8-2006

Modeling of Terrain Impact Caused by Off-road Vehicles

Qinghe Li
University of Tennessee - Knoxville

To the Graduate Council:

I am submitting herewith a dissertation written by Qinghe Li entitled "Modeling of Terrain Impact Caused by Off-road Vehicles." I have examined the final electronic copy of this dissertation for form and content and recommend that it be accepted in partial fulfillment of the requirements for the degree of Doctor of Philosophy, with a major in Biosystems Engineering.

Paul D. Ayers, Major Professor

We have read this dissertation and recommend its acceptance:

Alvin R. Womac, Eric C. Drumm, Jeffrey S. Freeman

Accepted for the Council:
Dixie L. Thompson

Vice Provost and Dean of the Graduate School

(Original signatures are on file with official student records.)

To the Graduate Council:
I am submitting herewith a dissertation written by Qinghe Li entitled "Modeling of Terrain Impact Caused by Off-road Vehicles". I have examined the final electronic copy of this dissertation for form and content and recommend that it be accepted in partial fulfillment of the requirements for the degree of Doctor of Philosophy, with a major in Biosystems Engineering.

Paul D. Ayers
Major Professor

We have read this dissertation
and recommend its acceptance:

Alvin R. Womac

Eric C. Drumm

Jefferey S. Freeman

Accepted for the Council:

Anne Mayhew
Vice Chancellor and Dean of
Graduate Studies

(Original signatures are on file with official student records)

MODELING of TERRAIN IMPACT CAUSED by OFF-ROAD VEHICLES

A Dissertation
Presented for the
Doctor of Philosophy Degree
The University of Tennessee, Knoxville

Qinghe Li
August 2006

Dedication

This dissertation is dedicated to my parents and my sister for their constant love and support.

Acknowledgments

I thank my mentor, Dr. Paul D. Ayers, for his consistent advice, patience, and encouragement in this study. He has been so enthusiastic and optimistic towards research, teaching, and life. It has been a great pleasure to be able to work with Dr. Ayers. My appreciation to Dr. Ayers is deep and sincere.

Many thanks go to Dr. Womac, Dr. Freeman, and Dr. Drumm for serving on my dissertation committee. They provided me instructions, valuable suggestions, reference materials, and encouragement during this study. Thanks also go to Alan Anderson who helped in arranging the field tests and collecting data in the field.

Thanks go to the faculties, staffs, and students in the Department of Biosystems Engineering and Soil Science for their support and assistance during the study. Thanks also go to the other members of the research group: Chelsea, Adam, Kate, Chris, Rob, and Matt. Your help in collecting data in the field and analyzing data in the laboratory made this research possible.

Abstract

Terrain impact models were developed for both wheeled vehicles and tracked vehicles based on the analysis of vehicle dynamics, soil mechanics, and geometric relationships between vehicle parameters and the disturbed width. The terrain impact models, including both disturbed width models and impact severity models, were developed separately for tracked vehicles and wheeled vehicles.

The disturbed width models of both vehicle types were primarily based on the geometric relationship between vehicle contact width and vehicle dynamic parameters. For both vehicle types, the impact severity was defined as the ratio between soil shear stress and soil shear strength. The impact severity model of wheeled vehicles was based on the balance between the centrifugal force of the vehicle and the soil shearing force that was related to vehicle dynamic parameters. For tracked vehicles, the soil shear stress was primarily derived from the lateral displacement of the tracks, not the centrifugal force, thus the impact severity model of tracked vehicles was based on the relationship between soil shear stress and soil lateral displacement caused by the lateral movement of the tracks.

Field tests of both wheeled vehicles and tracked vehicles were conducted at different test sites with different soil types and soil strength. The wheeled vehicles included a High Mobility Multipurpose Wheeled Vehicle (HMMWV), and a Light Armored Vehicle (LAV). The tracked vehicles included an M1A1 tank, an M577 armored personal carrier (APC), and an M548 cargo carrier.

The field test data supported the prediction of terrain impact models. The average percentage errors of the disturbed width model of the LAV and the HMMWV were $19.5\,\%$ and $8.6\,\%$, respectively. The average percentage errors of the impact severity model for the LAV were $48.5\,\%$ and $34.2\,\%$ for the high-speed ($9.6\,\mathrm{m/s}$) test and low-speed ($5.4\,\mathrm{m/s}$) test, respectively. The average percentage errors of the disturbed width model for the M1A1, M577, and the M548 were $10.0\,\%$, $27.3\,\%$, and $8.5\,\%$, respectively. The average percentage errors of the impact severity model of the M1A1 and M577 were $25.0\,\%$ and $21.4\,\%$, respectively.

Technical abstract

Off-road vehicles can damage the vegetative cover of the terrain and increase the potential of soil erosion. Theoretical models that can predict the terrain impact caused by off-road vehicles were developed and validated. Terrain impact was evaluated in terms of disturbed width and impact severity. Disturbed width is the width of disturbance caused by one pass of the vehicle and is an index of the size of the disturbed area that was measured perpendicular to the direction of travel. Impact severity indicates how severe the terrain was disturbed. The measurement of terrain impact severity was based on a guideline of initial severity of vehicle impact whose measurement ranging from $0\,\%$ to $100\,\%$.

Terrain impact models were developed for both wheeled vehicles and tracked vehicles based on the analysis of vehicle dynamics, soil mechanics, and geometric relationships between vehicle parameters and the disturbed width. Since the mechanism of operation of the wheeled vehicles and their interaction with terrain differs from that of the tracked vehicles, the terrain impact models, including both disturbed width models and impact severity models, were developed separately for tracked vehicles and wheeled vehicles.

The disturbed width model of wheeled vehicles was primarily based on the geometric relationship between vehicle contact width and vehicle dynamic parameters (vehicle speed and turning radius), as well as the tire cornering characteristics. The disturbed width model of the tracked vehicle was primarily based on the geometric relationship between vehicle

contact width and vehicle dynamic parameters, as well as the soil lateral resistance on the tracks.

For both wheeled vehicles and tracked vehicles, the impact severity was defined as the ratio between soil shear stress and soil shear strength. The impact severity model of wheeled vehicles was based on the balance between the centrifugal force of the vehicle and the soil shearing force that was related to vehicle dynamic parameters. For tracked vehicles, the soil shear stress was primarily derived from the lateral displacement of the tracks, not the centrifugal force, thus the impact severity model of tracked vehicles was based on the relationship between soil shear stress and soil lateral displacement caused by the lateral movement of the tracks. The soil lateral shear displacement was compared with the soil lateral shear deformation modulus that was determined based on previous studies of similar terrains.

Sensitivity analysis was conducted for some of the inputs to study their individual influences on terrain impact (disturbed width and impact severity). The disturbed width of wheeled vehicles was sensitive to cornering stiffness of tires especially at smaller turning radius. The most sensitive factor of disturbed width of tracked vehicles was track width. Impact severity of both types of vehicles were sensitive to vehicle speed at small turning radius. Impact severity of tracked vehicles was sensitive to soil shear modulus at small turning radius.

Field tests of both wheeled vehicles and tracked vehicles were conducted at different test sites with different soil types and soil strength. The wheeled vehicles included a four-wheeled vehicle, High Mobility Multipurpose Wheeled Vehicle (HMMWV), and an eight-wheeled vehicle, Light Armored Vehicle (LAV). The tracked vehicles included an M1A1 tank, an M577 armored personal carrier (APC), and an M548 cargo carrier. The test vehicles were operated in spiral patterns at different speed settings. The spiral-pattern maneuver resulted a wide range of turning radii ranging from 10 m to infinity.

Disturbed width and impact severity were measured within 24 hours at around 10 to 20 points along each spiral conducted by the test vehicles. Vehicle dynamic properties were collected using a Global Position System (GPS) receiver. Soil shear strength, used in the impact severity model of wheeled vehicles, were measured in situ by a soil torsional sheargraph. Soil samples were collected in the field for the analysis of soil texture in the laboratory.

The field test data supported the prediction of terrain impact models. The average percentage errors of the disturbed width model of the LAV and the HMMWV were $19.5\,\%$ and $8.6\,\%$, respectively. The average percentage errors of the impact severity model for the LAV on a soil with internal cohesion of $32.6\,\mathrm{kPa}$ and a friction angle of 26.6° were $48.5\,\%$ and $34.2\,\%$ for the high speed ($9.6\,\mathrm{m/s}$) test and low speed ($5.4\,\mathrm{m/s}$) test, respectively. The average percentage errors of the disturbed width model for the M1A1, M577, and the M548 were $10.0\,\%$, $27.3\,\%$, and $8.5\,\%$, respectively. The average percentage errors of the impact severity model of the M1A1 and M577 were $25.0\,\%$ and $21.4\,\%$, respectively, at a soil shear deformation modulus of 4 cm. The variation of the percentage errors were primarily due to the variation of soil strength parameters across the field, the operation of the vehicles during the spiral, and the variation of field measurement.

A comparison of terrain impact between wheeled vehicles and tracked vehicles was conducted based on an analysis of variance (ANOVA) of the field data. In the speed range tested in the field, the speed and turning radius of wheeled vehicles had strong interaction on terrain impact severity. However, the interaction of turning radius and speed for tracked vehicles was not significant.

Contents

List of Tables

List of Figures

Chapter 1

Introduction

Due to the wide application of off-road vehicles in agriculture, forestry, construction, and the military, the potential for damaging site productivity, increasing soil erosion, and deteriorating ecological quality has been a concern for land management. Off-road vehicles can damage the soil in the forms of compaction, ruts, vegetation cover removal, puddling, etc. Serious problems of adverse environmental effects resulting from off-road vehicle uses have been reported from the western United States, the Near-East deserts, North Africa, Peru, Australia, Russia, and China (Webb and Wilshire, 1983).

Military training land is one of the natural resources that off-road vehicles may damage. Vehicular military training is an intensive land use and can result in serious problems of terrain impact (Haugen et al., 2003). Figure 1.1 shows a parcel of the damaged terrain caused by vehicular military activities at Fort Riley, KS. Bare ground was exposed after the vegetation cover was completely scraped from the terrain surface. Rainfall and wind could cause serious soil erosion problems at this site. Figure 1.2 is an aerial image of Fort Riley, KS after vehicular training activities. The terrain impact caused by broad-scale uses of off-road vehicles degrades the terrain conditions extensively.

Figure 1.1: Terrain impact caused by off-road vehicle traffic at Fort Riley, KS

Figure 1.2: An aerial image of Fort Riley, KS after vehicular training activities, (from the GIS office, Fort Riley, 2005)

As a response to the concern of terrain impact caused by off-road vehicles, natural resource management organizations initiated various programs to study the potential deterioration of land resources due to vehicular activities. One of the largest federal land management organizations is the Department of Defense (DoD). The DoD is responsible for administering more than 25 million acres of federally owned land in the United States (Public Land Law Review Commission, 1970). Approximately half of the lands are available for a variety of training activities (Council on Environmental Quality, 1989). In order to become better stewards of the training land, the Army established the Integrated Training Area Management (ITAM) Program to manage these training lands. A Land Condition-Trend Analysis (LCTA) program was initiated to assess damage, identify potential problems, evaluate land conditions and allowable use, and monitor these conditions over time (Diersing et al., 1988). The Army Training and Testing Area Carrying Capacity (ATTACC) program was an initiative to estimate training land carrying capacity as well as land rehabilitation and maintenance costs associated with land-based training and other utilization (Anderson et al., 1996).

This dissertation focuses on the study of terrain impact that was evaluated in terms of disturbed width and impact severity caused by a single pass of off-road vehicles. The overall impact of a vehicle on soil and vegetation is a function of both the area impacted and the severity of impact within the disturbed area (Haugen, 2002). Disturbed width (DW) defines the width of disturbance caused by off-road vehicle traffic. Impact severity (IS) defines how severe the area was disturbed by a single pass of off-road vehicles. Knowledge of the disturbed width and impact severity is important for the estimation of the size of the impacted area, the amount of vegetation removal, and the potential of soil erosion.

Based on the design parameters of vehicles and the dynamic properties of soils and vehicles, theoretical models were developed to predict terrain impact (DW and IS) caused by off-road vehicles. As stated previously, terrain impact was evaluated with two indices,

disturbed width and impact severity. The disturbed width model and impact severity model were developed separately. Due to the differences of the mechanisms of operation and the vehicle-terrain interaction between the wheeled vehicles and the tracked vehicles, the development of disturbed width model and impact severity model for wheeled vehicles differs from that for tracked vehicles.

Field tests using both wheeled vehicles and tracked vehicles were conducted at different test sites. The test vehicles were operated in a spiral pattern at different speed settings. Disturbed width was measured perpendicular to the direction of travel in the field using a ruler. The measurement of terrain impact severity was based on a guideline of initial impact severity whose measurement step was 10% (Haugen, 2002). Vehicle static/dynamic properties and terrain properties were also recorded. The terrain impact models were supported by the field test data.

The terrain impact models would distinguish the influences of many vehicle/terrain parameters under general conditions. However, like many models in other fields, the models could not encompass the entire operation conditions, which would make the models exceedingly complicated, even make the development of the models hardly possible. Some assumptions were necessary during the development of the models. Major assumptions of the models are specified in the following list:

1. The models do not account for the scenario of vehicles running uphill or downhill. The vehicles were assumed to be operated on even ground with uniform vegetation cover.

2. Extreme operation conditions, such as the lateral sliding, sudden acceleration, and abrupt braking of the vehicles, are not considered.

3. For the disturbed width model of the wheeled vehicles, the tire contact width of all the tires of the wheeled vehicles is assumed to be the same.

4. The wheeled vehicles either have two axles or have four axles.

5. The lateral load transfer of a vehicle during a turn is not considered. The load transfer from one side to the other side of the vehicle not only changes the tire contact pressure or the track ground contact pressure, but also results in a slight increase of the slip angles of wheeled vehicles.

6. It is assumed that the slip angles developed under off-road conditions are consistent with that under on-road conditions, so that the equation to calculate slip angles of wheeled vehicles originally used under on-road conditions can be used under off-road conditions.

The remainder of this dissertation is structured as follows. Chapter 2 states the objectives of this study. Chapter 3 reviews previous studies on terrain impact, soil mechanics, and the application of GPS for vehicle tracking. Chapter 4 and 5 discuss the development of disturbed width model and impact severity model for wheeled vehicles and tracked vehicles respectively. Chapter 6 describes the method used to conduct field test. Chapter 7 states the results of field tests. Chapter 8 compares the difference of terrain impact between wheeled vehicles and tracked vehicles. Chapter 9 concludes the study.

Chapter 2

Objectives

Many of the previous models for terrain impact evaluation were empirical models based on statistical plot studies. The statistically based models were limited to be effective for a few vehicles at certain configurations under certain terrain conditions (Anderson et al., 2005). Development of theoretical models for terrain impact estimation based on vehicle design parameters and terrain conditions would compensate for these limitations and help the users better understand the mechanisms of terrain impact.

The objective of this study was to develop theoretical models for the estimation of disturbed width and impact severity of a single pass of off-road vehicles. Since there are two indices (disturbed width and impact severity) to describe terrain impact as well as two kinds of off-road vehicles (wheeled and tracked) to be studied, four individual models were developed. After the development of these models, field tests were conducted to test the models. Besides the measurement of disturbed width and impact severity, the input parameters of the models need to be determined in the field tests. These parameters included terrain properties and vehicle static/dynamic properties. Vehicle dynamic properties such as velocity and turning radius were determined by GPS tracking data. The specific objectives of this study were:

1. Develop a theoretical model to predict terrain disturbed width for wheeled vehicles;
2. Develop a theoretical model to predict terrain impact severity for wheeled vehicles;
3. Develop a theoretical model to predict terrain disturbed width for tracked vehicles;
4. Develop a theoretical model to predict terrain impact severity for tracked vehicles;
5. Conduct field tests and use field test data to validate the models.
6. Discuss and evaluate the utility and accuracy of each of the theoretical models;
7. Conduct sensitivity analysis to identify important parameters of the models;
8. Compare the difference between wheeled vehicles and tracked vehicles on terrain impact based on the field test data.

Chapter 3

Literature review

3.1 Terrain impact of off-road vehicles

3.1.1 The concern of terrain impact

Off-road vehicles are widely used in agriculture, forestry, construction, and the military. Intensive research has been conducted on the mobility and traction ability of off-road vehicles. In recent decades, the potential for damaging site productivity and ecological quality has been a concern in agriculture, forestry, and military land management. More and more researchers have begun to study the environmental damage, especially the terrain impact, caused by off-road vehicles (Braunack, 1986; Grantham et al., 2001; Thurow et al., 1993; Gatziolis et al., 2000; Shaw and Diersing, 1989). The terrain impact take various forms including ruts, compaction, change of plant species, reduction of vegetative cover, soil erosion, and change of the soil strength and the hydrologic characteristics of the soil. Intensive off-road vehicle maneuvers can alter the local ecological system (Wilshire, 1976).

In agriculture, ever since the extensive application of large farming equipment such as large 4WD and 2WD tractors, large combines, and auger wagons in the 1970's, farmers

have been concerned about soil damage caused by off-road vehicles (Janzen, 1990). Excessive compaction of soil caused by agricultural machinery can adversely influence crop production (Marsili et al., 1998). Oljaca (1994) conducted a field study of the soil compaction caused by tracked agricultural tractors. The soil type of the terrain was classified as silt clay loam with a moisture content of $15.20\,\%$-$18.73\,\%$. Due to the compaction of the tracked tractors, the increases of the penetraction resistance of the soil and bulk density of the soil ranged from $20.05\,\%$ to $150\,\%$ and from $0.21\,\%$ to $14.61\,\%$, respectively. The total soil porosity of the compacted soil decreased from $0.24\,\%$ to $15.41\,\%$. Petelkau and Dannowski (1990) found that grain yields declined up to 28.3% in the traffic lanes due to the compaction of soil resulting from different vehicle loads. Pytka (2005) measured the soil stress and soil deformation caused by agricultural tractors using a stress state transducer and an optical system, and found that deformations of soft soils were rapid and irreversible. The author stated that even advanced tillage practices did not restore the initial physical properties of compacted soil, such as bulk density, air, and water conditions. Compaction and deformation of the soil could damage soil ecological quality and significantly decrease the resulting yield capability.

In forestry management, the problem of soil damage caused by off-road machinery is of even greater concern because of the year-round operation of heavier machinery regardless of weather conditions (Matthes and Watson, 1989). A study reported that the increase of soil compaction during harvesting neotropical forest is related to traffic intensity of skidders (Donagh et al., 2002). In this study, these researchers suggested that an increase in number of logs logged in each pass might reduce the total number of passes and lessen the soil damage caused by skidders.

In the military, vehicular training is an intensive land use and can result in lost or disturbed vegetation and increased soil erosion (Haugen et al., 2003). The average off-road

impact area per vehicle for a three-day area security mission of the reconnaissance training exercise in Yakima Training Center, Washington was $1.958\,\mathrm{m}^2$ (Haugen et al., 2003). Off-road vehicle impacts can have detrimental environmental effects by removing vegetative cover and increasing soil erosion (Goran et al., 1983; Sullivan and Anderson, 2000). Various levels of ecological disturbance caused by U.S. Army tactical vehicle training on 12 training installations were reported (Goran et al., 1983). Vehicle training maneuvers resulted in the species replacement of both mammals and birds on major US Army installations (Goran et al., 1983). Significant biomass reduction, plant population reduction, and soil erosion on these installations were also reported. Soil disturbances produced during large-scale armored military maneuvers in the early 1940s were examined in 1981 in California's eastern Mojave Desert (Prose, 1985). The researcher reported that these soil disturbances were probably major factors in encouraging accelerated soil erosion throughout the maneuver area and also retarding or preventing the return of vegetation to its pre-disturbance conditions. A study on the vegetation impacts caused by tracked vehicles was conducted at the Pinon Canyon Maneuver Site, Colorado (Shaw and Diersing, 1990). The study shows that vehicular training not only significantly reduced vegetation cover and increased the percentage of bare ground, but also changed the plant species composition of the disturbed area. In the Netherlands, the area of irreparable damage had increased to $25\,\%$ of the $9000\,\mathrm{ha}$ of military training grounds (Payne et al., 1983).

3.1.2 Previous studies on the mechanisms of terrain impact

Researchers have studied a variety of factors that would influence terrain impact. These factors include the types of vehicle, number of passes of vehicles, moisture content of soil, and dynamic properties of off-road vehicles. Researchers also developed methods and models to evaluate terrain impact.

Different types of vehicle usually cause different degrees of terrain impact severity. By switching from wheeled tractors to tracked tractors, farmers improved in managing compaction and increased yield (Janzen, 1990). A field test conducted in northern Alaska studied the terrain impact of various types of vehicles including an air cushion vehicle, two light tracked vehicles, and three types of wheeled vehicles (Abele et al., 1984). The air cushion vehicle produced the least amount of soil damage. The wheeled vehicles, with multiple passes, caused longer-lasting damage than the light tracked vehicles.

Multiple off-road vehicle traffic causes more severe terrain impact than a single pass. Several vehicles traveling in line may produce an impact similar to a pivot turn (Wilson, 1988). A field test studied three levels of vehicle impact (2, 8, 32 trips over the same tracks) applied on rangelands near Ashland, Mont., using a four-wheel-drive vehicle (Payne et al., 1983). There was increasing likelihood of damage carrying over into subsequent years as the number of trips in the same track went up. A series of similar traffic tests was conducted in Alaska (Abele et al., 1984). The traffic impact was evaluated in terms of surface depression, effect on thaw depth, damage to vegetation, and visibility of traffic signature. The damage increased with the number of vehicle passes and with the increase in the tire or track's ground contact pressure. Another study reported that although the rapidly growing beach grass (Ammophila) recovers quickly after impact where conditions are favorable, the vegetation could be totally destroyed by even low-level, continuous off-road vehicle pressure (Leatherman and Godfrey, 1979). Although damage increases as the amount of repeated traffic increases, the initial pass had a prominent effect on soil compaction characterized by changes in the soil properties, such as dry density, specific volume, and penetration resistance (Abebe et al., 1989).

The moisture content of the soil influences the magnitude of terrain impact at the time of tracking (Thurow, 1990). A study indicated that damage was greater on very moist to wet soils than on dry soils (Payne et al., 1983). A field trial was conducted to examine the

effect of initial soil water content on soil disturbance caused by tracked military vehicles (Braunack and Williams, 1993). In the trial, deeper ruts were formed where the terrain had a higher water content.

Vehicle dynamic properties, such as turning radius, speed, and dynamic load on the wheel, affect the magnitude of impact as well. Vehicle maneuver patterns can dramatically influence the terrain impact (Thurow, 1990). A vehicle making sharp turns will disturb a larger width of soil than a vehicle traveling straight or making smooth turns (Ayers, 1994; Braunack, 1985). A single pivot turn of a tracked vehicle has an immediate and obvious impact on vegetation by exposing bare ground, destroying native plants, and allowing weeds to establish. By measuring soil dry bulk density, an experiment substantiated the theoretical prediction that increases in wheel load, at a given ground pressure, result in increases in soil compaction at greater depth but have less effect near the soil surface (Smith and Dickson, 1990). An increased dynamic load can increase both rut width and deformed soil cross-section area (Raper et al., 1995).

Several methods to judge the severity of terrain impact were proposed. Researchers developed a subjective impact rating method which assesses the impact ratings of three components, microrelief, soil, and vegetation, along the track of off-road vehicles (Slaughter et al., 1990). Then, a cumulative impact value was calculated by summing up the three individual impact ratings. Another method estimated soil erosion based on vegetative cover derived from remotely sensed imagery (Tweddale et al., 2000). Some studies rated the terrain impact by using the terms of disturbed width, percent bare soil, or vegetation removal area (Haugen et al., 2003; Ayers, 1994). The Army Training and Testing Area Carrying Capacity (ATTACC) methodology normalizes terrain impact in terms of Maneuver Impact Miles (MIM) which equals the impact of an M1A2 tank traveling 1 mile while participating in an armor battalion field training exercise (Anderson and Sullivan, 2002).

Researchers developed a variety of models to estimate the terrain damage problem caused by off-road wheeled vehicles, including models for estimating tire ground pressure (Dwyer, 1984), rut depth (Horn et al., 2004; Bekker, 1969; Freitag, 1965), and soil compaction or soil bulk density (Horn et al., 2004; Schwanghart, 1991), just to name a few. Some recent studies proposed empirical models to directly predict terrain impact caused by off-road vehicles. Ayers et al. (2000) empirically expressed impact severity and disturbed width of off-road vehicles as functions of vehicle turning radius and velocity. Wilson (1988) developed a model that related the composition of species and the amount of bare ground in mixed prairie to the frequency and season of military tank traffic. Wilson (1988)'s model was able to predict the number of tank passes that was sustainable by the vegetation without significant change in species composition. For the benefit of plant conservation, the model also advised the best season for military training. Diersing et al. (1988) developed a model that was able to estimate the allowable levels of sustained tracked vehicle use, such as the maximum allowable visible track coverage, based upon physical properties of the soil and biological attributes of the vegetation.

3.2 Soil mechanics and vehicle/terrain interaction

The understanding of soil is of great importance for this study. This section reviews the definition and classification of soil, then discusses various parameters describing soil strength as well as their measuring techniques, and finally lists some models on vehicle-terrain interaction. Some of the techniques of measuring soil strength are used in this study, and will also be mentioned in other chapters.

3.2.1 Soil definition and classification

Soil is defined as "masses of mineral particles mixed with varying proportions of water, gases and salts, and often organic matter" (McKyes, 1989). The particles are classified into three types, sand, silt, and clay (McKyes, 1989). According to the USDA classification scheme, the particle sizes of sand, silt, and clay are divided into three major size classifications: $2.0\,\mathrm{mm}$-$0.05\,\mathrm{mm}$, $0.05\,\mathrm{mm}$-$0.002\,\mathrm{mm}$, and less than $0.002\,\mathrm{mm}$, respectively (Soil Survey Division Staff, 1993). The texture of the soil, or the relative distribution of various sized particles, can be looked up from the USDA textural triangle, which is a graphical representation of the 12 soil textural classes shown in Figure 3.1 (Soil Survey Division Staff, 1993).

Due to the variation of soil textures and the complexity of the spatial arrangement of particles in soil, it is almost impossible to conduct a rigorous mathematical analysis of soils. The character of plasticity increases as the texture of a soil changing from sand to clay. The behaviors of a friction soil (sand) and a cohesion soil (clay) are different. For example, the trafficability of a friction soil has little variation due to the change of water content, whereas the change soil moisture of a cohesion soil would influence the trafficability significantly (McKyes, 1989).

3.2.2 Soil shearing strength

Soil shearing strength is a major dynamic property of soil. As Equation 3.1 shows, Coulomb defined soil shearing strength as a function of the applied normal stress and strength parameters of the soil (Wong, 2001).

$$\tau = c + \sigma \cdot \tan\phi \tag{3.1}$$

Where,

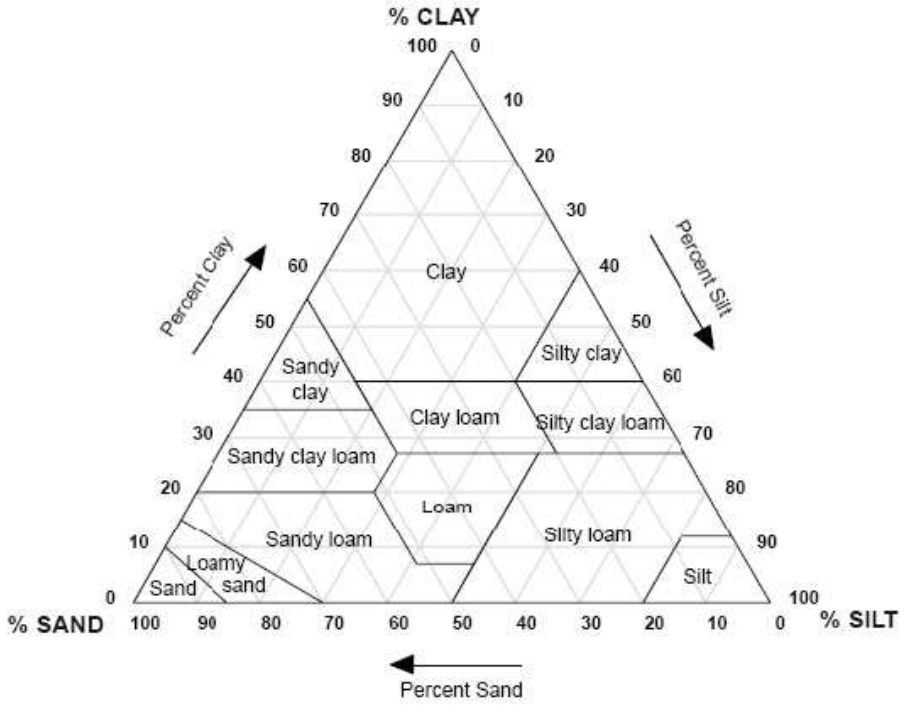

Figure 3.1: The USDA soil texture triangle (McKyes, 1989)

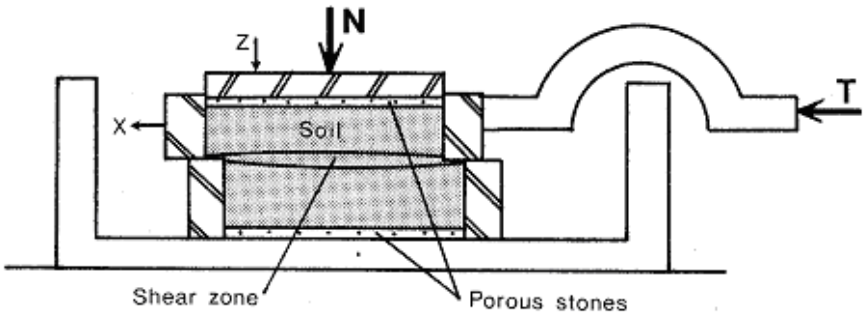

Figure 3.2: The direct shear box (McKyes, 1989)

τ is the shearing strength of the soil (psi),

σ is the applied normal stress (psi),

ϕ is the angle of internal friction (deg), and

c is the internal cohesion of the soil (psi).

The soil strength parameters in the equation not only change with soil texture and structure, but also change with soil moisture and density. A study discussed the effects of moisture and density on soil shear strength parameters measured with a torsional sheargraph for coarse-grained soils (Ayers, 1987). The study shows that values for both the soil cohesion and friction angle increase with an increase in soil density.

Researchers have developed a variety of measurement techniques to measure the angle of internal friction and the internal cohesion of soil. The direct shear box, shown in Figure 3.2, is a simple device that measures soil strength in the laboratory (McKyes, 1989). The triaxle soil testing device, shown in Figure 3.3, is more complex than the direct shear box (McKyes, 1989). It provides the ability to control soil strains and stress combinations.

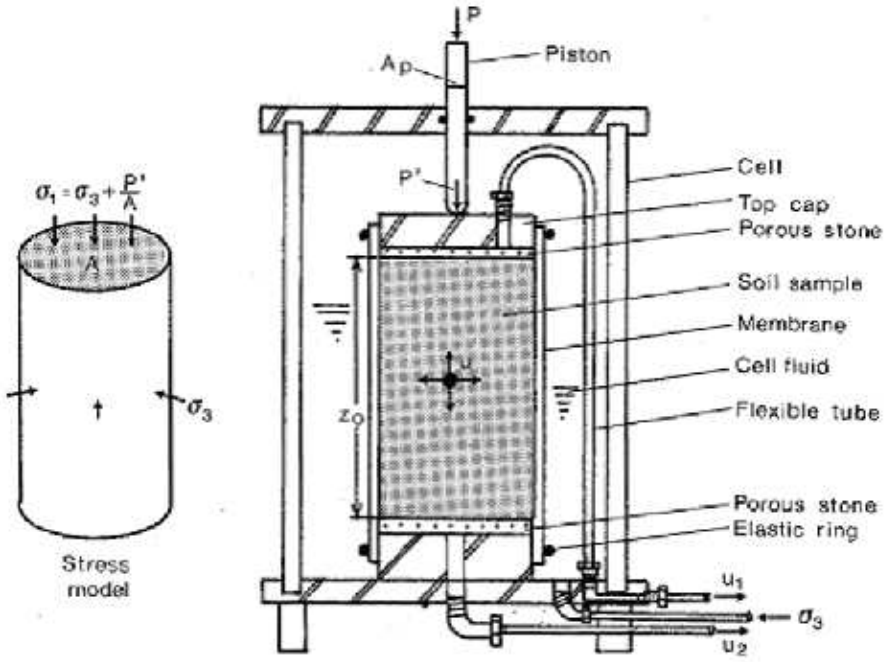

Figure 3.3: The triaxle soil testing device (McKyes, 1989)

Figure 3.4 shows an instrument called the soil torsional sheargraph (Cohron, 1962). The instrument consists of a shear head, a pointer, a spiral spring, a recording graph, and a handle. By applying a combination of normal-torsional load through the handle, a shear stress-normal stress curve is recorded on the graph by the pointer that is attached to the shear head. The instrument is convenient to estimate the parameters of the Coulomb equation in situ. The soil torsional sheargraph is easier to use than the triaxial soil test device, which requires the removal of a sample of soil from the test site to the laboratory. Figure 3.5 shows the measurement result of a Torsional Sheargraph test (McKyes, 1989). It can be read from the test result sheet that the internal friction angle and the internal cohesion are 25° and $3\,\mathrm{psi}$, respectively (McKyes, 1989).

3.2.3 Soil penetration resistance

Soil penetration resistance depends on the cone area, angle of penetration, velocity of penetration, and the depth of penetration (ASAE, 1999). The penetrometer is widely used when the measurement of soil penetration resistance is needed. Figure 3.6 shows the structure of a penetrometer. The operation of the soil penetrometer should follow the ASAE standard EP542 (ASAE, 1999):

> The cone should be pushed into the soil at a uniform rate of approximately $30\,\mathrm{mm/s}$ ($72\,\mathrm{in./min}$). The surface reading is measured at the instant the base of the cone is flush with the soil surface. Subsequent readings should be made continuously, or as frequently as possible while maintaining a $30\,\mathrm{mm/s}$ ($72\,\mathrm{in./min}$) penetration rate.

Equation 3.2 is a model to calculate soil penetration resistance (Ayers and Perumpral, 1982). Four parameters of the model need to be determined from field measurement data.

$$q = \frac{C_1 \cdot g^{C_4}}{C_2 + (MC - C_3)^2} \tag{3.2}$$

Figure 3.4: The Torsional Sheargraph

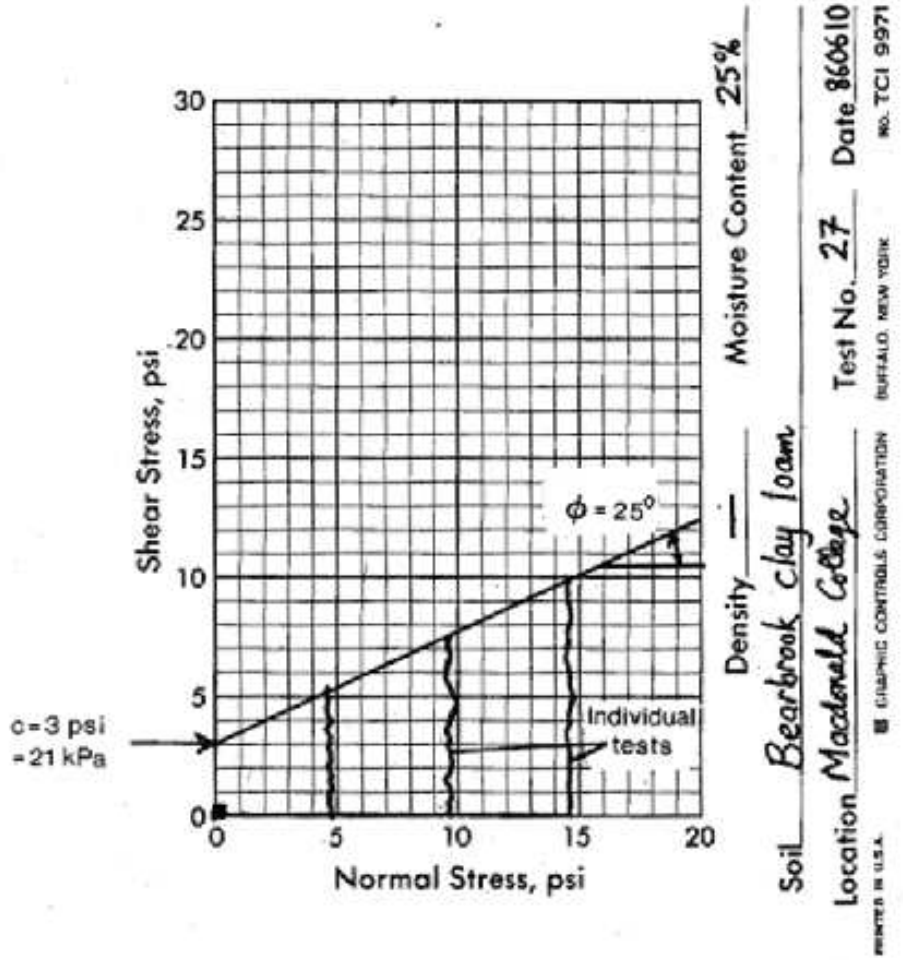

Figure 3.5: The test sheet of Torsional Sheargraph (McKyes, 1989)

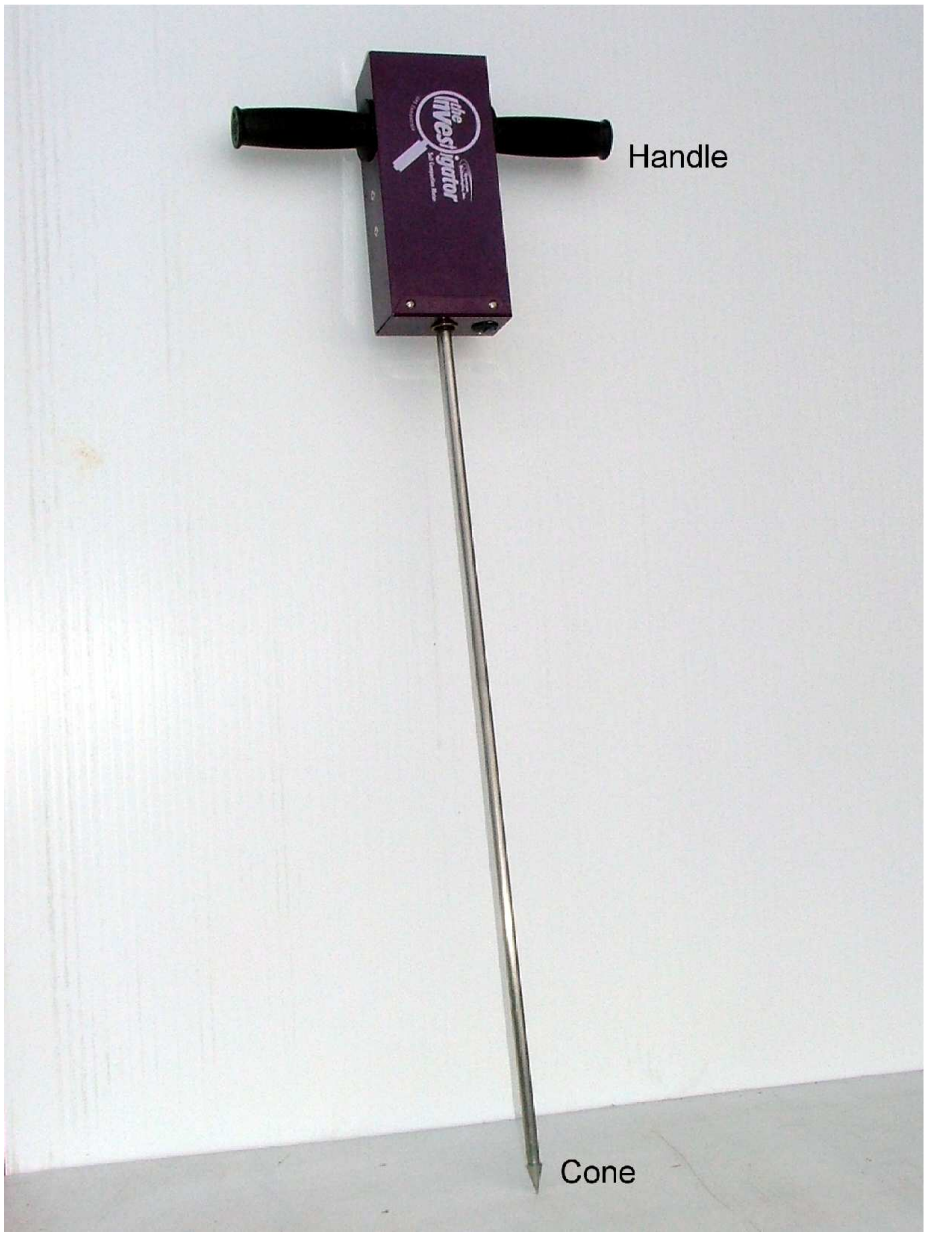

Figure 3.6: The soil penetrometer

Where,

q is the penetratioin resistance (kPa),

g is the soil dry density ($\mathrm{kg/m^3}$),

MC is the moisture content, (dry weight percentage), and

$C_1 - C_4$ are constants to be estimated.

Another technique to measure soil penetration resistance is to use a drop-cone penetrometer. The technique consists of releasing a $2\,\mathrm{kg}$, 30° apex angle cone from a height of $1\,\mathrm{m}$ and measuring its penetration (Godwin et al., 1991). Godwin et al. (1991) also found that cone penetration is in linear relationships with soil moisture content, vane shear strength, and rut depth resulting from machinery operations.

3.2.4 Soil bearing capacity and rut depth (sinkage) models

Soil bearing capacity is usually considered as the maximum allowable wheel/track contact pressure. Table 3.1 shows the bearing capacity of different soil types (Saarilahti, 2002). Due to the low bearing capacity of wet clay, alluvial soils, and peatlands, these types of terrain are considered unsuitable for wheeled forwarder traffic (Saarilahti, 2002). The Waterways Experiment Station (WES) models use the Cone Index, measured by using a soil penetrometer, to evaluate soil bearing capacity.

Researchers have developed sinkage models to describe soil bearing capacity. Bekker proposed a model, shown in Equation 3.3, to describe the relationship between track pressure and sinkage, (Bekker, 1969).

$$p = (\frac{k_c}{b} + k_\phi) \cdot z^n \tag{3.3}$$

Where,

p is the contact pressure of track (Pa),

Table 3.1: Bearing capacity of different soil types (Saarilahti, 2002)

Soil description	Bearing capacity, kPa
Moraine, dry	400-800
Moraine, moist, fine	200-500
Moraine, moist, granular	300-600
Gravel, dry	300-700
Gravel, moist	400-800
Sand, dry	150-250
Sand, moist	300-500
Clay, dry	400-1200
Clay, moist	200-300
Clay, wet	50-150
Peatland, wooded	40-70
Peatland, open	10-40
Snow, virgin	10-30
Snow, old, -10C	50-100
Snow, compressed, -10C	200-500
Snow, hard packed, -10C	400-800
Ice	1000-2000

b is the smaller dimension (width of a rectangular contact area or radius of a circular contact area) of the contact patch (m),

z is the sinkage depth (m),

n is the soil deformation exponent (unitless),

k_c is a soil deformation modulus related to the cohesion and friction components ($\mathrm{N/m^{(n+1)}}$), and

k_ϕ is another soil deformation modulus related to the cohesion and friction components ($\mathrm{N/m^{(n+2)}}$).

Equation 3.4 describes an empirical single-pass rutting model used to evaluate the impact severity of wheeled vehicles in the ATTACC (Army Training and Testing Area Carry and Capacity) program (Sullivan and Anderson, 2000). The sinkage of wheeled vehicles is described as the function of the Rating Cone Index ($RatingConeIndex$) of the soil, Tire Diameter ($TireDia$), Single Tire Width ($TireWidth$), Total Vehicle Weight ($VehWeight$), Total Number of Wheels ($NumWheel$), Tire Deflection ($TireDefl$), and Tire Section Height ($TireSectHt$).

$$Sinkage = \frac{5 \times TireDia}{\left[\frac{RatingConeIndex}{\left[\frac{VehWeight/NumWheel}{TireDia \times tireWidth}\right] \times \left[1 - \frac{TireDefl}{TireSectHt}\right]^{3/2} \times 0.724\,779\,7}\right]^{5/3}} \tag{3.4}$$

Where,

$Sinkage$ is Wheel Sinkage or Rut Depth ($\mathrm{in.}$),

$RatingConeIndex$ is Rating Cone Index of the soil (unitless),

$TireDia$ is Tire Diameter ($\mathrm{in.}$),

$TireWidth$ is Single Tire Width ($\mathrm{in.}$),

$VehWeight$ is Total Vehicle Weight (lb),

$NumWheel$ is Total Number of Wheels (unitless),

$TireDefl$ is Tire Deflection ($\mathrm{in.}$), and

$TireSectHt$ is Tire Section Height (in.).

Equation 3.5 describes an empirical single-pass rutting model used to evaluate the terrain impact of tracked vehicles in the ATTACC program (Sullivan and Anderson, 2000). In this model, sinkage is described as the function of the Track length ($TrLen$), Track width ($Trwidth$), Vehicle weight ($VehWeight$), Number of Track ($NumTrack$) and Rating Cone Index ($RatingConeIndex$) of the soil.

$$Sinkage = TrLen \times 0.0043 \times e^{[\frac{5.887\times(\frac{VehWeight/NumTrack}{TrLen\times Trwidth})}{RatingConeIndex}]} \tag{3.5}$$

Where,

$Sinkage$ is Wheel Sinkage or Rut Depth (in.),

$RatingConeIndex$ is Rating Cone Index of the soil (unitless),

$TrLen$ is Track Length (in.),

$VehWeight$ is Total Vehicle Weight (lb),

$NumTrack$ is Total Number of Tracks (unitless), and

$Trwidth$ is Track Width (in.).

3.2.5 The WES models

The Waterways Experiment Station (WES) is headquarters for the U.S. Army Engineer Research and Development Center (ERDC). In order to provide military personnel simple methods to evaluate the mobility of vehicles, the WES developed a variety of empirical models of wheel-terrain interaction. These methods were based on the measurement of the Cone Index (CI), which can be easily measured by using a cone penetrometer.

The CI is used to calculate a wheel numeric (or tire numeric), which contains both the characteristics of soil and the parameters of the wheel. The wheel numeric helps to describe the status of wheel-soil contact. Due to the variation of different soil type characteristics,

the wheel numeric is not in a unique form. Equations 3.6, 3.7, and 3.8 are used to calculate tire numeric for tires operating in purely cohesive soil, purely friction soil, and soils with both cohesive and frictional properties, respectively (Wong, 2001).

$$N_C = \frac{CI \cdot b \cdot d}{W} \cdot \sqrt{\frac{\delta}{h}} \cdot \frac{1}{1 + \frac{b}{2d}} \tag{3.6}$$

$$N_S = \frac{G \cdot (b \cdot d)^{3/2}}{W} \tag{3.7}$$

$$N_{CS} = \frac{CI \cdot b \cdot d}{W} \tag{3.8}$$

Where,

b is the tire section width (m),

CI is the cone index (Pa),

d is the tire diameter (m),

G is the sand penetration resistance gradient $(\mathrm{Pa/m})$,

h is the unloaded tire section height (m),

W is the tire load (N), and

δ is the tire deflection (m).

Using the wheel numeric as input, researchers have developed a variety of models to predict parameters of vehicle mobility. For example, these models include rolling resistance (Equation 3.9, (Dwyer, 1984)), thrust (Equation 3.10, (MacLaurin, 1997)), rut depth (Equation 3.11, (MacLaurin, 1997)), as well as drawbar pull.

$$u_R = 0.049 + \frac{0.287}{N_{CI}} \tag{3.9}$$

$$u_P = 0.817 - \frac{3.2}{N_{CI} + 1.91} + \frac{0.453}{N_{CI}} \tag{3.10}$$

$$z = d \cdot \frac{0.224}{N_{CI}^{1.25}} \tag{3.11}$$

Where,

u_R is the rolling resistance coefficient (unitless),

u_P is the thrust coefficient (unitless),

z is the rut depth (m),

N_{CI} is the tire numeric (unitless), and

d is the tire diameter (m).

3.3 Using GPS for vehicle tracking

Researchers found that vehicle dynamic parameters, such as speed and turning radius, could influence the severity of terrain impact. These parameters need to be determined in order to evaluate their influence. The Global Positioning System (GPS) provides a method that is not only able to determine the position of off-road vehicles but also able to derive their dynamic parameters.

3.3.1 The application of GPS tracking

GPS systems have been widely used for a variety of tracking applications (Ayers et al., 2000; Dougherty, 2000; Markgraf et al., 2002; Moen et al., 1996; Turner et al., 2001; Veal et al., 2001; Zito et al., 1995). Haugen (2002) used the autonomous Garmin GPS35-HVS receivers to track 20 military vehicles during a military training exercise. The accuracy of tracking forest machines with GPS was studied (Veal et al., 2001). The researchers in this

study used two commercially available GPS receivers to track forest machine movement. The GPS receivers were hand-held models manufactured by Trimble Navigation, Ltd. The receivers were the ProXR and the GeoExplorer II. The forest machine, a wheeled skidder, was tracked in three different canopy conditions and at two different ground speeds. Their study found that positions collected by the ProXR and the GeoExplorer receivers had mean errors of $1.34\,\mathrm{m}$ and $2.75\,\mathrm{m}$ respectively. The changing of conditions from open to heavy canopy deteriorated the accuracy of position tracking. The skidder speeds tested did not appear to affect the accuracy of GPS tracking. In a study, researchers used a GPS tracking system to determine the dynamic properties (vehicle velocity and turning radius) of off-road vehicles (Ayers et al., 2000). The static/dynamic accuracy of GPS receivers is discussed in section 3.3.2.

A study reviewed the fusion of GPS position fixes with dead-reckoning sensors (Abbott and Powell, 1999). The combination of GPS position fixes and other navigation aids helps to enhance the overall performance of navigation. Dead-reckoning is the ability to determine the current location of a vehicle by knowing the movement information, such as heading and velocity, from a previous position. Although the dead-reckoning prediction will drift over long time periods, it is accurate in measuring changes over short time periods and will reduce the short-term errors of GPS position fixes. The errors of GPS position fixes and dead-reckoning predictions are complementary. Figure 3.7 shows the functional schematic of the land-vehicle navigation system. The system contains a GPS receiver and a dead-reckoning unit that includes a rate Gyro, a compass, and an odometer (Abbott and Powell, 1999). A Kalman filter can take advantage of the complementary errors, and produce a better performance of positioning than each individual sensor (Abbott and Powell, 1999).

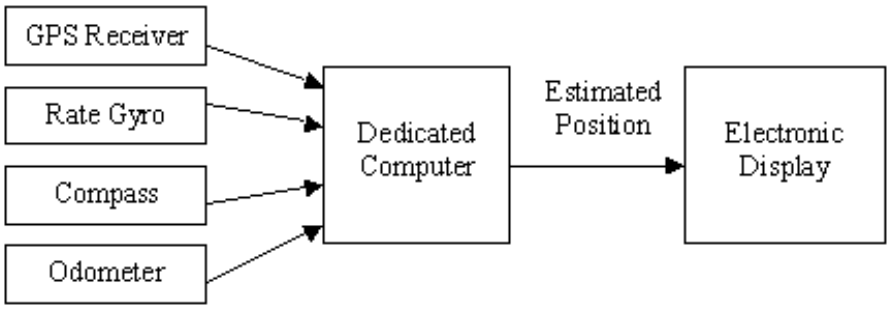

Figure 3.7: Function schematic of land-vehicle navigation system, (Abbott and Powell, 1999)

3.3.2 The evaluation of the accuracy of GPS receivers

Evaluations of the dynamic performance of GPS receivers have been recently conducted. Static performance of receivers was not indicative of dynamic performance (Stombaugh et al., 2002). A study shows that the cross track errors were less than $0.15\,m$ for high-level GPS receivers (Taylor and Schrock, 2003).

Researchers evaluated the static and dynamic accuracy of autonomous Garmin GPS 35 and Omnistar Trimble AgGPS 132 differential GPS receivers (Ayers et al., 2004). Figure 3.8 shows the placement of GPS receivers for static accuracy test. The AgGPS 132 receiver was placed in the center. The Garmin GPS 35 receivers were surrounding the AgGPS 132 in a circle. The GPS data were recorded at a frequency of $1\,\mathrm{Hz}$. The Trimble AgGPS 132 GPS receiver produced expected accuracies of $0.44\,\mathrm{m}$, $0.37\,\mathrm{m}$, and $0.93\,\mathrm{m}$ for Mean, Circular Error Probable (CEP) and 2 Distance Root Mean Square (2DRMS), respectively. The mean error for the Garmin 35 was $4.03\,\mathrm{m}$, much higher than the receiver with differential correction.

Figure 3.8: The placement of GPS receivers for static accuracy test (Ayers et al., 2004)

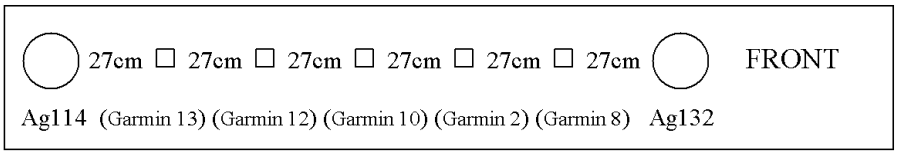

Figure 3.9: The placement of GPS receivers for dynamic accuracy test (Ayers et al., 2004)

In the same study, an in-line tracking test was conducted to examine the dynamic accuracy of both DGPS receivers and autonomous GPS receivers (Ayers et al., 2004). The GPS data logging frequency was $1\,\mathrm{Hz}$. Figure 3.9 illustrates the placement of the receivers. Two DGPS receivers, Trimble Ag 132 and Ag 114, were mounted at the front and the rear ends of the mounting plate. Five autonomous Garmin-35 GPS receivers were mounted in between Ag 132 and Ag 114. All of the receivers were separated in a $27\,\mathrm{cm}$ interval (Ayers et al., 2004).

Figure 3.10 shows the tracking data of all the receivers along the travel line of the truck in the test (Ayers et al., 2004). The 'true' track line of the truck was determined using the least square fitting of the tracking data of the five Garmin receivers. Then the mean cross track error of the receivers was determined. Table 3.2 lists the error of both the Garmin receivers and the Trimble receivers. The mean error of the autonomous Garmin receivers was $1.92\,\mathrm{m}$. The mean error of the DGPS Trimble receivers was $0.14\,\mathrm{m}$, which was much smaller than that of the Garmin receivers (Ayers et al., 2004). This test showed the superior ability of DGPS receivers for deriving dynamic properties of off-road vehicles.

Besides the accuracy of static and dynamic positioning, researchers also examined the accuracy of GPS receivers on determining velocity and turning radius of vehicles. A study compared the accuracy of the Ag 132 receiver with a radar speed sensor on determining velocity (Ayers et al., 2000). When the reading of the radar speed sensor was $2.38\,\mathrm{m/s}$ and $6.76\,\mathrm{m/s}$, the velocity calculated from the GPS data was $2.33\,\mathrm{m/s}$ and $6.84\,\mathrm{m/s}$, respectively. The accuracy of the calculated velocity from the GPS data decreases with increasing

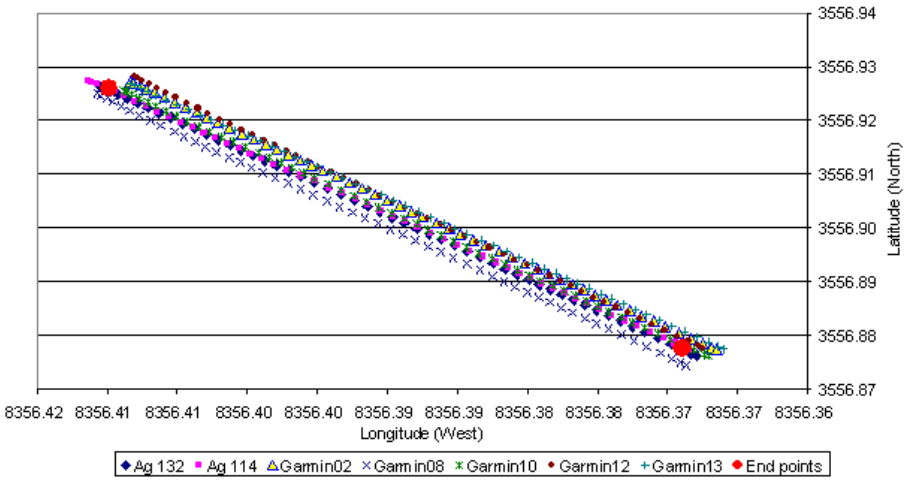

Figure 3.10: Positions of the GPS receivers during the in-line tracking test (Ayers et al., 2004)

Table 3.2: Summary of the in-line tracking errors (meters) (Ayers et al., 2004)

	mean_error	std_error
Garmin	1.918	1.194
Trimble	0.138	0.084

velocity, but the error is small compared to the actual velocity. Turning radius was also able to be accurately calculated from GPS data (Ayers et al., 2000). When the actual turning radius of the tested vehicle was $10\,\mathrm{m}$, the turning radius was calculated as $10.3\,\mathrm{m}$ with a standard deviation of $0.9\,\mathrm{m}$.

3.4 Summary of literature

Previous studies on terrain impact were reviewed. Terrain impact of off-road vehicles depend on a variety of factors including soil properties and vehicle static/dynamic properties. Although some empirical terrain impact models exist, none of these models and/or methods were developed based on the analysis of vehicle dynamics, soil mechanics, and the mechanism of vehicle/terrain interaction. The empirical models only accounted for limited factors that could influence terrain impact. This chapter also reviewed studies on soil mechanics as well as some WES models of terrain-vehicle interaction. Some applicable apparatuses that can measure soil properties in situ during field tests were discussed. Since vehicle dynamic parameters play an important role on influencing terrain impact, vehicle tracking technology was required by this study. Literature on the application of GPS technology and its accuracy on vehicle tracking was reviewed.

Chapter 4

Model development for wheeled vehicles

4.1 Disturbed width model for wheeled vehicles

4.1.1 Model development for an eight-wheeled vehicle

The army is transforming to new easily deployable vehicles such as the light armored vehicle (LAV). The LAV, shown in Figure 4.1, is an eight-wheeled vehicle. Transformation to the LAV results in a change of the patterns of training activities and a possible change in terrain impact. The army has been interested in quantifying the impact caused by the new vehicles (Haugen, 2002).

Disturbed width is defined as the maximum width of the tire contact area on the terrain, measured perpendicular to the traveling direction of the vehicle. There are a variety of factors that can influence the disturbed width. The influence of turning radius is obvious. As vehicle goes straight, because the treads of tires overlap with each other, the disturbed width is minimum. As the vehicle turns, the treads of tires would separate and result increase of the disturbed with.

The development of a theoretical model of disturbed width for an eight-wheeled vehicle was based on the dynamic properties and geometric relationships of the vehicle. The

Figure 4.1: Light armored vehicle (LAV)

centrifugal force cannot be neglected when a vehicle is negotiating a turn at moderate or higher speeds. Figure 4.2 shows the geometric relation and dynamic condition of an eight-wheeled four-axle vehicle when negotiating a turn with a constant turning radius and a constant forward speed. The pair of tires on each axle is represented by a single tire with double the cornering stiffness. Because the tires must develop appropriate cornering force (F_{yf} and F_{yr}) to balance the centrifugal force, the tires will develop slip angles α_f and α_r (Wong, 2001).

From the geometry shown in Figure 4.2, a triangle is formed by the center of front tire (f), the center of the rear tire (r) and the turning center (O). L is the wheel base which is defined in this study as the distance from the front axle center to the rear axle center. R_r and R_f are the lengths from the turning center to the center of the rear tire and to the center of the front tire, respectively. R is the length from the turning center to the junction point of the centrifugal force line and the line connecting the front and rear tires. The three angle values of the triangle are approximately given by

$$\angle O \approx \frac{L}{R} \tag{4.1}$$

$$\angle r = \frac{\pi}{2} - \alpha_r \tag{4.2}$$

$$\angle f = \frac{\pi}{2} + \alpha_r - \frac{L}{R} \tag{4.3}$$

It is noted that $\angle O$ is approximated as $\frac{L}{R}$ in Equation 4.1. The approximation is reasonable as long as $\angle O$ is a small angle. It is discussed in detail in section 4.1.2.

Turning radius (TR) here is defined as the distance from the turning center of the vehicle to the center of the vehicle body. B (not shown in the figure) represents the tread width, which is the distance between the center of the two front tires or the two rear tires.

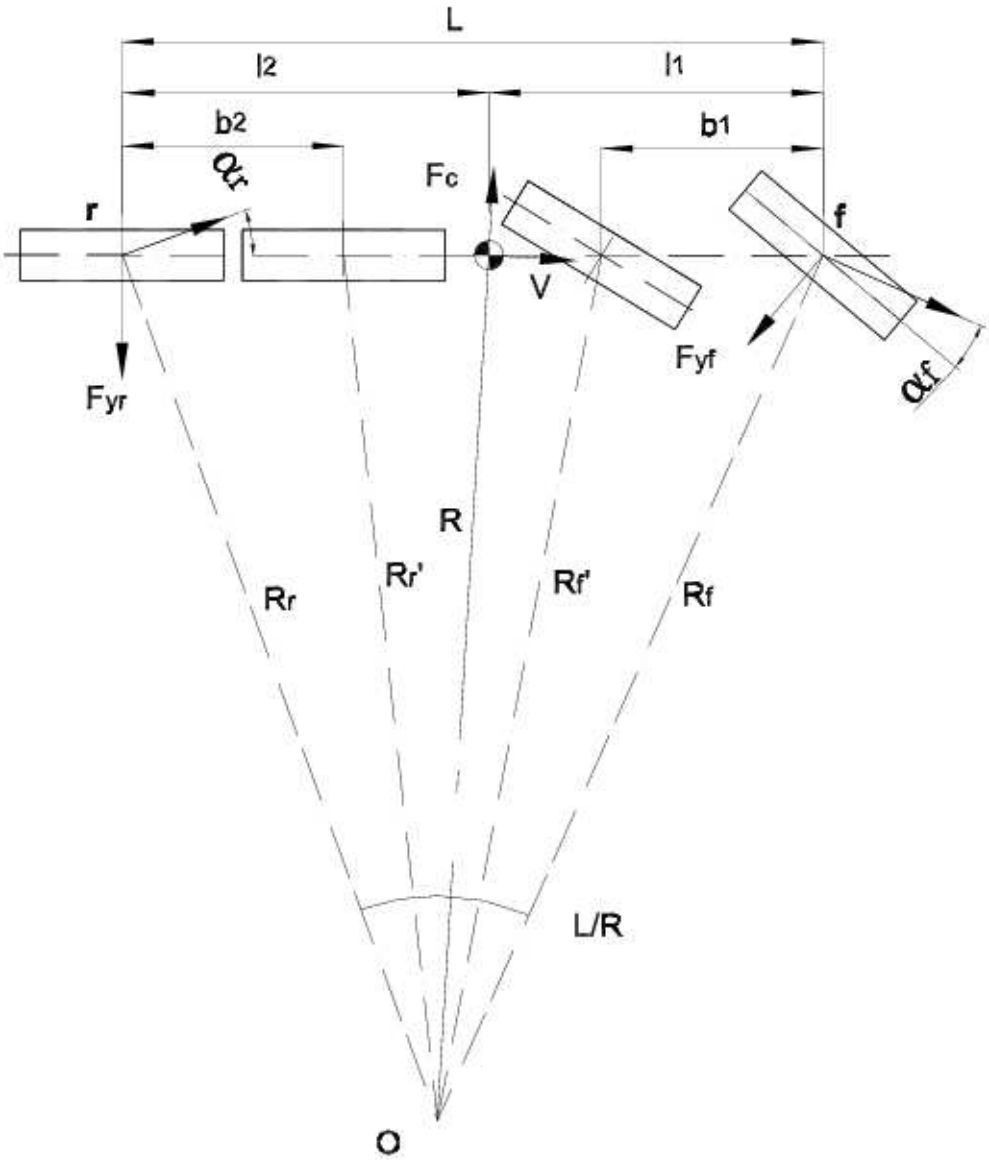

Figure 4.2: Geometric relation and dynamic condition of an eight-wheeled vehicle (modified from (Wong, 2001))

In this model, the front tread width and the rear tread width are assumed to be the same. For the calculation of disturbed width of the inner side tires in the following procedure, the parameter of R can be approximated by

$$R = TR - \frac{B}{2} \tag{4.4}$$

Note that R should be substituted with the sum of TR and $B/2$ in order to calculate the disturbed width of the outside tires.

According to triangle geometry, the following relationships exist:

$$\frac{L}{\sin(\frac{L}{R})} = \frac{R_f}{\sin(\frac{\pi}{2} - \alpha_r)} \tag{4.5}$$

$$\frac{L - b_1}{\sin(\frac{L-b_1}{R})} = \frac{R'_f}{\sin(\frac{\pi}{2} - \alpha_r)} \tag{4.6}$$

$$\frac{L - b_2}{\sin(\frac{L-b_2}{R})} = \frac{R'_r}{\sin(\frac{\pi}{2} + \alpha_r - \frac{L}{R})} \tag{4.7}$$

$$\frac{L}{\sin(\frac{L}{R})} = \frac{R_r}{\sin(\frac{\pi}{2} + \alpha_r - \frac{L}{R})} \tag{4.8}$$

R_f, R'_f, R'_r, and R_r can be calculated by solving Equations 4.5 to 4.7.

$$R_f = \frac{L \cdot \sin(\frac{\pi}{2} - \alpha_r)}{\sin(\frac{L}{TR-B/2})} \tag{4.9}$$

$$R'_f = \frac{(L - b_1) \cdot \sin(\frac{\pi}{2} - \alpha_r)}{\sin(\frac{L-b_1}{TR-B/2})} \tag{4.10}$$

$$R'_r = \frac{(L - b_2) \cdot \sin(\frac{\pi}{2} + \alpha_r - \frac{L}{TR - B/2})}{\sin(\frac{L - b_2}{TR - B/2})} \tag{4.11}$$

$$R_r = \frac{L \cdot \sin(\frac{\pi}{2} + \alpha_r - \frac{L}{TR - B/2})}{\sin(\frac{L}{TR - B/2})} \tag{4.12}$$

When the vehicle is going straight ahead, the rear tire track completely overlaps the front tire track. In this case, the disturbed width (DW) of the vehicle is equal to the tire-terrain contact width (TW). As the vehicle starts negotiating a turn, the rear tire track will move away from the front tire track. The disturbed width increases as the overlapped track area decreases.

R_f, R'_f, R'_r, and R_r can then be ranked into R_1, R_2, R_3, and R_4, so as to make $R_1 \geq R_2 \geq R_3 \geq R_4$. The total disturbed width can be represented by the summation of three parts: DW_1, DW_2, and DW_3. Figure 4.3 shows a scenario of the relationships between DW, TW, DW_1, DW_2, DW_3, R_1, R_2, R_3, and R_4. These relationships are more explicitly defined from 4.13 to 4.19

$$DW = DW_1 + DW_2 + DW_3 \tag{4.13}$$

Where,

$$DW_1 = 1.5 \cdot TW \qquad \text{if } R_1 - R_2 \geq TW \tag{4.14}$$

$$DW_1 = R_1 - R_2 + 0.5 \cdot TW \qquad \text{if } R_1 - R_2 < TW \tag{4.15}$$

$$DW_2 = TW \qquad \text{if } R_2 - R_3 \geq TW \tag{4.16}$$

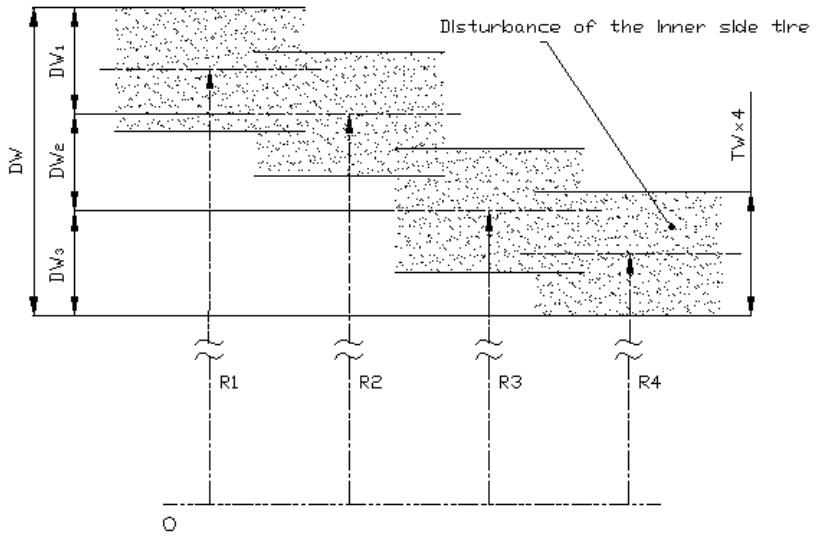

Figure 4.3: A scenario of the relationship between DW, R_1, R_2, R_3, and R_4

$$DW_2 = R_2 - R_3 \qquad \text{if } R_2 - R_3 < TW \tag{4.17}$$

$$DW_3 = 1.5 \cdot TW \qquad \text{if } R_3 - R_4 \geq TW \tag{4.18}$$

$$DW_3 = R_3 - R_4 + 0.5 \cdot TW \qquad \text{if } R_3 - R_4 < TW \tag{4.19}$$

Wong (2001) reported that for slip angles below a certain value, the cornering force is approximately proportional to the slip angle. In this study the slip angle and cornering force are considered to be in a linear relationship with a slope equal to the cornering stiffness of the tires. It is assumed that the slip angle of the rear tires of the vehicle under off-road conditions can be approximated by Equation 4.20 (Wong, 2001).

$$\alpha_r = \frac{W_r}{C_{\alpha r}} \frac{V^2}{g \cdot TR} \tag{4.20}$$

Where,

W_r is the static normal load on each of the rear tires (N),

V is the velocity of the vehicle ($\mathrm{m/s}$),

$C_{\alpha r}$ is the cornering stiffness of each of the rear tires ($\mathrm{N/rad}$),

g is the acceleration of gravity ($\mathrm{m/s^2}$), and

TR is the turning radius of the vehicle (m).

Equations 4.9 to 4.20 define the model of DW for an eight-wheeled vehicle. DW is a function of L, TR, B, b_1, b_2, TW, W_r, V, and $C_{\alpha r}$. In this model, it is assumed that the tires of the vehicle does not slide laterally, which can be caused by a sharp turn at an extreme high speed. The lateral load transfer, which can result in a slight increase in the slip angle of the tires, is not considered in the model development (Wong, 2001).

4.1.2 Approximation analysis

Angle $\angle O$ is approximated as $\frac{L}{R}$ in Equation 4.1. The approximation holds true as long as $\angle O$ is a small angle. This section discusses the validity of this approximation.

Figure 4.4 is modified from Figure 4.3. A triangle is formed by lines $\overline{AB}$, $\overline{OA}$, and $\overline{OB}$. The length of line $\overline{OA}$ is equal to the length of line $\overline{OB}$. Line $\overline{OC}$ is perpendicular to line $\overline{AB}$, thus divides $\angle O$ evenly into two small angles whose values are equal to θ. Theoretically, the following equations hold true:

$$\angle O = 2 \times \theta \tag{4.21}$$

$$\theta = \arcsin(\frac{L}{2R}) \tag{4.22}$$

So,

$$\angle O = 2 \times \arcsin(\frac{L}{2R}) \tag{4.23}$$

Equation 4.23 is a theoretical calculation of angle $\angle O$; whereas Equation 4.1 is an approximation. If $\angle O$ is a small angle, Equation 4.1 is a valid approximation. Because the turning radius of the LAV is around $10\,\mathrm{m}$ to $150\,\mathrm{m}$, whereas the wheel base of the vehicle is $3.86\,\mathrm{m}$, angle $\angle O$ usually is less than 22°.

Table 4.1 compares the calculation results of $\angle O$ from the theoretical equation and the approximation equation. When turning radius is $10\,\mathrm{m}$, the theoretical result is only $0.6\,\%$ higher than the approximation. The approximation approaches the true value as turning radius increases. The approximation in Equation 4.1 is reasonable.

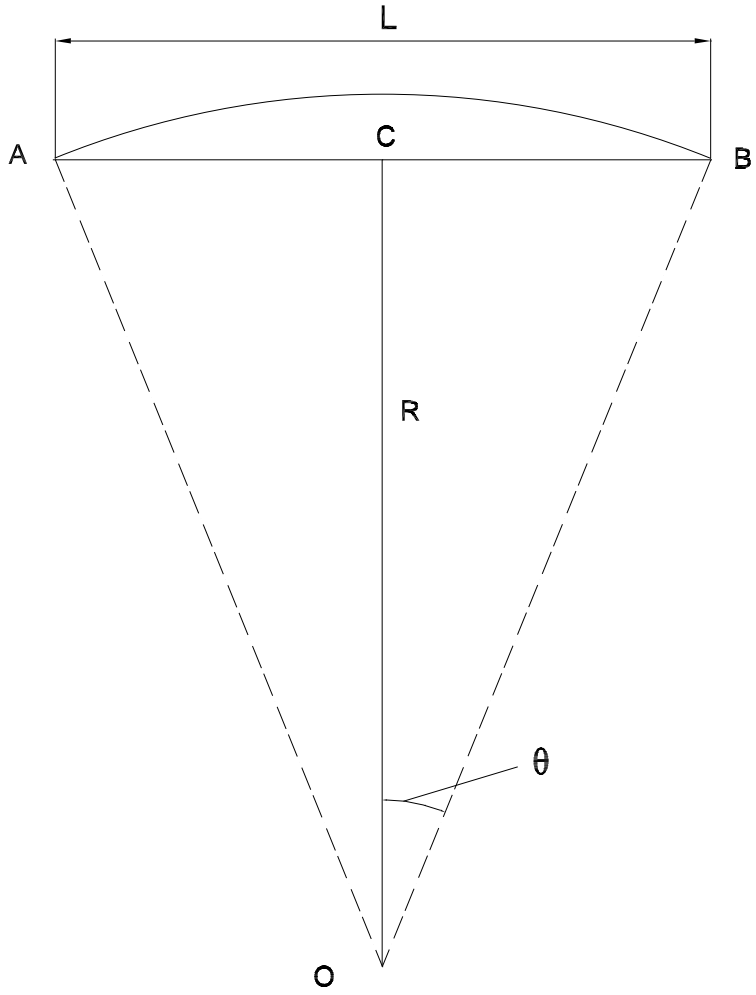

Figure 4.4: Approximation of a small angle

Table 4.1: Comparison of the approximation and the theory values of $\angle O$

Turning radius	Theory	Approximation	Percentage error
$10\,\mathrm{m}$	22.26	22.12	0.6%
$150\,\mathrm{m}$	1.47	1.47	0.0%

4.1.3 Model development for a four-wheeled vehicle

The DW model of the eight-wheeled vehicle can be extrapolated to a four-wheeled vehicle. Figure 4.5 shows the geometric relation and dynamic condition of a four-wheeled vehicle when negotiating a turn with a constant turning radius and a constant forward speed.

For a vehicle moving at a constant speed, the turning radius for a total separation of the front tire track and the rear tire track can be calculated by solving Equation 4.24

$$R_f - R_r = TW \tag{4.24}$$

For a vehicle moving at a turning radius larger than the turning radius at separation, the disturbed width of the inner side tires of the vehicle can be calculated by Equation 4.25. For a vehicle moving at a turning radius smaller than the turning radius at separation, the disturbed width of the inner side tires of the vehicle is equal to twice of the tire width, shown in Equation 4.26. The disturbed width of a wheeled vehicle is given by

$$DW = (R_f + \frac{TW}{2}) - (R_r - \frac{TW}{2}) \qquad \text{if } R_f - R_r \leq TW \tag{4.25}$$

$$DW = 2 \cdot TW \qquad \text{if } R_f - R_r > TW \tag{4.26}$$

Where R_f and R_r can be calculated by Equations 4.9 and 4.12, respectively.

In general, disturbed width of the inside tires of a wheeled vehicle can be expressed by

$$\begin{aligned} DW &= \frac{L}{\sin(\frac{L}{TR-B/2})} \cdot [\sin(\frac{\pi}{2} - \frac{W_r}{C_{\alpha r}} \frac{V^2}{g \cdot TR}) - \sin(\frac{\pi}{2} - \frac{W_r}{C_{\alpha r}} \frac{V^2}{g \cdot TR} - \frac{L}{TR - B/2})] + \\ &\quad + TW \qquad \text{if } R_f - R_r \leq TW \end{aligned} \tag{4.27}$$

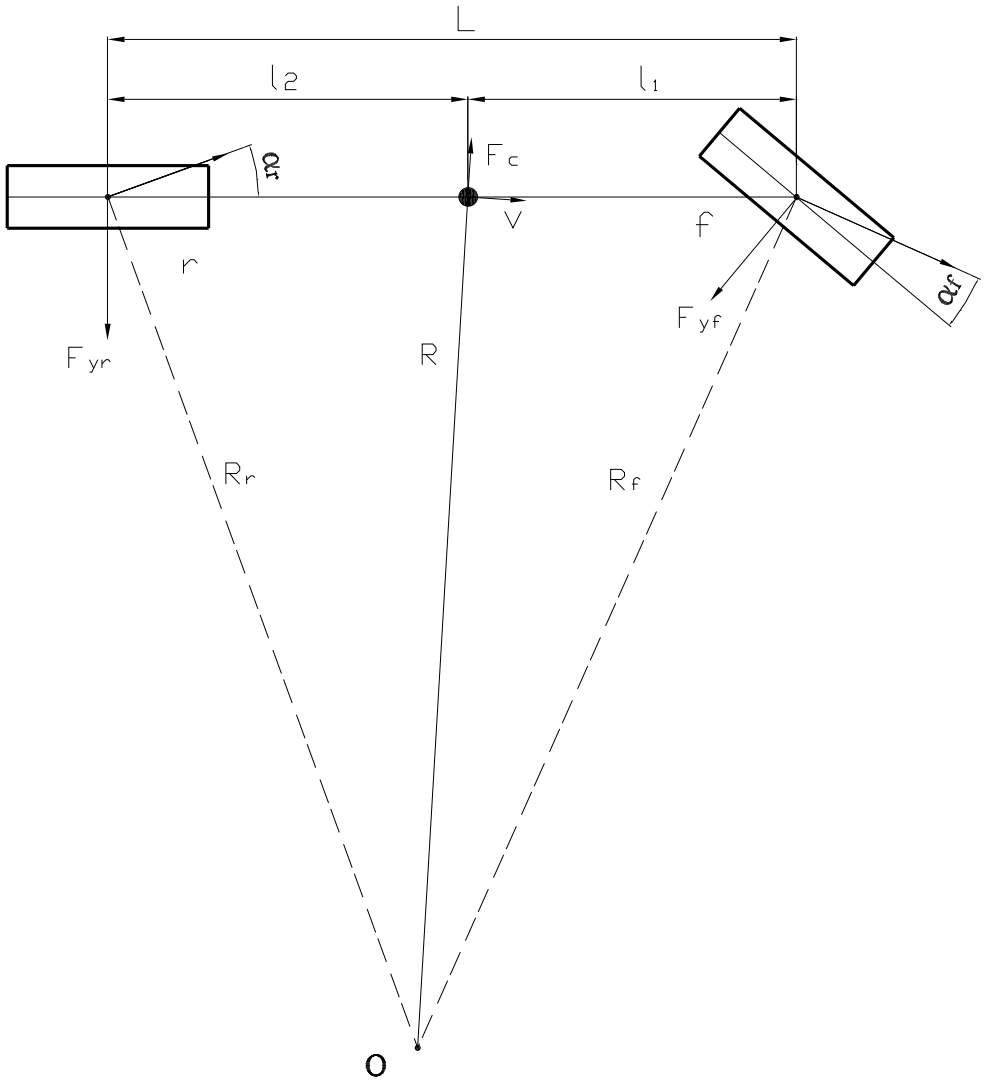

Figure 4.5: Geometric relation and dynamic condition of a four-wheeled vehicle (modified from (Wong, 2001))

$$DW = 2 \cdot TW \qquad \text{if } R_f - R_r > TW \tag{4.28}$$

In this model, the tire-soil contact area is assumed to be circular with a diameter equal to TW. It is noted that $TR - B/2$ should be substituted with $TR + B/2$ in Equation 4.27 in order to calculate the disturbed width of the outside tires.

4.2 Impact severity model for wheeled vehicles

Besides disturbed width, impact severity is another index to describe terrain impact. Disturbed width is an index of the size of the disturbed area, whereas impact severity describes how severe the area was impacted. Impact severity models of wheeled vehicles will be developed in this section.

It is assumed that the higher the shear stress caused by off-road vehicles the higher the impact severity. When the shear stress reaches the soil shear strength, vehicle sliding will happen as the soil fails. In this scenario, soil impact severity will reach the maximum value. Soil impact severity will reach the maximum value when the shear stress reaches the soil shear strength. Soil shearing and vehicle sliding will happen at this condition. Therefore soil impact severity can be related to the ratio between the actual shear stress and the soil shear strength.

The Mohr-Coulomb equation defines soil shearing strength as a function of the applied normal stress and strength parameters of the soil (Wong, 2001).

$$\tau = c + \sigma \tan \phi \tag{4.29}$$

Where,

τ is the shearing strength of the soil (Pa),

σ is the applied normal stress (Pa),

ϕ is the angle of internal friction (deg), and

c is the internal cohesion of the soil (Pa).

When the soil shear stress reaches the soil strength laterally, the centrifugal force will be balanced by soil shear force as shown in Equation 4.30. During turning, the centrifugal force produces weight shift from inside tires to outside tires. The centrifugal force is in equilibrium of the summation of the soil shear forces on both the inside tires and the outside tires.

$$\frac{m \cdot V^2}{TR} = [c + \frac{(\frac{mg}{2} + \frac{m \cdot V^2}{TR} \cdot \frac{H}{B})}{A_{out}} \cdot \tan\phi] \cdot A_{out} + [c + \frac{(\frac{mg}{2} - \frac{m \cdot V^2}{TR} \cdot \frac{H}{B})}{A_{in}} \cdot \tan\phi] \cdot A_{in} \quad (4.30)$$

It can be simplified as

$$\frac{m \cdot V^2}{TR} = c \cdot A + mg \cdot \tan\phi \quad (4.31)$$

Or,

$$\frac{m \cdot V^2}{TR \cdot A} = c + \frac{mg \cdot \tan\phi}{A} = \tau \quad (4.32)$$

Where,

m is the vehicle mass (kg),

V is the velocity ($\mathrm{m/s}$),

TR is the turning radius (m),

A_{out} is the contact area of out side tires (m^2),

A_{in} is the contact area of inside tires (m^2),

A, equal to $A_{out} + A_{in}$, is the tire-terrain contact area (m^2),

H is the height of center of gravity (m),

B is the tread width (m),

Table 4.2: Lookup table for parameter k (Koolen and Kuipers, 1983)

Ply rating	4 and 6	8	10 and 12	16
k	1.1	1.15	1.2	1.25

g is the acceleration of gravity ($\mathrm{m/s^2}$), and

τ is the soil shear stress (Pa).

As the vehicle speed increases, the soil shear stress increases. Eventually the speed would increase to a critical value, then any further increase of speed beyond this critical velocity will cause the vehicle to slide laterally. Simultaneously the soil shear stress reaches the soil shear strength. This scenario is described in Equation 4.33. The critical velocity, V_{cri} , can be derived from Equation 4.34.

$$\frac{m \cdot V_{cri}^2}{TR \cdot A} = \tau_{max} \tag{4.33}$$

Where,

V_{cri} is the critical velocity ($\mathrm{m/s}$), and

τ_{max} is the soil shear strength (Pa).

$$V_{cri} = \sqrt{\frac{TR \cdot (c \cdot A + mg \cdot \tan\phi)}{m}} \tag{4.34}$$

The tire-terrain contact area can be calculated by Equation 4.35 (Koolen and Kuipers, 1983).

$$A = \frac{mg}{k \cdot p_i} \tag{4.35}$$

Where,

p_i is the tire inflation pressure (Pa), and

k can be determined from Table 4.2 (Koolen and Kuipers, 1983).

Equation 4.32 shows that soil shear stress is linearly related to the square of velocity. The proposed theory impact severity, which is a ratio between the actual shear stress and the soil shear strength, can be expressed by

$$IS_{theory} = \frac{\tau}{\tau_{max}} = (\frac{V_{act}}{V_{cri}})^2 \times 100\% \qquad \text{if } V_{act} \leq V_{cri} \tag{4.36}$$

$$IS_{theory} = 100\% \qquad \text{if } V_{act} > V_{cri} \tag{4.37}$$

Where V_{act} is the actual vehicle velocity.

Chapter 5

Model development for tracked vehicles

5.1 Disturbed width model for tracked vehicles

Besides wheeled vehicles, tracked vehicles such as the M1A1 tank are also widely used in the army. Because the locomotion systems are different, the mechanism of terrain impact of tracked vehicles is different from wheeled vehicles. When a tracked vehicle moves, the track pads lay down as the roadwheels roll over. As the tracked vehicle makes a turn, the lateral movement of the tracks increases the disturbed width.

A theoretical disturbed width model of tracked vehicles was developed based on vehicle dynamic properties and geometric relationships. Figure 5.1 shows the geometric relationship between turning radius (TR) and disturbed width (DW) of a tracked vehicle. DW in this study is defined as the width of the contact area of vehicle track on soil. TL, TW and B represent track length, track width, and tread width, respectively. C is the geometric center of the projection of the tracks. O is the instantaneous turning center when the vehicle is moving at a speed of V with a turning radius of TR. D represents the distance between the instantaneous turning center (O) and the geometric center (C) in the traveling direction of the vehicle. D can be calculated by Equation 5.1 (Le, 1999).

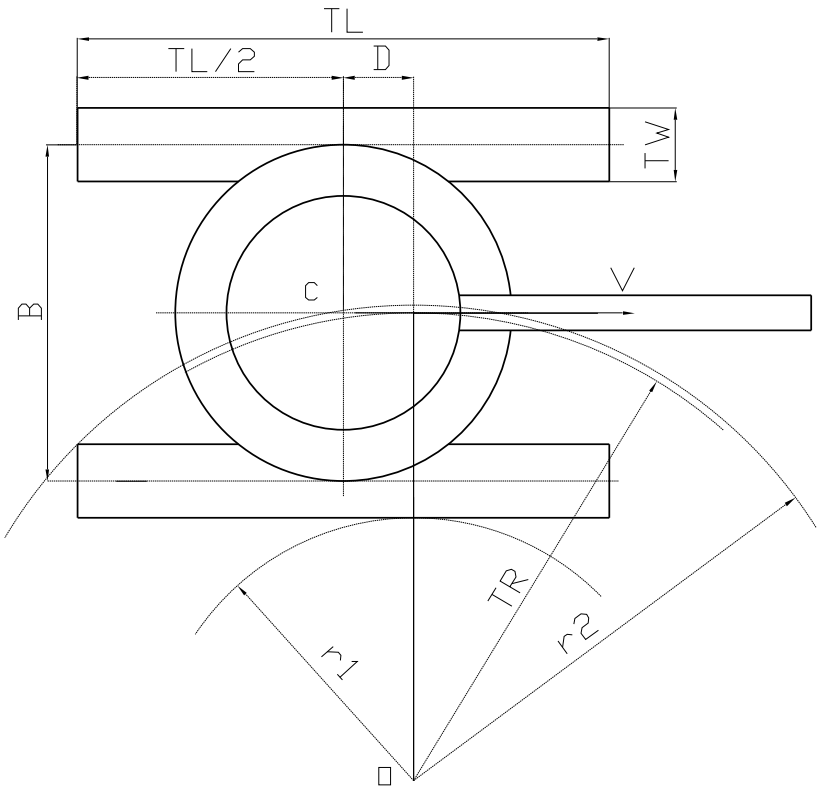

Figure 5.1: Geometric relationship of a tracked vehicle

$$D = \frac{V^2 \cdot TL}{4g\mu_l \cdot TR} \tag{5.1}$$

Where,

V is the velocity of the vehicle ($\mathrm{m/s}$),

g is the acceleration of gravity ($\mathrm{m/s^2}$),

μ_l is the coefficient of soil lateral resistance (unitless), and

TR is the turning radius of the vehicle (m).

The distance from the instantaneous turning center (O) to the inner side edge of the inside track is represented by r_1. The distance between O and the furthest corner of the inside track is represented by r_2. If the vehicle maintains a constant speed at a given turning radius, its path forms a complete circle. A disturbed area in the shape of an annulus with radii r_1 and r_2 will be formed due to the movement of the inside track. The disturbed width (DW) is defined as the difference between r_1 and r_2 .

$$DW = r_1 - r_2 \tag{5.2}$$

According to the geometric relationships in Figure 5.1, r_1 and r_2 are defined by Equations 5.3 and 5.4.

$$r_1 = TR - \frac{B}{2} - \frac{TW}{2} \tag{5.3}$$

$$r_2 = \sqrt{(\frac{TL}{2} + \frac{\nu^2 \cdot TL}{4g\mu_l \cdot TR})^2 + (TR - \frac{B}{2} + \frac{TW}{2})^2} \tag{5.4}$$

Substituting Equations 5.3 and 5.4 for r_1 and r_2 in Equation 5.2 derives the disturbed width model, Equation 5.5. Inputs of the DW model include vehicle geometric dimensions, vehicle speed, turning radius, and coefficient of soil lateral resistance. In this model, vehicle

mass has no influence on disturbed width. The equation of the disturbed width model of the outside track can be easily extrapolated from Equation 5.5 by simply substituting $TR+B/2$ in the equation for $TR - B/2$.

$$DW = \sqrt{(\frac{TL}{2} + \frac{\nu^2 \cdot TL}{4g\mu_l \cdot TR})^2 + (TR - \frac{B}{2} + \frac{TW}{2})^2} - (TR - \frac{B}{2} - \frac{TW}{2}) \quad (5.5)$$

5.2 Impact severity model for tracked vehicles

5.2.1 Review of the relationship between shear stress and shear displacement of the soil

As a tracked vehicle turns, the tracks slide laterally. The lateral movement of the tracks of a turning vehicle will produce shear stress, and cause shear displacement of the soil. It is expected that a higher shear displacement would cause a higher impact severity. A study of the relationship between shear stress and shear displacement of soils helps the development of impact severity model. Wong (2001) indicated that there are three types of relationships between shear stress and shear displacement. The variation of strain-stress relationship was caused by the texture, structure, moisture content, and bulk density of soils. Researchers have developed models to simulate these strain-stress relationships.

The first type of strain-stress relationship is for loose sand, saturated clay, and dry fresh snow. Figure 5.2 shows the features of this type of strain-stress relationships. The shear stress rises up rapidly with the increase of soil displacement. Finally, it levels off at the maximum shear strength. Janosi and Hanamoto (1961) proposed a model, shown in Equation 5.6, to describe this relationship.

$$\tau = \tau_{max} \cdot (1 - e^{-j/K}) = (c + \sigma \cdot \tan\phi) \cdot (1 - e^{-j/K}) \quad (5.6)$$

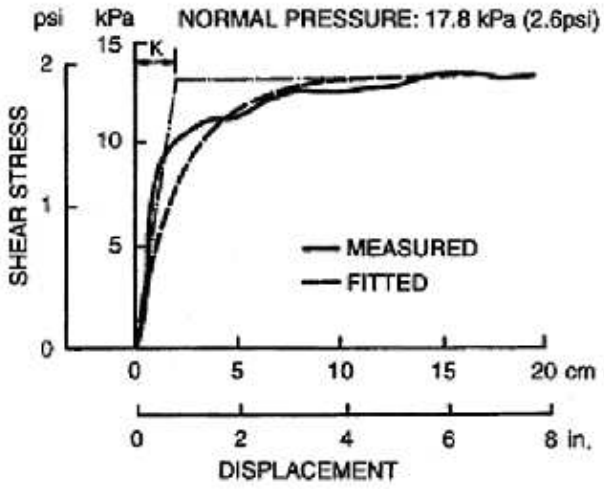

Figure 5.2: Shear stress and displacement relationship of loose sand (Wong, 2001)

Where,

τ is the shear stress (Pa),

j is the shear displacement (m),

c is the internal cohesion of the soil (Pa),

ϕ is the angle of internal friction of the soil (deg), and

K is defined as the shear deformation modulus (m).

The shear deformation modulus, K, is considered as "a measure of the magnitude of the shear displacement that develops the maximum shear strength" (Wong, 2001). The value of K for sandy terrain varies from $1\,\mathrm{cm}$ to $2.5\,\mathrm{cm}$. For undisturbed, fresh snow, the value of K varies from $2.5\,\mathrm{cm}$ to $5\,\mathrm{cm}$ (Wong, 2001). As quoted below, Wong (2001) proposed several methods to determine K:

> "Its value may be represented by the distance between the vertical axis and the point of intersection of the straight line tangent to the shear curve at the origin and the horizontal line representing the maximum shear stress τ_{max}. The slope

of the shear curve at the origin can be obtained by differentiating τ with respect to j in Equation 5.6:

$$\frac{d\tau}{dj}|_{j=0} = \frac{\tau_{max}}{K} e^{-j/K}|_{j=0} = \frac{\tau_{max}}{K} \tag{5.7}$$

Thus, the value of K can be determined from the slope of the shear curve at the origin and τ_{max}.

The value of K may also be taken as $1/3$ of the shear displacement where the shear stress τ is $95\,\%$ of the maximum shear stress τ_{max}.

The optimum value of K that minimizes the overall error in fitting Equation 5.6 to the measured curve may be obtained from the following equation, based on the weighted least squares principle:

$$K = -\frac{\sum(1 - \frac{\tau}{\tau_{max}})^2 j^2}{\sum(1 - \frac{\tau}{\tau_{max}})^2 j[\ln(1 - \frac{\tau}{\tau_{max}})]} \tag{5.8}$$

Where τ_{max} is the measured maximum shear stress, and τ and j are the measured shear stress and the corresponding shear displacement, respectively."

The second type of strain-stress relationship is for organic terrain with vegetation cover on the surface and saturated peat beneath it. The relationship of strain-stress of this type of terrain is different from the type of loose sand. Figure 5.3 shows the features of this type of strain-stress relationship. Rather than maintain the maximum value after the shear stress reaches the maximum shear strength, the stress will decrease with a further increase of the soil displacement.

Equation 5.9 characterizes this type of shearing behavior (Wong, 2001). Different from the shear deformation modulus, K_w is the shear displacement where the maximum shear

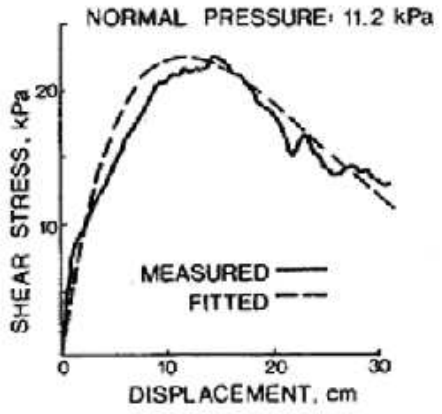

Figure 5.3: Shear stress and displacement relationship of organic terrain (Wong, 2001)

stress occurs. The value of K_w varies from $14.4\,\mathrm{cm}$ to $16.4\,\mathrm{cm}$ for various types of organic terrain tested in the Petawawa area, Ontario, Canada (Wong, 2001).

$$\tau = \tau_{max} \cdot (j/K_w) \cdot e^{1-j/Kw} \tag{5.9}$$

The third type of strain-stress relationships is for compact sand, silt, loam, and frozen snow. Figure 5.4 characterizes the strain-stress relationship of this type of terrain. The shear stress approaches a constant residue after it reaches the maximum shear strength. Wong (2001) proposed the following model, shown in Equation 5.10, to characterize this behavior.

$$\begin{aligned} \tau &= \tau_{max} \cdot K_r(1 + [\frac{1}{K_r(1-1/e)} - 1] \cdot e^{1-j/Kw}) \cdot \\ &\quad \cdot [1 - e^{-j/Kw}] \end{aligned} \tag{5.10}$$

Where,

K_r is the ratio of the residual shear stress to the maximum shear stress (unitless), and

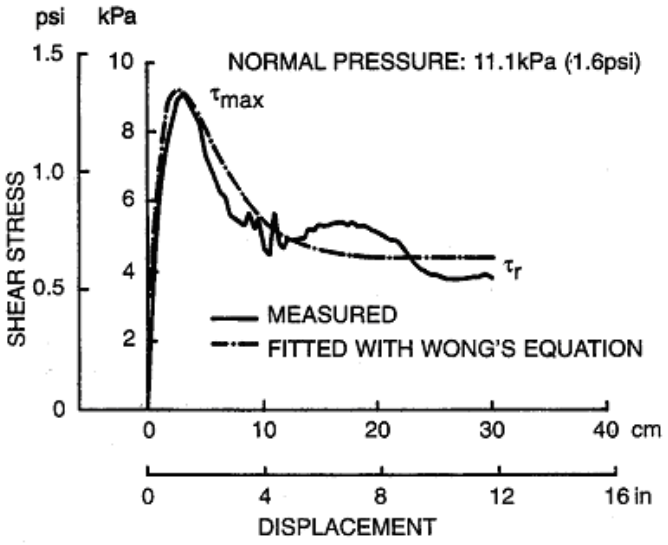

Figure 5.4: Shear stress-displacement relationship of silt (Wong, 2001)

K_w is the shear displacement where the maximum shear stress occurs (m).

5.2.2 Development of impact severity model for tracked vehicles

Soil impact severity is mainly attributed to the shear displacement of the vegetation cover and the surface soil caused by lateral movement of pads. It is noted that the more the shear stress produced in the terrain surface, the more the soil shear displacement, and the more the impact severity. The vegetation cover and the surface soil will be completely scraped away when the shear stress reaches the maximum shear strength of the soil. Any further shear displacement beyond this point will cause $100\,\%$ impact severity.

As in the wheeled vehicle model, the impact severity is a ratio of the actual shear stress to the maximum shear strength. It is expected that the curve that defines the relationship between impact severity and shear displacement is similar as the curve shown in Figure 5.2. After the shear stress reaches the maximum shear strength, even though the shear strength may decrease for some types of terrain, the impact severity will maintain $100\,\%$ with any further increase of the soil displacement. Based on this reasoning, the impact severity can be expressed as a function of the shear displacement, shown in Equation 5.11.

$$IS = \frac{\tau}{\tau_{max}} = (1 - e^{-j/K}) \times 100\% \tag{5.11}$$

Where,

τ is the shear stress (Pa),

τ_{max} is the shear strength (Pa),

j is the shear displacement (m), and

K is the shear deformation modulus (m).

The value of K depends on the type of soils and a variety of soil conditions. Based on experimental data collected, Table 5.1 lists the K values of some soil types under different

Table 5.1: K values of different soil types (developed from Wong (2001))

Soil type and conditions	K value (cm)
Firm sandy terrain	1
Loose sand	2.5
Clay at maximum compaction	0.6
Undisturbed, fresh snow	2.5-5
Organic terrain with a mat of living vegetation on the surface and saturated peat beneath it	4.8-5.5*
Compact sand, silt, loam, and frozen snow	0.9-2.4*

conditions (Wong, 2001). The value of K is $0.6\,\mathrm{cm}$ for clay at maximum compaction. The value of K increases from $1\,\mathrm{cm}$ for firm sandy terrain to $2.5\,\mathrm{cm}$ for loose sand. The value of K varies from $4.8\,\mathrm{cm}$ to $5.5\,\mathrm{cm}$ for the organic terrain that Wong (2001) studied. For compact sand, silt and loam, and frozen snow, the value of K is approximately $0.9\,\mathrm{cm}$ to $2.4\,\mathrm{cm}$.

When the vehicle moves straight, there is no lateral movement of the tracks, thus Equation 5.11 indicates $0\,\%$ impact severity. The model needs to be modified in order to account for the effect of compaction and slippage produced by the vehicle moving straight. The normal stress in the soil caused by the compaction of the tracks produces imprint type impact.

Based on field observation, the impact severity caused by compaction and slippage was approximately $20\,\%$ as discussed in future sections. Equation 5.12 shows that a constant, -0.223, is added to the original equation to reflect the impact severity under no-lateral-shear-stress condition. The modified equation will generate an impact severity of $20\,\%$ when there is only compaction and slippage caused by the vehicle.

$$IS = (1 - e^{-j/K - 0.223}) \times 100\% \tag{5.12}$$

*Derived from K_w using $K = \frac{1}{3}K_w$. K_w is the shear displacement where the maximum shear stress occurs. The value of K_w varies from $14.4\,\mathrm{cm}$ to $16.4\,\mathrm{cm}$ for organic terrain, and is about $2.7\,\mathrm{cm}$ to $7.1\,\mathrm{cm}$ for compact sand, silt, loam, and frozen snow (Wong, 2001).

Chapter 6

Field test methodology

In order to validate the influence of velocity and turning radius on terrain impact, field tests of a variety of wheeled and tracked vehicles were conducted. This chapter described the detailed procedure of the field tests. The vehicle tracking method was discussed. Techniques of the measurement of terrain impact were introduced. Pre-analysis of field data was explained.

6.1 The vehicle tracking system

For the validation of the relationship between terrain impact and the vehicle dynamic properties, the use of differential Global Positioning System (DGPS) was required to provide accurate vehicle positions and dynamic properties. The vehicle tracking system used in this study consists of an Ominstar DGPS receiver, a pocket PC, a data storage card, a battery, and a case. These individual units are described in detail in the following sections.

Figure 6.1: The DGPS Ag 114 receiver

6.1.1 DGPS receiver

The Trimble DGPS Ag 132 and Ag 114 receivers were used in the vehicle tracking system. Both receivers are able to calculate sub-meter positions in real-time by utilizing either free public or subscription-based differential correction services. The Trimble DGPS Ag 132 receiver has a control panel for the setup of its parameters. Its standard features include the internal L-Band satellite differential receiver, the internal MSK Beacon receiver, and the internal WAAS/EGNOS receiver. The satellite-based OmniStar differential correction services were subscribed for this receiver. The Wide Area Augmentation System (WAAS) differential corrections can also be used. The Trimble DGPS Ag 114, shown in Figure 6.1, was also used in the study. The features of the Ag 114 receiver are similar as the Ag 132 receiver except that the Ag 114 receiver does not provide a control panel. Table 6.1 lists the performance characteristics of the Ag 132 receiver.

Table 6.1: Performance characteristics of Ag 132 receiver (http://www.trimble.com)

Feature	Description
General	12 channel L1 code phase receiver
Maximum update rate	10 Hz
Static position accuracy(year-to-year)	submeter differential
Dynamic pass-to-pass accuracy	4 in.-12 in. (10 cm-30 cm) RMS 15 min
Time to first fix	Less than 30 s, typical
NMEA messages	GGA, GGL, GRS, GST, VTG, RMC, GSA, GSV, XTE, ZDA, ALM, MSS
Communication Ports	2 RS-232, 2 J1939 (CAN 2.0B)

6.1.2 Data recorder

The Compaq IPAQ 3150 was selected to record the GPS data for the tracking system. Figure 6.2 shows the Compaq IPAQ 3150 pocket PC. Table 6.2 lists the features of the pocket PC. A $128\,\mathrm{MB}$ Compact Flash card was used for data storage in the pocket PC. The data recorder is able to inform the user that GPS data is recording from the scrolling National Marine Electronics Association (NMEA) strings on the screen at the beginning of the tracking activity.

6.1.3 Power supply, power accessories, and protective case

A 12-volt direct current power supply was used in the vehicle tracking system. The Odyssey rechargeable Drycell 12-volt battery (P/N PC625), shown in Figure 6.3, can provide 12 volts for 17 amp-hours, which corresponds to approximately 4 days of power consumption of the GPS receiver and pocket PC. The Odyssey rechargeable Drycell $12\,\mathrm{V}$ DC battery is of starved electrolyte dry cell electrochemical design and can be air-freighted. Simple 12-volt automotive plugs are used to attach the battery to the GPS receiver and pocket PC.

The Pelican Protector 1300 Case, shown in Figure 6.4, was used to house the vehicle tracking equipment. The case is watertight and shock proof. A hole was drilled in the side of the case for the GPS receiver cable. The size of the case ($10.75'' \times 9.75'' \times 7''$ outside, $9.5'' \times 7.5'' \times 6.5''$ inside) fits the pocket PC, one battery, all wire connections, and the power accessories. The weight of the case with one battery and all equipment is approximately $15\,\mathrm{lbs}$. The protective case makes the vehicle tracking system to be easily moved and secured in a vehicle.

Figure 6.2: Compaq IPAQ 3150 pocket PC

Table 6.2: Features of the Compaq IPAQ 3150 (Compaq Computer Corporation)

Feature	Description
Processor	Intel StrongARM SA-110 206 MHz
OS	Windows CE 3.0
Memory	16 MB RAM, 24 MB ROM
Display	16-gray backlit semi-transmissive LCD
Digitizer	Pressure-sensitive panel
Storage	Internal RAM or via PC Card or CF card expansion jacket
Size	$3.25'' \times 5.1'' \times 0.62''$
Weight	6.4 oz
Power	Li-Polymer (up to 10 hours)
Interface	Serial, Irda 1.1, expansion
Options	CF card and PC Card expansion sleeves

Figure 6.3: The Odyssey P/N PC625 battery

Figure 6.4: The Pelican Protector 1300 Case

6.1.4 The placement of GPS unit

The ideal position to set the GPS receiver is near the geometric center of the tested vehicle. Any deviation from the geometric center leads to error of positioning the vehicle based on GPS data. Usually the GPS receiver can be set directly on top of a steel structure of the vehicle using the magnet bottom of the receiver. If the test vehicle did not have a steel structure at the appropriate position, a steel plate that was taped on a non-steel structure would be able to provide a magnet mounting for the receiver. Some extension tools could also be used to create mounting positions for GPS receivers. Figure 6.5 shows that a short folding ladder was secured in the loading bay of a High Mobility Multi-purpose Wheeled Vehicle (HMMWV) to provide a mounting position for the GPS receiver.

Other devices of the GPS unit, such as the handheld PC, battery, cables, and power splitters should be placed securely at any convenient position. Any collision of these items during the maneuver of the test vehicle could cause a break of the cable connection and lose the tracking data. Figure 6.6 illustrates that the handheld PC, batteries, and all the extra cables were set in a solid protective case. The case was secured using duct tape. The AgGPS 132 receiver has a control panel unit. Figure 6.7 shows that the control panel was secured inside the driving cab using bungee cords.

6.1.5 Setup of the GPS receiver

The Trimble AgGPS 132 receiver has a control panel for the setup of its parameters. For an AgGPS 114 receiver, the PC based AgRemote software helps to set up the receiver parameters (Trimble, 2004). The AgRemote has a GUI interface whose menu looks similar as the physical control panel.

There were a variety of receiver parameters needed to be set up. Baud rate was usually set to be 9600. The frequency for GPS data output was set to $1\,\mathrm{Hz}$, which means that the datalogger recorded GPS signals every second.

Figure 6.5: Mounting GPS receivers on a HMMWV

Figure 6.6: Arrangement of data recording devices

Figure 6.7: Mounting of the control panel

Table 6.3: Frequencies of the Omnistar Satellite Beacon (MHz)

Zone	Frequency
Eastern USA	1556.825
Central USA	1554.497
Western USA	(1) 1551.429; (2) 1551.489

Omnistar differential function should be enabled. There are three zones in North America: the west coast, the middle, and the east coast. The frequencies of the Omnistar Satellite Beacon are listed in Table 6.3. An appropriate frequency needed to be selected according to the location of the test site.

6.1.6 Setup of the data recorder

A datalogging software, VxHpc, was used on the handheld PC to communicate with the GPS receiver. VxHpc is a high performance serial and Telnet communications software for Windows CE and Pocket PC (http://www.cam.com/vxhpc.html). The software recorded the data to a newly created file on a memory card inserted in the handheld PC.

Serial communication using RS-232 was used to connect the GPS receiver and the handheld PC. The communication requires specifying four parameters, the baud rate of the transmission, the number of data bits encoding a character, the optional parity bit, and the number of stop bits. The options of these parameters are listed in Table 6.4. Each character transmitted from the GPS receiver to the handheld PC is packaged in a character frame that consists the following parts in sequence: a single start bit, the data bits, the optional parity bit, and the stop bit or bits. A start bit is physically a voltage transition from negative to positive; its duration in seconds is the reciprocal of the baud rate. For example, the setting of 9600-8-N-1 represents 9600-baud, 8 data bits, no parity bit, and 1 stop bits. All of the four parameters of both the GPS receiver and the handheld PC should share the same values.

Table 6.4: Serial communication parameters

Parameter	Settings
Baud rates	300, 600, 1200, 1800, 2400, 3600, 4800, 7200, 9600, 14 400, 19 200, 28 800, 38 400, or 57 600
Data bits	5, 6, 7, or 8
Parity	odd, even, or none
Stop bits	1, 1.5, or 2

A null modem, or a RS-232 Pin 2/3 reverser, was used to reverse pin 2 (transmit data) and pin 3 (receive data) in the serial connection cable between the GPS receiver and the handheld PC. A gender changer was used to allow the female end of the null modem to connect to the female end of the serial port of the handheld PC.

6.2 Operation of the test vehicles in the field

Plots of relatively flat area were used for terrain impact study. The areas were large enough for off-road vehicles to conduct several maneuvers in spiral pattern. A relatively uniform vegetation cover was advisable for the comparison of terrain impact.

The test vehicles were operated to run from going straight to turning sharper and sharper, so that the track of the vehicles would form a spiral pattern. This maneuver pattern resulted a wide range of turning radii. The vehicle speed was maintained stable during each spiral. The drivers were instructed to operate the vehicles in a high speed and a low speed typically used during training activities, in order to disclose the influence of different speeds on terrain impact. Actual speed of the vehicles was derived from the GPS data recorded at 1 Hz. Figures of the GPS tracking data of some of the test vehicles were listed in the Appendix.

6.3 Data collection in the field

6.3.1 Introduction of data collection in the field

After the terrain was trafficked, the measurement of terrain impact and soil properties was conducted within 24 hours. The terrain impact data included disturbed width and impact severity. Field properties such as the shearing strength, soil penetration resistance, and soil moisture content were determined. Soil samples were also collected in the field.

6.3.2 A field data collection unit using backpack GPS and ArcPad software

The hardware of the data collection unit included a GPS receiver (Trimble AgGPS 132 or AgGPS 114), batteries, and a handheld PC. The GPS receiver provided the position and dynamic properties of the vehicle during the field tests. The field measurement data was input to the handheld PC using the ArcPad software. The handheld PC also logged the GPS coordinates simultaneously.

The ArcPad software was developed by ESRI, which produced a series of GIS and mapping software. Arcpad provided a data collection solution in the field with the real-time positioning ability using a GPS receiver. Data entry forms were customized in ArcPad using ArcPad Application Builder. The interface and data entry forms were created to adapt the field mission of this study. The ArcPad customization was performed on a desktop PC before the deployment on the handheld PC. Figures 6.8 and 6.9 show the customized forms used in ArcPad.

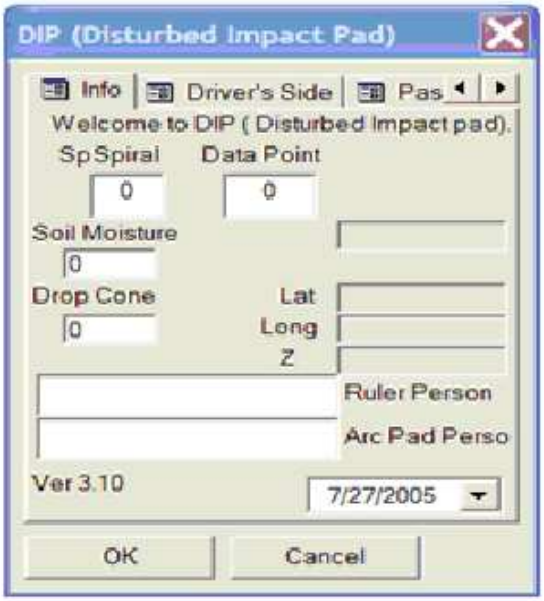

Figure 6.8: The information page of the customized forms

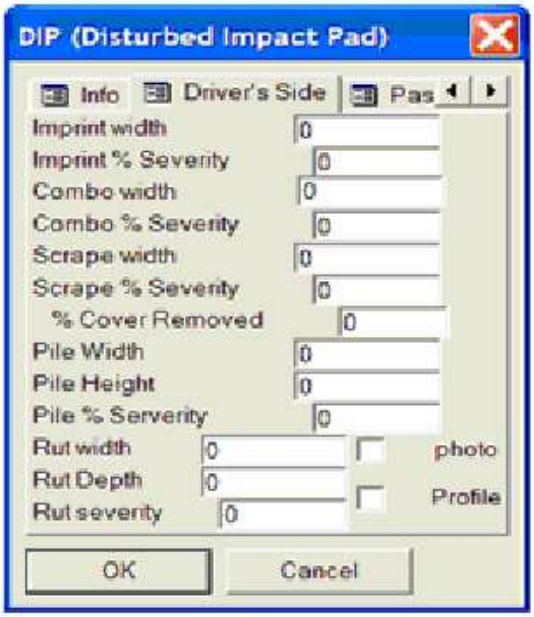

Figure 6.9: The data collection entry page of the customized forms

6.3.3 Measurement of terrain impact

Two people were required for the measurement of terrain impact. One person was in charge of the measurement. The other person with the backpack GPS unit and data logger, standing in the middle of the inside track and the outside track, was in charge of recording the measurement data to the handheld PC. Figure 6.10 shows the collection of terrain impact data in the field.

Terrain impact was measured along both the inside track and the outside track. Usually ten to twenty points along one spiral were measured. The measurement points had intervals of $2\,\mathrm{m}$ to $3\,\mathrm{m}$, and covered all the range of the turning radii of the spiral. When the terrain impact was measured, GPS coordinates of the center between the inside track and the outside track were recorded. Figure 6.11 shows the GPS points of measurement along one spiral.

Disturbed width was measured perpendicular to the direction of travel of the vehicle in the field using a ruler. The disturbed width could be classified into four types: the imprint width, the scrape width, the combination width, and the pile width. Imprint impacts were compressed soil and vegetation in the vehicle track. Scrape impacts were soil and vegetation that had been stripped away from the vehicle track. Combination impacts showed characteristics of both the imprint type and scrape type impacts. The pile of sheared soil was formed on the edge of tracks sometimes when the vehicle made sharp turns at a relatively high speed. Figure 6.12 shows the measurement of impact width. Besides impact width, rut depth and pile height were also measured using rulers in the field.

In this study, the measurement of impact severity was based on an initial impact severity guideline. The guideline scales impact severity from $0\,\%$ to $100\,\%$ (Haugen, 2002). Table 6.5 shows the initial impact severity guidelines.

Figure 6.10: Collection of terrain impact data in the field

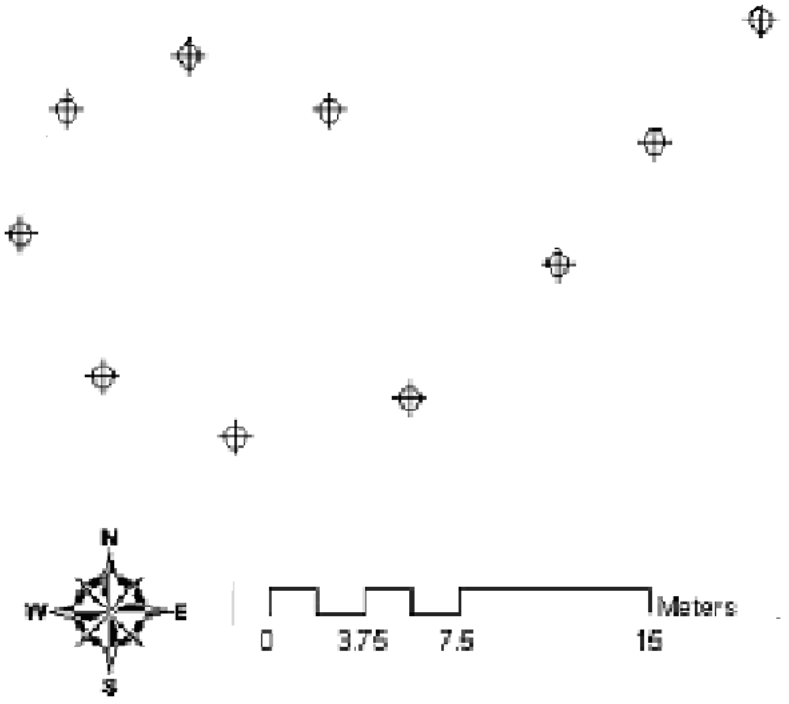

Figure 6.11: Measurement points along one spiral

Figure 6.12: Disturbed width measurement

Table 6.5: Initial impact severity guidelines (Haugen, 2002)

Impact Severity (%)	Guidelines
0	No visible disturbance as compared to surrounding vegetation/area
10	Laying down of vegetation; will recover quickly; few, if any, broken stems; no evidence of vegetative shearing; very difficult to see impact after a few days
20	Some broken stalks/plants; no possibility of these stalks/plants straightening or returning to initial conditions within a few days; visible for a couple of months after impact; visible soil disturbance, possibly exposing bare soil, due to vehicle weight
40	Obvious depressed soil and vegetation with slight vegetation removal and significant vegetative damage; crushing, shearing and slight removal of vegetation likely; piling on track edge evident due to turning radius and weight of vehicle; movement of plants/soil towards the edge of vehicle track without completely shearing plant at roots; some bare soil exposed
60	About one third of vegetation still present and intact on the track; significant amount of bare soil exposed; larger piling of vegetation on edge of track due to shearing motion of the vehicle, fully removing species from the track; some of the pile has overturned, exposing some roots to air suggesting vegetation may not recover
80	Few vegetative species still intact on vehicle path; some vegetation has been sheared down to just above roots, so very little of plant remains above ground, while other vegetation has been fully sheared, removing roots; piling of vegetation and soil on the edge of the path; pile is completely overturned, exposing roots, suggesting the majority of species will not recover.
100	Complete removal of vegetation and soil; shearing action of vehicle has left vehicle track bare; sheared vegetation and soil are piled on edge of track.

6.3.4 Measurement of field properties

Field properties were measured in situ. A torsional sheargraph measured the soil shear strength in the middle of each spiral. A cone penetrometer measured the soil penetration resistance when applicable (ASAE, 1999). A time-domain reflectometer (TDR, shown in Figure 6.13) measured the soil moisture content. The soil moisture content could also be measured in the laboratory if soil samples were collected in the field. The measurement of drop cone (shown in Figure 6.14) was also conducted (Godwin et al., 1991). A small can of soil sample was collected from the upper $10\,\mathrm{cm}$ soil surface in the center of each spiral. Laboratory analysis of these samples revealed the details of soil texture.

6.4 Pretreatment of the field data

6.4.1 Transformation of the GPS data from the geographic coordinates to UTM

The unit of GPS data is in decimal degrees of the coordinate system, WGS 84 (World Geodetic System). The calculation of turning radius requires projecting the WGS 84 coordinate system into the Universal Transverse Mercator (UTM) system which provided units of meters for position. The Geographic Calculator software developed by Blue Marble Geographics performed this transformation (http://www.bluemarblegeo.com). Table 6.6 lists the parameters of the UTM system.

6.4.2 Turning radius calculation

The vehicle dynamic parameters, such as speed and turning radius, can be derived from the GPS tracking data. Speed can be directly read from the NMEA string of GPS data. Haugen (2002) developed a three-point method to calculate turning radius from GPS data.

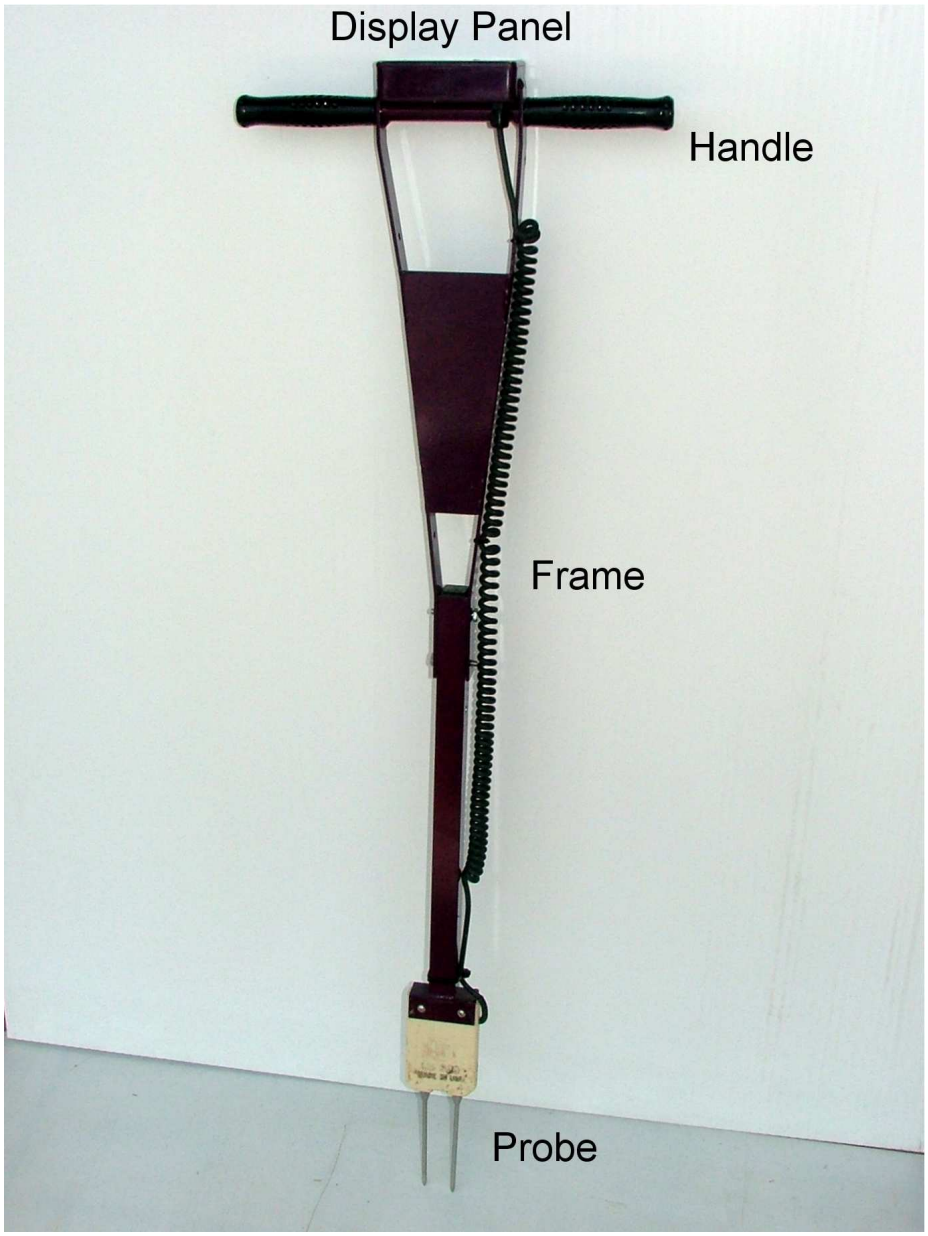

Figure 6.13: Time-domain reflectometer

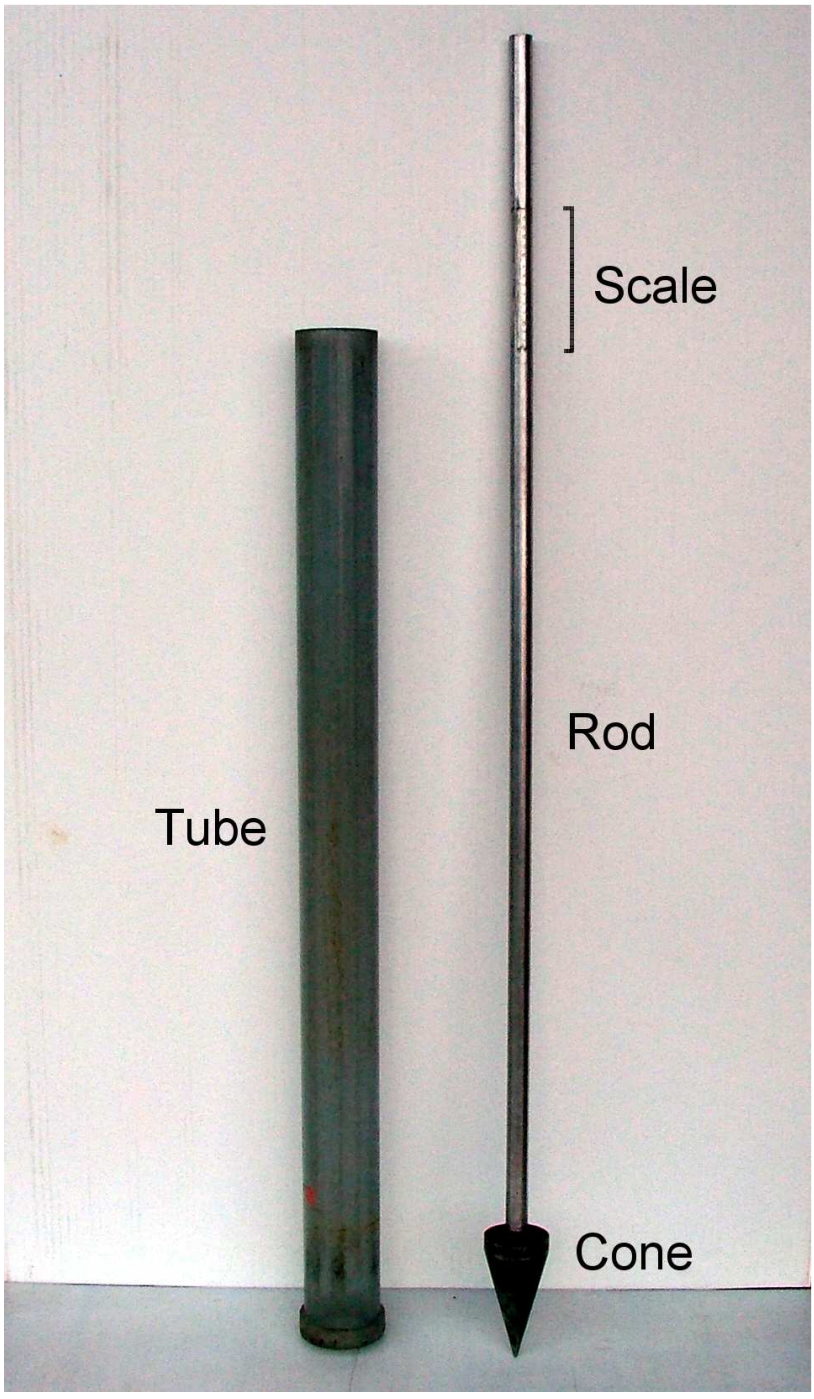

Figure 6.14: Drop cone

Table 6.6: Parameters of the UTM system

Feature	Description
Datum	North American Datum 1983
Spheroid	GRS 1980
False Easting	$500\,000$
False Northing	0
Units	Meters

The three point method was found to be able to accurately calculate the turning radius (Haugen, 2002).

The three-point method utilizes the current position, the position immediately before the current position, and the position immediately after the current position to calculate turning radius. Figure 6.15 shows a diagram that is used in the three-point method for turning radius calculation (Haugen, 2002). The current position, the position immediately before the current position, and the position immediately after the current position are labeled B, A, and C respectively. Point 1 and point 2 are the bisect points of line $\overline{AB}$ and line $\overline{BC}$. Line $\overline{1-I}$ and line $\overline{2-I}$ are the perpendicular bisect lines of line $\overline{AB}$ and $\overline{BC}$. The center of turn is point I, which is the intersect of line $\overline{1-I}$ and line $\overline{2-I}$. The turning radius is the distance from the current GPS position, point B, to the point I.

Using subscript E and N as indication of Easting longitude and Northing latitude, the coordinates of points A, B, C, and I can be written as (A_E, A_N), (B_E, B_N), (C_E, C_N), and (I_E, I_N). Equations 6.1 and 6.2 calculate the slopes of lines $\overline{AB}$ and $\overline{BC}$ in the plane using Easting longitude and Northing latitude as coordinate axes.

$$m_{AB} = \frac{B_N - A_N}{B_E - A_E} \tag{6.1}$$

$$m_{BC} = \frac{C_N - B_N}{C_E - B_E} \tag{6.2}$$

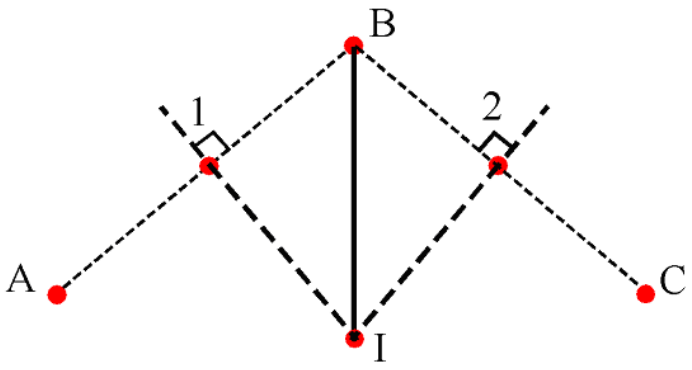

Figure 6.15: The three-point method of turning radius calculation (Haugen, 2002)

Equations 6.3 and 6.4 calculate the slopes of lines $\overline{1-I}$ and $\overline{2-I}$ that are perpendicular to lines $\overline{AB}$ and $\overline{BC}$ respectively.

$$m_{1-I} = \frac{-1}{m_{AB}} \tag{6.3}$$

$$m_{1-I} = \frac{-1}{m_{BC}} \tag{6.4}$$

Equations 6.5 and 6.6 calculate the intercepts of lines $\overline{1-I}$ and $\overline{2-I}$ on the Northing latitude axis.

$$b_{1-I} = \frac{1}{2}(A_N + B_N) - m_{1-I} \cdot \frac{1}{2}(A_E + B_E) \tag{6.5}$$

$$b_{2-I} = \frac{1}{2}(B_N + C_N) - m_{2-I} \cdot \frac{1}{2}(B_E + C_E) \tag{6.6}$$

Since the point I is the intersection of lines $\overline{1-I}$ and $\overline{2-I}$, in other words, the point is on both line $\overline{1-I}$ and line $\overline{2-I}$, I_E and I_N can be expressed in both Equation 6.7 (the equation of line $\overline{1-I}$) and Equation 6.8 (the equation of line $\overline{2-I}$). The coordinates of the center of turn, (I_E, I_N), can be calculated by solving the Equations 6.7 and 6.8.

$$I_N = m_{1-I} \cdot I_E + b_{1-I} \tag{6.7}$$

$$I_N = m_{2-I} \cdot I_E + b_{2-I} \tag{6.8}$$

By far, both the coordinates of the current GPS point (B_E, B_N) and the center of turn (I_E, I_N) were calculated. Equation 6.9 determines the turning radius (TR), which is the distance from point B and point I.

$$TR = \sqrt{(I_N - B_N)^2 + (I_E - B_E)^2} \tag{6.9}$$

6.4.3 Joining of the vehicle tracking data and the field measurement data using ArcGIS

The data collected in the field using the ArcPad software does not contain the vehicle dynamic information, such as turning radius and speed. The vehicle dynamic information was derived from the GPS tracking data. The measurement data of terrain impact were then combined with the GPS tracking data, which contained the turning radius and vehicle speed information. This combined result contained both the information of terrain impact and vehicle dynamic parameters.

The Join function in the ArcGIS software provides a solution to combine two separate data sets (http://www.esri.com/software/arcgis). Figure 6.16 shows both the data of the points of vehicle tracking and the points of the measurement of terrain impact along one spiral. Both of these data sets need to be input to ArcGIS as separate layers first. The GPS tracking data with the information of turning radius and speed was joined to the measurement data of terrain impact. The joining result contained both the information of terrain impact and vehicle dynamic parameters.

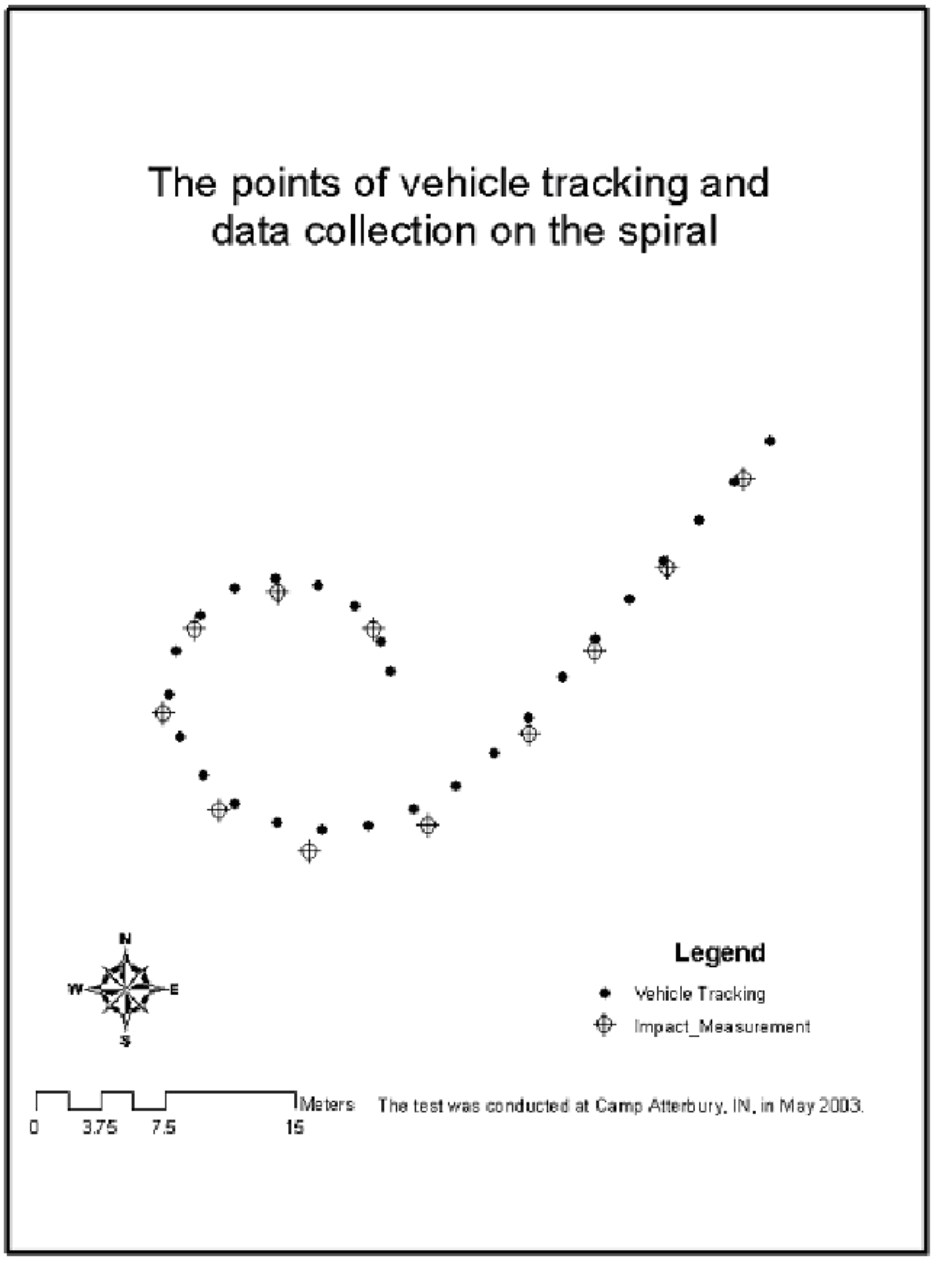

Figure 6.16: The points of vehicle tracking and measurement of terrain impact along one spiral

Chapter 7

Field test results

7.1 Disturbed width of wheeled vehicle

7.1.1 Eight-wheeled vehicle

The eight-wheeled test vehicle was a Light Armored Vehicle (LAV), shown in Figure 7.1. The LAV was a diesel fueled eight-wheeled vehicle with a maximum curb weight of $13\,930\,\mathrm{kg}$. The tires were Michelin 12R20 XML TL 149J with an inflation pressure of $480\,\mathrm{kPa}$. Other information of the vehicle is shown in Table 7.1.

A field test of the LAV was conducted at Fort Lewis, WA, in June 2002 to validate the models of wheeled vehicles developed in Chapter 4. A plot of flat area with relatively uniform vegetation cover was selected for the terrain impact test. The area was large enough for the LAV to conduct several maneuvers in a spiral pattern. Five spirals were conducted for each of the low speed and the high speed settings.

The test field of Fort Lewis was classified as sandy loam (Lombardi, 2004). A particle size analysis found that the soil was $67\,\%$ sand, $29\,\%$ silt, and $4\,\%$ clay (Simmons, 2004). The test field was covered with sod-forming grassy vegetation (Simmons, 2004). The most common type of grass at the site was Colonial (Lombardi, 2004).

Figure 7.1: The eight-wheeled light armored vehicle (LAV)

Table 7.1: Information of the test vehicle, LAV

Tread width (B)	Tire-terrain contact Width (TW)	Wheel Base (L)	Front Wheel Gap (b_1)	Rear Wheel Gap (b_2)	Cornering Stiffness ($C_{\alpha r}$)	Normal Load (W_r)
$2.37\,\mathrm{m}$	$0.21\,\mathrm{m}$	$3.86\,\mathrm{m}$	$1.22\,\mathrm{m}$	$1.22\,\mathrm{m}$	$1.1 \times 10^5\,\mathrm{N/rad}$	$17\,064\,\mathrm{N}$

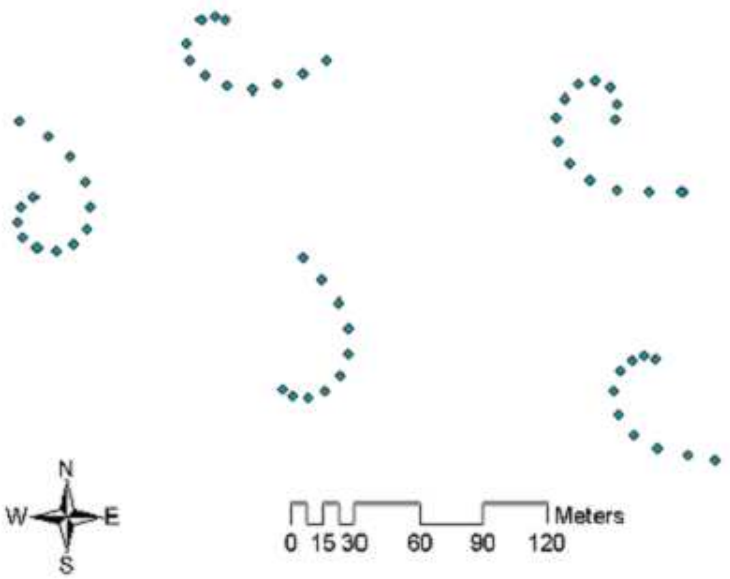

Figure 7.2: GPS tracking points of the high-speed spirals

The disturbed width was measured approximately fifteen points along each spiral using a ruler. At each point of measurement, a backpack GPS unit was used to record the coordinates of Latitude and Longitude. Figure 7.2 shows the GPS points collected along the high-speed spirals while conducting measurement.

A group of data of 40 measurement points with similar speed value was sampled from the raw field data. The average speed value of the sampled data was $3.7\,\mathrm{m/s}$ with a standard deviation of $0.5\,\mathrm{m/s}$. By using the disturbed width model equations developed in Chapter 4, the relationship between turning radius and disturbed width of the LAV is shown in Figure 7.3. Both the field data and the theoretical model show that the disturbed width increases as turning radius decreases. The disturbed width increases more sharply at a smaller turning radius until it reaches $0.84\,\mathrm{m}$. The leveling off of disturbed width is due to the complete separation of the treads. Measured values of DW above $0.84\,\mathrm{m}$ may be caused by vehicle sliding or skidding during the turn. The average percent error of the prediction is $19.5\,\%$ with a standard deviation of $18.3\,\%$.

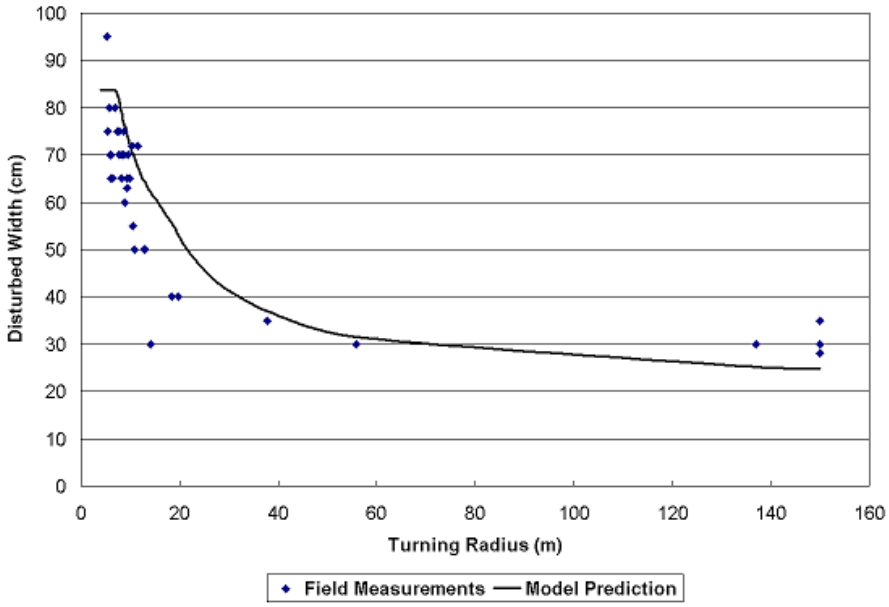

Figure 7.3: LAV field data and theoretical prediction curve

7.1.2 Four-wheeled vehicle

A field test of the four-wheeled vehicle was conducted at Yuma Proving Ground (YPG), AZ in March 2003. of YPG, AZ was without vegetation cover. The soil samples of the test field were analyzed in the Soil, Water and Plant Testing Laboratory at Colorado State University. The analysis of the soil samples showed that the soil composed of sand, moisture, silt, and clay at percentages of $94\,\%$, $0.27\,\%$, $4\,\%$, and $2\,\%$, respectively. Since the test site was sand field without vegetation cover, the field data was only used to test the disturbed width model.

The four-wheeled test vehicle was an M1097 High Mobility Multipurpose Wheeled Vehicle (HMMWV), shown in Figure 7.4. The tires used in the test were Dick Cepek F-C Kevlar $38/15.50 \times 16.5$ LRC. Table 7.2 shows the information of the test vehicle. The test procedure of the HMMWV was discussed in Chapter 6, and was similar as the LAV discussed in section 7.1.1.

A group of data of 19 measurement points with similar speed value was sampled from the raw field data. The average speed value of the test vehicle was $5.0\,\mathrm{m/s}$ with a standard deviation of 0.6 m/s. The turning radius at the total separation point of the front tire track and the rear tire track was calculated by Equation 4.24 as 15.5 meters. By using the model equations, the relationship between the turning radius and the disturbed width (in meters) of the inside tires of the M1097 HMMWV is given by

$$\begin{aligned} DW &= \frac{3.3}{\sin(\frac{3.3}{TR-0.895})} \cdot [\cos(\frac{0.908}{TR}) - \cos(\frac{0.908}{TR} - \frac{3.3}{TR-0.895})] + \\ &\quad + 0.295 \qquad \text{if } TR \geq 10.25\,\mathrm{m} \end{aligned} \tag{7.1}$$

$$DW = 0.59 \qquad \text{if } TR < 10.25\,\mathrm{m} \tag{7.2}$$

Figure 7.4: The high mobility multipurpose wheeled vehicle (HMMWV)

Table 7.2: Information of the test vehicle, M1097

Tread width (B)	Tire-terrain contact Width (TW)	Wheel Base (L)	Cornering Stiffness ($C_{\alpha r}$)	Normal Load (W_r)
$1.79\,\mathrm{m}$	$0.295\,\mathrm{m}$	$3.30\,\mathrm{m}$	$3.8 \times 10^4\,\mathrm{N/rad}$	$6.9 \times 10^3\,\mathrm{N}$

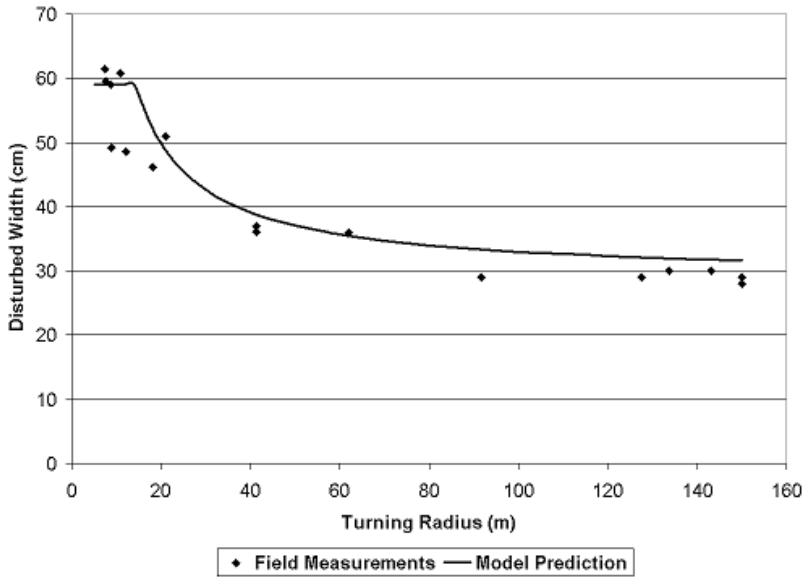

Figure 7.5: M1097 field data and theoretical prediction curve

Figure 7.5 shows the relationship between the disturbed width of the inner side tires and the turning radius of the wheeled vehicle M1097. Both field data and the theoretical model show that the disturbed width increases as turning radius decreases. The disturbed width increased more sharply at a smaller turning radius. The prediction curve shows that the disturbed width reaches $0.59\,\mathrm{m}$ if the turning radius is smaller than 15.5 meters. The leveling off of disturbed width is due to the complete separation of the front tread and the rear tread. The average percentage error of the prediction value is $8.6\,\%$ with a standard deviation of $6.2\,\%$.

7.2 Impact severity of wheeled vehicle

Impact severity data were also collected from the field test of LAV at Fort Lewis, WA. The measurement of impact severity was based on an impact severity guideline using a scale from $0\,\%$ to $100\,\%$ (Haugen, 2002). A torsional sheargraph instrument was used to

measure the soil strength of the test site (Cohron, 1962). A linear regression of the soil strength data measured across the field showed that the soil had an internal cohesion of $32.59\,\mathrm{kPa}$, and a friction angle of $26.6°$. The Coulomb equation can be written as

$$\tau = 32.59 + 0.501\sigma \tag{7.3}$$

Where,

τ is the soil shearing stress (kPa), and

σ is the soil normal stress (kPa).

The mass of the LAV was $13\,930\,\mathrm{kg}$. The tire-terrain contact area of the vehicle was calculated as $0.631\,\mathrm{m}^2$ from Equation 4.35. Substituting these parameters to Equation 4.34, the critical velocity was determined by Equation 7.4. The centrifugal force of the vehicle operating at critical velocity reaches the maximum lateral force that the soil can provide at its given shear strength.

$$V_{cri} = \sqrt{\frac{TR \cdot (32.59 \times 10^3 \cdot 0.631 + 0.501 \cdot 13930 \times 9.8)}{13930}} = 2.53\sqrt{R} \tag{7.4}$$

Figure 7.6 shows the velocity data of both the high speed and low speed operations of the test vehicle (LAV) compared to its calculated critical velocity at different turning radii. The critical velocity decreases with decreasing turning radius. Corresponding to the high-speed spirals and low-speed spirals during field test, the measured velocity data were separated into two groups. Since the data of the high-speed operation were closer to the critical velocity curve than the low-speed operation, the high speed operation would cause a higher impact severity.

Because the vehicle slowed during the turn, the velocity data in Figure 7.6 were not uniform. In order to analyze the relationship between impact severity and turning radius at

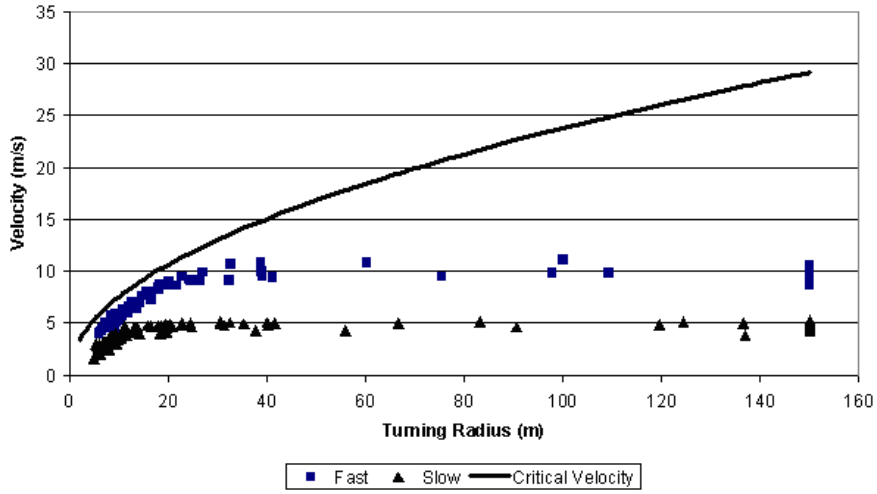

Figure 7.6: Velocity data compared to the critical velocity at different turning radius of the LAV

a constant velocity, a group of data was sampled to have an average velocity of $9.6\,\mathrm{m/s}$. The velocity values of the chosen data have a standard deviation of $0.7\,\mathrm{m/s}$. Figure 7.7 shows both the measured impact severity and the predicted impact severity in relationship with turning radius.

The predicted impact severity value was derived from Equation 4.36 and Equation 4.37. Equation 7.5 generates a zero impact severity when turning radius is infinity. Based on field observation, the average imprint impact was $10\,\%$ when the vehicle was moving straight. In order to compensate for the imprint impact, the impact severity was assigned a value of $10\,\%$ when the calculation result is smaller than $10\,\%$. The assigned value of impact severity could change with soil conditions and/or vegetation type.

$$IS_{theory} = (\frac{9.6}{2.53\sqrt{R}})^2 \times 100 = \frac{1440}{R} \tag{7.5}$$

Figure 7.7 shows both the field data of 79 measurement points and the theoretical impact severity curve. As the turning radius deceases, the impact severity increases. The average percentage error between the predicted impact severity value and the measured value is $48.5\,\%$ with a standard deviation of $55.5\,\%$.

Another group of data was sampled with an average speed value of $5.4\,\mathrm{m/s}$. The standard deviation is $0.35\,\mathrm{m/s}$. The theoretical impact severity was calculated by Equation 7.6. Again, the impact severity was assigned a value of $10\,\%$ when the calculation result was smaller than $10\,\%$.

$$IS_{theory} = (\frac{5.4}{2.53\sqrt{R}})^2 \times 100 = \frac{456}{R} \tag{7.6}$$

Figure 7.8 shows both the impact severity data of 50 measurement points and the predicted impact severity in relationship with turning radius. The average percentage error

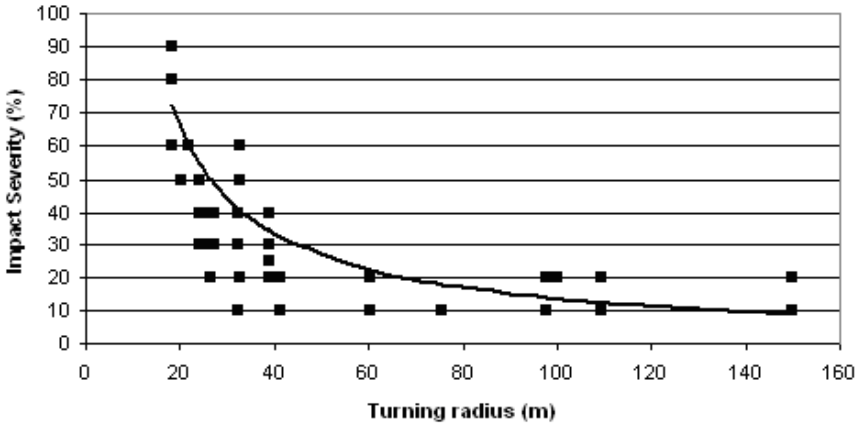

Figure 7.7: Measurement and prediction of the impact severity of the LAV at high speed

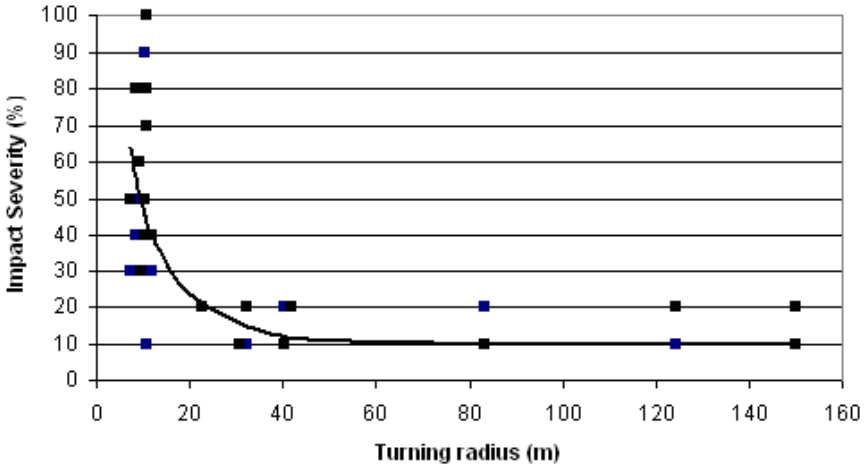

Figure 7.8: Measurement and prediction of the impact severity of the LAV at low speed

between the predicted impact severity value and the measured value is $34.2\,\%$ with a standard deviation of $55.8\,\%$. Comparing with Figure 7.7, it is noted that at a lower speed, severe impact severity can only be caused at smaller turning radii. Both field data and the theoretical prediction curve show that impact severity increases as turning radius decreases.

Theoretical IS models were successfully applied to the 8-wheeled vehicle, LAV, at both low and high speed settings. At a small turning radius, the test vehicle operating at the high speed setting ($9.6\,\mathrm{m/s}$) caused more severe impact than at the low speed setting ($5.4\,\mathrm{m/s}$). However, the influence of speed on terrain impact diminishes as the turning radius increases. The worst scenario happens when the wheeled vehicle negotiates a sharp turn at a high speed.

7.3 Disturbed width of tracked vehicle

A field test of the M1A1 combat tank was conducted at Yakima Training Center (YTC) in Yakima, WA in June 2002. YTC is located in central Washington about 11 km north of the city of Yakima (Haugen, 2002). Dominant native plants are bluebunch wheatgrass

Table 7.3: Yakima Training Center study site description (Haugen, 2002)

Feature	Description
Dominant Vegetation	Bluebunch Wheatgrass
Soil Type	Silt loam
Site Elevation	$915\,\mathrm{m}$
Precipitation Zone	$23\,\mathrm{cm}$-$30\,\mathrm{cm}$
Drop Cone	$7.4\,\mathrm{cm}$

and big sagebrush; cheatgrass is an important invader (Goran et al., 1983). The soil type was classified as silt loam composed by $55\,\%$-$56\,\%$ sand, $34\,\%$-$35\,\%$ silt, and $10\,\%$ clay. Table 7.3 shows the description of the study site of YTC.

Both turning radius and speed of the vehicle influence the magnitude of the disturbed width. In order to validate the influence of these vehicle dynamic properties on the disturbed width, the M1A1 was operated in a spiral pattern similar to that described in section 7.1.1: starting from driving straight, the vehicle turned sharper and sharper, so that the tread of the vehicle appeared as a spiral on the terrain. The vehicle was operated at both low speed (4 spirals) and high speed (4 spirals).

Equation 5.5 of the disturbed width model requires an estimate of the coefficient of soil lateral resistance, μ_l, of the study site. The coefficient of lateral resistance is defined as the ratio of lateral soil resistance force acting on the track to the normal load of the track when shearing a block of soil. The coefficient of soil lateral resistance can be calculated by Equation 7.7

$$\mu_l = \frac{F}{N} \tag{7.7}$$

Where, F is the lateral resistance force of soil acting on the track (N), and

N is the normal load of the track (N).

Equation 7.8 calculates F.

$$F = \tau \cdot A = (c + \sigma \cdot \tan\phi) \cdot A \tag{7.8}$$

Where, τ is the shearing stress of the soil (Pa),

A is the track-terrain contact area (m^2),

c is the internal cohesion of the soil (Pa),

σ is the normal stress (Pa), and

ϕ is the angle of internal friction of the soil (deg).

Then,

$$\mu_l = \frac{F}{N} = \frac{(c + \sigma \cdot \tan\phi) \cdot A}{N} \tag{7.9}$$

Since $N = \sigma \cdot A$, Equation 7.9 can be simplified as

$$\mu_l = \frac{c}{\sigma} + \tan\phi \tag{7.10}$$

In this study, c and ϕ of the study site was approximated using a torsional sheargraph instrument (Cohron, 1962). The sheargraph relates the shearing strength to the normal stress. Figure 7.9 shows the torsional sheargraph measurement data and its linear regression curve. The slope of the curve approximated a $\tan\phi$ of 0.64. The intercept of the curve on the shear strength axis indicated that the internal cohesion of the soil, c, was $2.00\,\mathrm{psi}$.

The combat tank M1A1, shown in Figure 7.10, was a tracked armored tank with a combat weight of $1.26 \times 10^5\,\mathrm{lbs}$. The vehicle had an overall length of $355.6\,\mathrm{in.}$, a height of $113.6\,\mathrm{in.}$, and a width of $144\,\mathrm{in.}$. The track length and track width were measured as $179.1\,\mathrm{in.}$ ($4.55\,\mathrm{m}$) and $24.8\,\mathrm{in.}$ ($0.63\,\mathrm{m}$), respectively. The ground pressure, σ can be calculated as $14.2\,\mathrm{psi}$.

The parameters of $\tan\phi$, c, and σ are 0.64, $2.00\,\mathrm{psi}$, and $14.2\,\mathrm{psi}$, respectively. The coefficient of soil lateral resistance, μ_l, can be calculated by Equation 7.10 as 0.78. Sensitivity analysis of the influence of μ_l on disturbed width was studied in section 7.6.

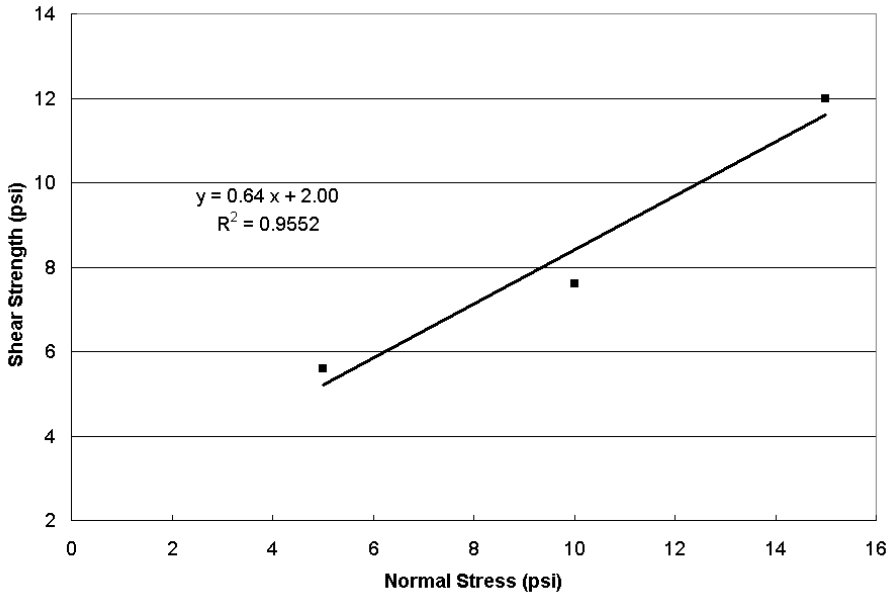

Figure 7.9: Soil shear strength and normal stress curve (Yakima)

Figure 7.10: The M1A1 combat tank

Table 7.4: Information of the M1A1 vehicle and the field

Track Length (TL)	Track Width (TW)	Tread Width (B)	Vehicle Speed (V)	Resistance coefficient (μ_l)
$4.55\,\mathrm{m}$	$0.63\,\mathrm{m}$	$2.88\,\mathrm{m}$	$3.85\,\mathrm{m/s}$	0.78

Table 7.4 shows the information of the vehicle dimensions, speed setting, and the lateral resistance coefficient of the test field. The data of 25 measurement points used for validation had an average vehicle speed of $3.85\,\mathrm{m/s}$ with a standard deviation of $0.18\,\mathrm{m/s}$. Given all these parameters, disturbed width of the M1A1 tank can be calculated by Equation 7.11, which is derived from Equation 5.5 of the theoretical model.

$$DW = \sqrt{(2.28 + \frac{2.21}{TR})^2 + (TR - 1.13)^2} - (TR - 1.76) \tag{7.11}$$

Figure 7.11 shows the relationship between disturbed width and turning radius. Both the prediction curve and the field data of 25 measurement points were shown in the figure. The average percentage error of the prediction value is $9.5\,\%$ with a standard deviation of $6.2\,\%$. Both field data and the theoretical model show that the smaller the turning radius the larger the disturbed width.

An M1A1 combat tank was also tested at Fort Riley, Kansas in October 2004. The installation is located in a semi-arid, tallgrass-prairie ecosystem (Althoff and Thien, 2005). The soil texture was classified as silt loam on uplands composed of nearly level ground and gentle slopes in broad areas (Althoff and Thien, 2005).

According to the test procedures described in Chapter 6, the M1A1 tank was operated in spiral patterns at both high speed and low speed settings. Approximately fifteen measurement points were selected in an interval of $2\,\mathrm{m}$ to $3\,\mathrm{m}$ alone each of the spirals.

Figure 7.12 shows the torsional sheargraph measurement data and its linear regression curve. The slope of the curve approximated a $\tan\phi$ of 0.73. The intercept of the curve

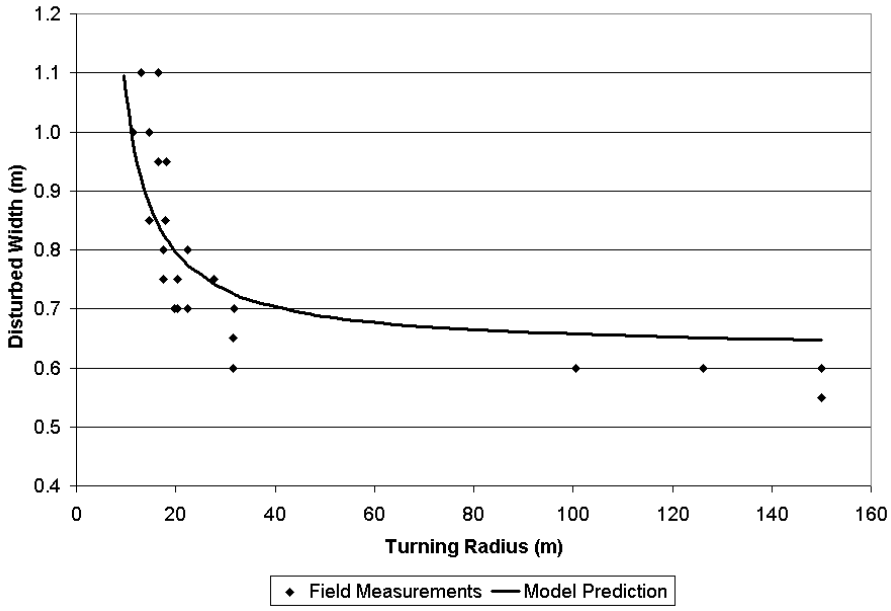

Figure 7.11: M1A1 field measurements and model prediction curve (Yakima)

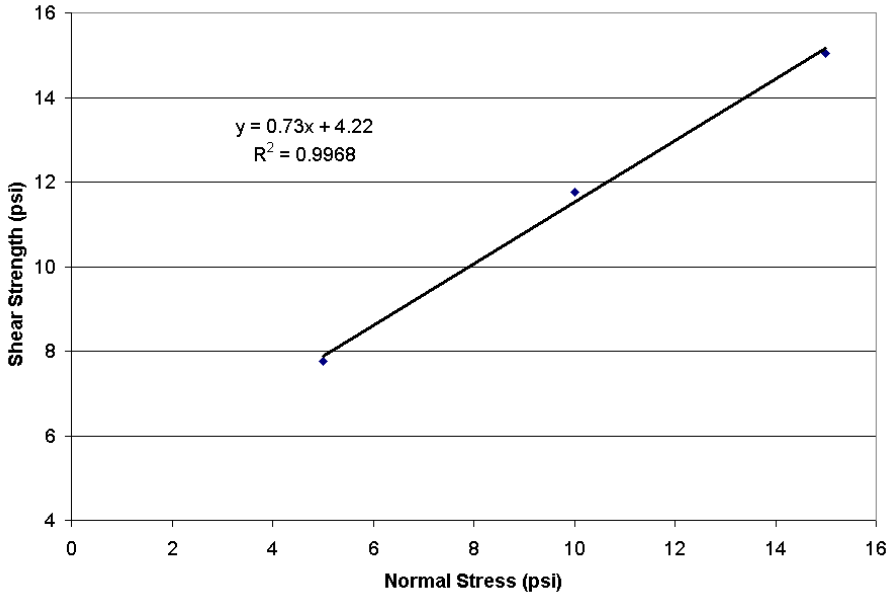

Figure 7.12: Soil shear strength and normal stress curve (Riley)

on the shear strength axis indicated that the internal cohesion of the soil, c, was $4.22\,\mathrm{psi}$. Again, the ground pressure of the M1A1 tank, σ, was $14.2\,\mathrm{psi}$. Given all these parameters, the coefficient of soil lateral resistance, μ_l, can be calculated by Equation 7.10 as 1.03.

The specifications of the vehicle were the same as the M1A1 tested at Yakima training center. The data of 26 measurement points used for validation had an average vehicle speed of $5.35\,\mathrm{m/s}$ with a standard deviation of $0.67\,\mathrm{m/s}$. Using Equation 5.5 of the theoretical disturbed width model, disturbed width of the M1A1 tank can be calculated by Equation 7.12.

$$DW = \sqrt{(2.28 + \frac{3.22}{TR})^2 + (TR - 1.13)^2} - (TR - 1.76) \tag{7.12}$$

Figure 7.13 shows the relationship between disturbed width and turning radius. The average percentage error of the prediction value is $10.0\,\%$ with a standard deviation of $9.2\,\%$. Both field data and the theoretical model show that the smaller the turning radius

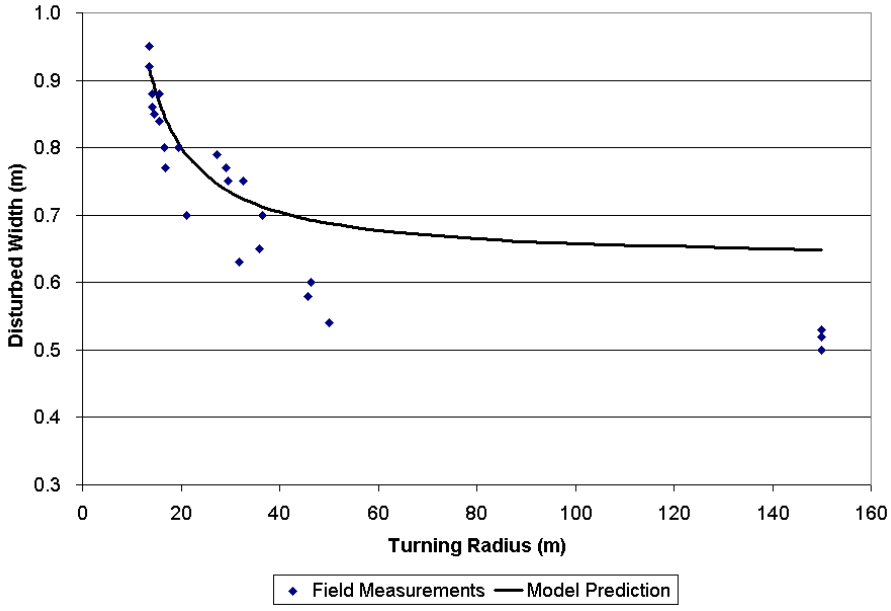

Figure 7.13: M1A1 field measurements and model prediction curve (Riley)

the larger the disturbed width. It is noted that the disturbed width measured in the field was less than the track width when the vehicle moved straight. When the vehicle made a relatively large turning or moved straight, the tracks did not have a full width contact with the soil. The contact only happened between the rubber pads and the soil, thus results larger prediction error when turning radius was large.

Another vehicle tested together with the M1A1 at Fort Riley, Kansas in October 2004 was an Armored Personal Carrier (APC) M577A2, shown in Figure 7.14. The Armored Personnel Carrier M577A2 was a tracked vehicle with a combat weight of $25\,813\,\mathrm{lbs}$. The vehicle overall length was $191\,\mathrm{in.}$, the overall height was $106.5\,\mathrm{in.}$, and the overall width was $106\,\mathrm{in.}$.

Table 7.5 shows the information of the vehicle dimensions, speed setting, and the lateral resistance coefficient of the test field. The data of 25 measurement points used for validation had an average vehicle speed of $4.33\,\mathrm{m/s}$ with a standard deviation of $0.77\,\mathrm{m/s}$. The ground pressure of the APC was $8.3\,\mathrm{psi}$; thus the coefficient of soil lateral resistance, μ_l,

Figure 7.14: The Armored Personal Carrier (APC)

Table 7.5: Information of the APC vehicle and the field

Track Length (TL)	Track Width (TW)	Tread Width (B)	Vehicle Speed (V)	Resistance coefficient (μ_l)
$2.64\,\mathrm{m}$	$0.38\,\mathrm{m}$	$2.2\,\mathrm{m}$	$4.33\,\mathrm{m/s}$	1.24

can be calculated by Equation 7.10 as 1.24. Using Equation 5.5 of the theoretical model, disturbed width of the APC can be calculated by Equation 7.13.

$$DW = \sqrt{(1.32 + \frac{1.04}{TR})^2 + (TR - 1.01)^2} - (TR - 1.29) \tag{7.13}$$

Figure 7.15 shows the relationship between disturbed width and turning radius. The average percentage error of the prediction value is $27.3\,\%$ with a standard deviation of $12.0\,\%$. Again, the disturbed width measured in the field was less than the track width when the vehicle moved straight. Because the contact only happened between the rubber pads and the soil, larger prediction error was produced when turning radius was large.

Another field test was conducted at Camp Atterbury, Indiana, in May 2003. Camp Atterbury is located in central Indiana approximately 7 km east of Columbus. The training area encompasses about 144 square kilometers of lush vegetation including species such as common ragweed (ambrosia artemisifolia), giant ragweed (ambrosia trifida), common milkweed (asclepias syriaca), mustard (brassicaceae species), etc. (Haugen, 2002). The soil type was classified as sandy loam composed by $55\,\%$ sand, $30\,\%$ silt, and $15\,\%$ clay. Moisture content was $28\,\%$.

The test vehicle was a tracked cargo carrier, M548, shown in Figure 7.16. The gross weight of the vehicle was $28\,290\,\mathrm{lbs}$. The vehicle had an overall length of $230\,\mathrm{in.}$, an overall height of $105\,\mathrm{in.}$, and an overall width of $106\,\mathrm{in.}$.

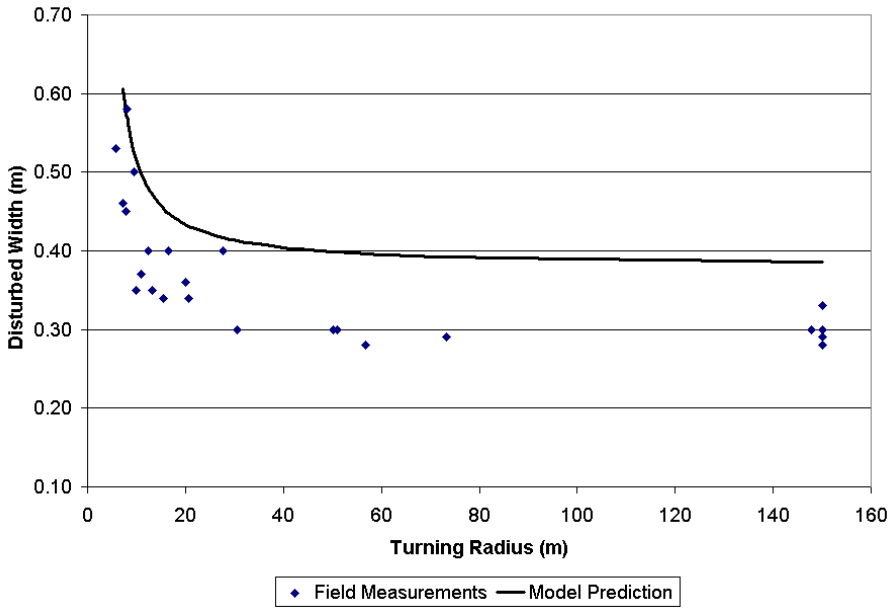

Figure 7.15: APC field measurements and model prediction curve (Riley)

Figure 7.16: The tracked cargo carrier, M548

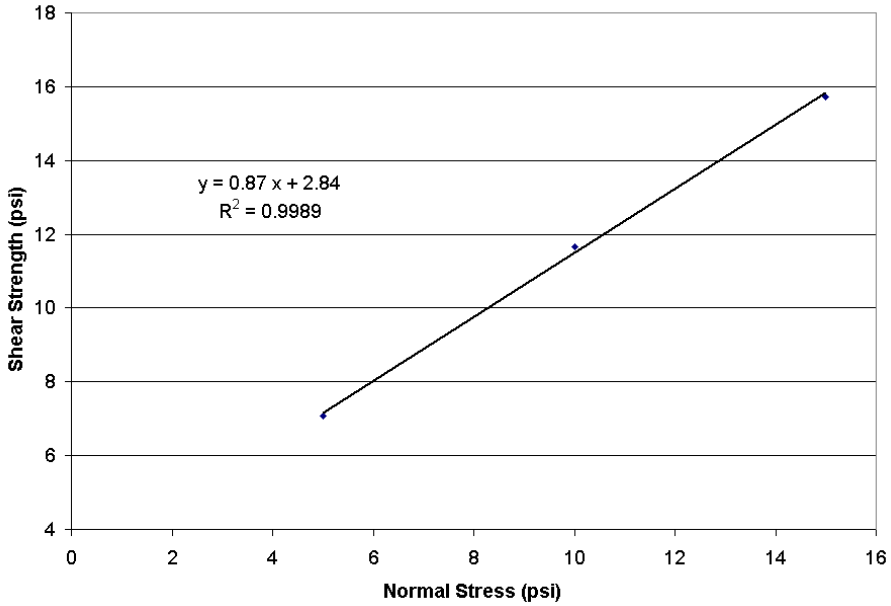

Figure 7.17: Soil shear strength and normal stress curve (Atterbury)

Figure 7.17 shows the torsional sheargraph measurement data and its linear regression curve at Camp Atterbury. The slope of the curve approximated a $\tan\phi$ of 0.87. The intercept of the curve on the shear strength axis indicated that the internal cohesion of the soil, c, was $2.84\,\mathrm{psi}$. The ground pressure of the M548 was $8.7\,\mathrm{psi}$; thus the coefficient of soil lateral resistance, μ_l, can be calculated by Equation 7.10 as 1.20. Other information of the vehicle and the field is shown in Table 7.6.

The vehicle was tested according to similar procedures described in section 7.1.1. The data of 23 measurement points used for validation had an average vehicle speed of $3.32\,\mathrm{m/s}$ with a standard deviation of $0.16\,\mathrm{m/s}$. Using the parameters given in Table 7.6, Equation 7.14 was derived from the theoretical model equation. Equation 7.14 expresses the disturbed width of the inside track of the M548 vehicle as a function of turning radius.

$$DW = \sqrt{(1.39 + \frac{0.65}{TR})^2 + (TR - 0.89)^2} - (TR - 1.27) \tag{7.14}$$

Table 7.6: Information of the M548 vehicle and the field

Track Length (TL)	Track Width (TW)	Tread Width (B)	Vehicle Speed (V)	Resistance coefficient (μ_l)
$2.77\,\mathrm{m}$	$0.38\,\mathrm{m}$	$2.16\,\mathrm{m}$	$3.32\,\mathrm{m/s}$	0.84

Figure 7.18 shows the disturbed width data of the M548 vehicle along with the theoretical prediction curve. Similar as the test results of the M1A1 vehicle, the M548 test also indicates that the smaller the turning radius, the larger the soil disturbed width. The average percentage error of the the field measurement from the model prediction is $8.5\,\%$ with a standard deviation of $7.8\,\%$. The average percentage error of the predictions of both the M1A1 model and M548 model is below $10\,\%$.

7.4 Impact severity of tracked vehicle

The study of impact severity was also conducted using the M1A1 combat tank and the Armored Personal Carrier M577A2 in the field test at Fort Riley, Kansas in October 2004. The test site was described in section 7.3. The measurement of impact severity was based on a guideline that helps to judge the impact severity on a scale of $0\,\%$ to $100\,\%$ as discussed in the previous chapter (Haugen, 2002).

According to Equation 5.12, two parameters needed to be determined prior to the application of the impact severity model. The first parameter was the lateral shear displacement, j, of the soil. When the tracked vehicle moved straight in a flat field, although slippage of the tracks existed, there was no lateral shear displacement; and the disturbed width (DW) was approximately equal to the track width (TW). When the vehicle started to make a turn, the lateral movement of the tracks laterally sheared the soil. The lateral shear displacement

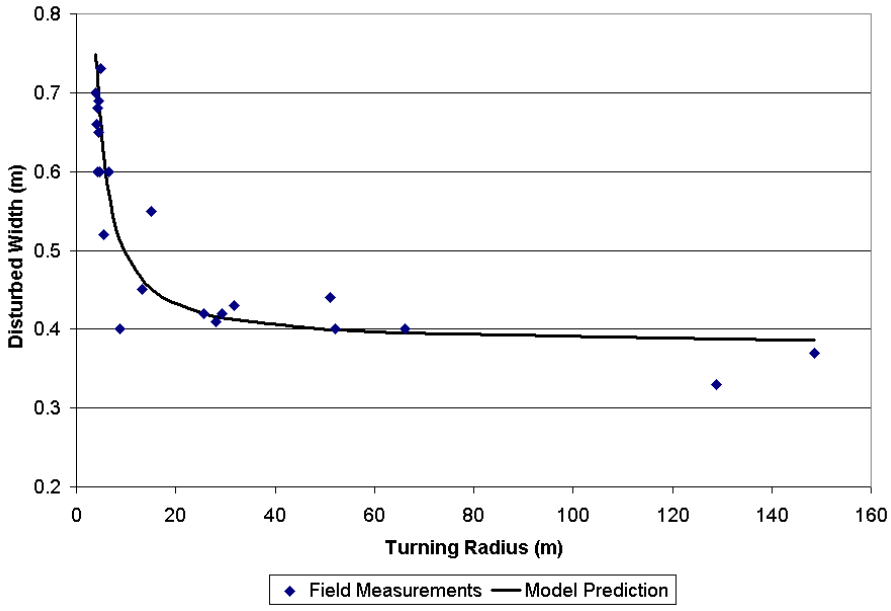

Figure 7.18: M548 field measurements and model prediction curve (Atterbury)

of the soil was equal to the difference between the disturbed width and the track width, thus the lateral shear displacement, j, can be calculated by Equation 7.15.

$$j = DW - TW \tag{7.15}$$

The second parameter to be determined was the value of the shear deformation modulus, K. Wong (2001) studied the shear deformation modulus of various terrains. Table 5.1 shows that K varies from $0.6\,\mathrm{cm}$ to $5.5\,\mathrm{cm}$ for different terrain types and soil conditions (Wong, 2001). Organic matters of the terrain influences the shear deformation modulus. Wong (2001) studied the characteristics of the shear stress-displacement relationships of various types of organic terrain tested in Petawawa area, Ontario, Canada. Based on the experimental data, the value of K varied from $4.8\,\mathrm{cm}$ to $5.5\,\mathrm{cm}$ for the organic terrain.

Kogure et al. (1982) used a shear ring test apparatus to measure the soil shear deformation modulus. Three different sizes of the shear ring was used. The shear ring is similar as the shear head of a torsional sheargraph. During measurement, the shear ring was applied a normal pressure, and was rotated 3 degrees per second. The shear ring test apparatus was able to measure the angular displacement of the shear ring as well the torque that was applied on the shear ring. The test field was excavated at a depth of $40\,\mathrm{cm}$. The water content of the soil was $40.1\,\%$. Based on the grain size distribution of the soil from the test site, the soil contained approximately $10\,\%$ sand, $60\,\%$ silt, and $30\,\%$ clay. The soil texture can be classified as silty clay loam based on the USDA soil texture triangle shown in Figure 3.1. The soil texture is very similar as that of the test site of Fort Riley, KS. The soil deformation modulus, K, obtained at the test site using the shear ring test apparatus ranged from $6.0\,\mathrm{cm}$ to $8.0\,\mathrm{cm}$ (Kogure et al., 1982).

Wong (1980) measured the soil shear deformation modulus of a natural sandy terrain using a bevameter that employed an annular shear plate. The average density of the soil sample was $1.6\,\mathrm{g/cm^3}$. The shear deformation modulus ranged from $3.0\,\mathrm{cm}$ to $4.1\,\mathrm{cm}$

for the sandy terrain with moisture content of less than $1\,\%$, and ranged from $4.0\,\mathrm{cm}$ to $4.5\,\mathrm{cm}$ for the sandy terrain with moisture content of $12\,\%$. Wong (1980) also compared his measurement with a full sized tracked vehicle (M113A1) with its tracks locked and being pulled horizontally with a winch. The value of K of the full sized vehicle test was derived from the pulling force and the corresponding shear displacement of the track. The average K value was $3.6\,\mathrm{cm}$, which supported the value of K measured by the bevameter using an annular shear plate. The value of K obtained using an annular shear plate is appropriate to predict the shearing characteristics of a full sized vehicle.

In another study, Wong et al. (1982) measured the shear characteristics of muskeg in its natural condition. Two test sites were studied. The ground of Site A was saturated. The surface of site A was almost all non-woody and fairly fragile sedge. The field was of low-trafficability, and could easily be disturbed by vehicles. Site B was relatively drier and firmer. The site was dominated by low woody and non-woody short vegetation. Moisture content of site B was $91\,\%$. The mat density was measured as $0.051\,\mathrm{g/cm^3}$. The soil shear deformation modulus of the test sites was measured using a vehicle-mounted bevameter. The value of K ranged from $3.9\,\mathrm{cm}$ to $9.8\,\mathrm{cm}$ for site A, and ranged from $3.3\,\mathrm{cm}$ to $6.5\,\mathrm{cm}$ for site B.

Literature shows that larger values of K were observed in terrains under their natural conditions than that of soil samples measured in laboratory conditions. The difference could be due to the mutation of the physical structure of the soil and the influence of the vegetation cover and its roots. Unlike the terrain in its natural conditions, the soil samples tested in laboratory usually were pure soil containing no vegetation, thus the influence of grass root was not considered.

A reasonable initial estimate of the value of K was $4\,\mathrm{cm}$ based on the soil characteristics and terrain conditions of the test site, shown in Figure 7.19. As a comparison, a smaller K value of $2\,\mathrm{cm}$ was also used to test the impact severity model. Sensitivity analysis of the shear deformation modulus, K, was conducted in section 7.6. Given the parameters of j as $DW - 63$ and K as $4\,\mathrm{cm}$ in Equation 5.12 of the theoretical model, the impact severity model is expressed as Equation 7.16. The model defines the relationship between impact severity and the disturbed width.

$$IS = (1 - e^{-(DW-63)/4-0.223}) \times 100\% \tag{7.16}$$

The original model, Equation 5.11, only considers the influence of lateral shear movement of the tracks. Certain amount of terrain impact could also be caused by a straight-moving vehicle by its compaction and longitudinal slippage. According to the initial impact severity guidelines of Table 6.5, an impact severity of $20\,\%$ was observed when the tracked vehicle (M1A1) was moving straight in the field. In order to compensate for this no-lateral-shear-stress impact, a constant, -0.223, was appended to the original impact severity equation in Chapter 5. The impact severity is assigned a value of $20\,\%$ when the calculation result is less than $20\,\%$.

Figure 7.20 shows both the curve of the impact severity model and the field data of 63 measurement points of the M1A1 tank. Average percentage error of the prediction curve is $19.7\,\%$ with a standard deviation of $23.3\,\%$. The curve with the shear deformation modulus of $4\,\mathrm{cm}$ fits the measurement data better than the curve with the shear deformation modulus of $2\,\mathrm{cm}$ whose average percentage error is $39.7\,\%$ with a standard deviation of $26.6\,\%$. An increase of the disturbed width, which means an increase of the shear displacement, causes an increase of the impact severity.

For the the Armored Personal Carrier M577A2 vehicle, the track width is $38\,\mathrm{cm}$, so the parameter of j is equal to $DW - 38$. Given K as $4\,\mathrm{cm}$ in Equation 5.12 of the theoretical

Figure 7.19: The test field at Fort Riley, KS

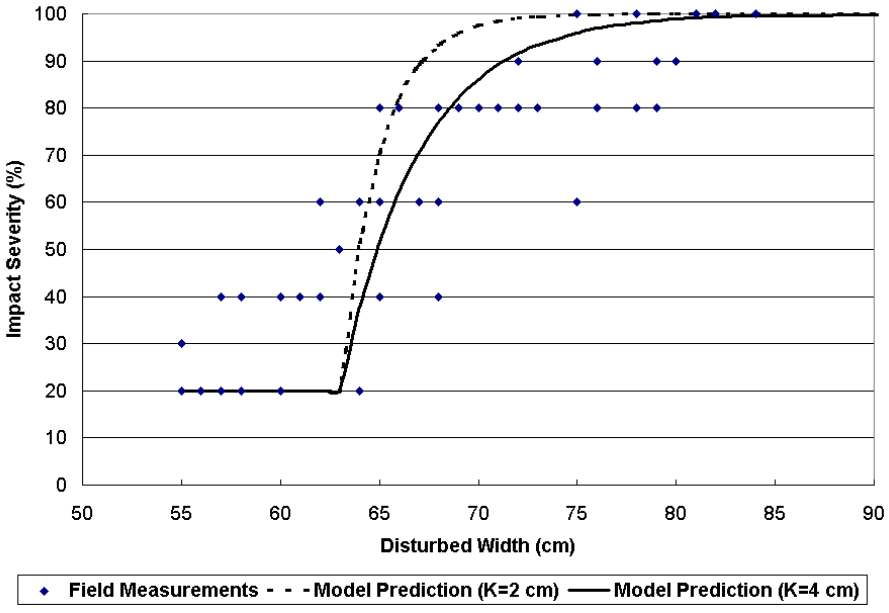

Figure 7.20: Relationship between IS and DW of the M1A1 (Fort Riley)

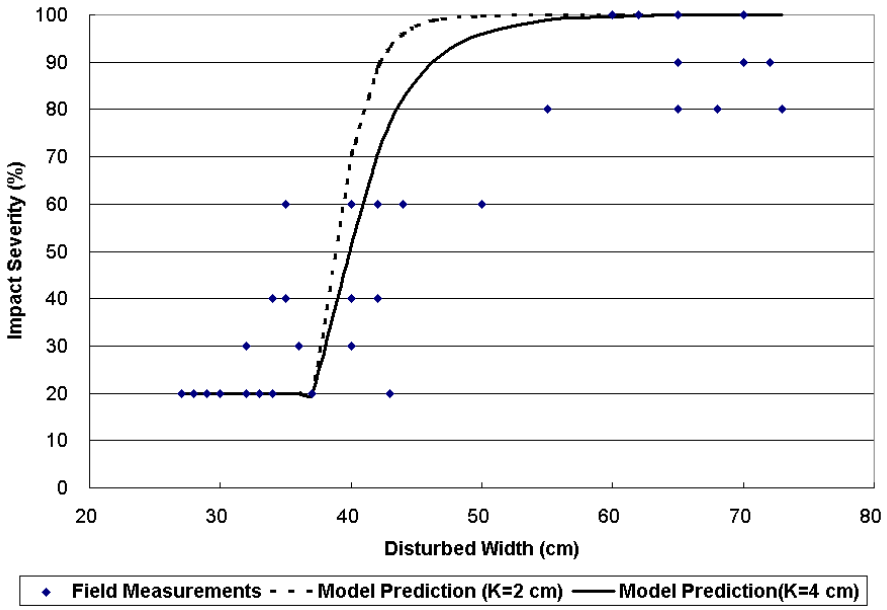

Figure 7.21: Relationship between IS and DW of the APC (Fort Riley)

model, the impact severity model of the Armored Personal Carrier is expressed as Equation 7.17. Again, the impact severity is assigned a value of $20\,\%$ when the calculation result is less than $20\,\%$.

$$IS = (1 - e^{-(DW-38)/4-0.223}) \times 100\% \tag{7.17}$$

Figure 7.21 shows both the curve of the model and the field data of 51 measurement points. Average percentage error of the curve of the shear deformation modulus of $4\,\mathrm{cm}$ is $21.4\,\%$ with a standard deviation of $44.3\,\%$. Again, it is a better fit of the measurement data than the curve with the shear deformation modulus of $2\,\mathrm{cm}$ whose average percentage error is $28.7\,\%$ with a standard deviation of $59.1\,\%$. An increase of the disturbed width causes an increase of the impact severity.

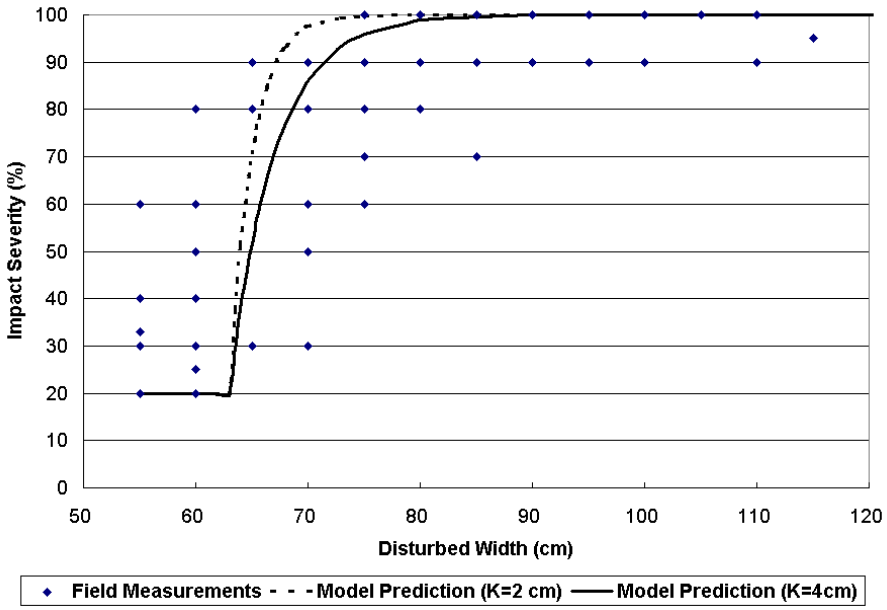

Figure 7.22: Relationship between IS and DW of the M1A1 (YTC)

Another field test of impact severity of the M1A1 tank was conducted at Yakima Training Center (YTC), WA. The test site, test procedure and vehicle were discussed in section 7.3 for the disturbed width test. Figure 7.22 shows both the curve of the theoretical model and the field data of 107 measurement points. Average percentage error of the prediction curves are $25.0\,\%$ with a standard deviation of $28.0\,\%$ for a shear deformation modulus of $4\,\mathrm{cm}$, and $27.3\,\%$ with a standard deviation of $32.9\,\%$ for a shear deformation modulus of $2\,\mathrm{cm}$. The curve with the shear deformation modulus of $4\,\mathrm{cm}$ has a better fit of the measurement data. The impact severity increases with the increase of disturbed width.

The impact severity can also be directly determined by turning radius. Equation 7.11 is able to calculate disturbed width using turning radius as input. Since impact severity is determined by disturbed width in Equation 7.16, the combination of Equations 7.11 and 7.16 defines the relationship between impact severity and turning radius. For example, Figure 7.23 shows the relationship of impact severity and turning radius for the M1A1 tank

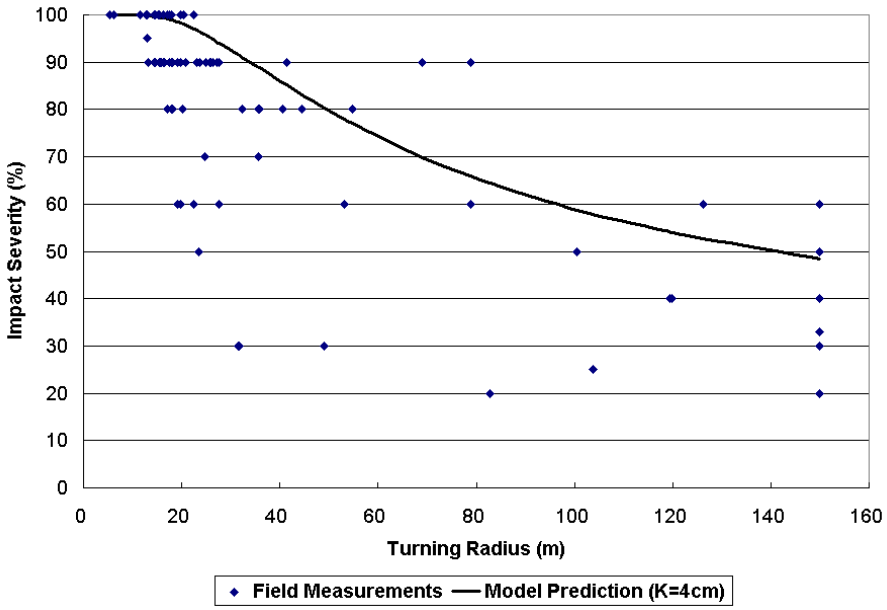

Figure 7.23: Relationship between IS and TR of the M1A1 (YTC)

test at YTC. Average percentage error of the prediction curve is $28.1\,\%$ with a standard deviation of $47.7\,\%$. The impact severity increases with the decrease of the turning radius.

7.5 Summary of the test results

Field tests of terrain impact of both wheeled vehicles and tracked vehicles were conducted in different test sites. Due to the complicated test conditions, a certain amount of variability existed in the field data. However, the terrain impact models fit the data trends.

Table 7.7 is a summary of the tests and percentage errors of the predictions of the wheeled vehicles. The average percentage errors of the disturbed width model for the LAV and HMMWV were $19.5\,\%$ and $8.6\,\%$, respectively. The average percentage errors of the impact severity model of the eight-wheeled LAV were less than $48.5\,\%$ and $34.2\,\%$ for the high speed test and the low speed test, respectively.

Table 7.7: Wheeled vehicle test summary and percentage errors of the predictions

	LAV (Lewis)	HMMWV (Yuma)
DW (Stdev)	$19.5\,\%$ ($18.3\,\%$)	$8.6\,\%$ ($6.2\,\%$)
IS (Stdev)	$48.5\,\%$ ($55.5\,\%$) (High speed) $34.2\,\%$ ($47.8\,\%$) (Low speed)	N/A

Table 7.8: Tracked vehicle test summary and percentage errors of the predictions

	M1A1 (YTC)	M1A1 (Riley)	APC (Riley)	M548 (Atterbury)
DW (Stdev)	$9.5\,\%$ ($6.0\,\%$)	$10.0\,\%$ ($9.2\,\%$)	$27.3\,\%$ ($12.0\,\%$)	$8.5\,\%$ ($7.8\,\%$)
IS (Stdev)	$25.0\,\%$ ($28.0\,\%$)	$19.7\,\%$ ($23.3\,\%$)	$21.4\,\%$ ($44.3\,\%$)	N/A

Table 7.8 is a summary of the tests and percentage errors of the predictions of the tracked vehicles. The average percentage errors of the disturbed width model for the M1A1, M577, and the M548 were $10.0\,\%$, $27.3\,\%$, and $8.5\,\%$, respectively. The average percentage errors of the impact severity model of the tracked vehicles were less than $25.0\,\%$.

7.6 Sensitivity analysis

Configurations of the training vehicles may change. There are certain amount of variability in the field conditions. Any change of these parameters and/or inputs of the models could influence the magnitude of the output. Sensitivity analysis helps users of the models to understand the patterns of such influences. This section studies the sensitivity of vehicle conditions (cornering stiffness of tires, speed, track length, and track width) and soil conditions (lateral resistance coefficient and shear deformation modulus) on the disturbed width and impact severity of off-road vehicles.

7.6.1 Sensitivity of DW to cornering stiffness of tires for wheeled vehicle

Figure 7.24 shows the effect of cornering stiffness of tires on disturbed width of wheeled vehicles. The disturbed width of the M1097 HMMWV was calculated at cornering stiffness of tires at $20\,\mathrm{kN/rad}$, $38\,\mathrm{kN/rad}$, and $80\,\mathrm{kN/rad}$, respectively. The disturbed width increases as cornering stiffness increases. The influence of cornering stiffness becomes more obvious as the turning radius decreases. However, the influence vanishes after the separation of the front tire tread from the the rear tire tread.

7.6.2 Sensitivity of IS to speed for wheeled vehicle

Figure 7.25 shows the effect of speed on impact severity of wheeled vehicles. The impact severity of the LAV was calculated at vehicle speed at $5.4\,\mathrm{m/s}$, $7.0\,\mathrm{m/s}$, and $9.6\,\mathrm{m/s}$, respectively. The impact severity increases as vehicle speed increases. However, the influence of speed decreases as the turning radius increases. In the speed range shown in the figure, it is hard to observe any influence of vehicle speed on the impact severity if the turning radius is more than $140\,\mathrm{m}$.

7.6.3 Sensitivity of DW to speed for tracked vehicle

Figure 7.26 shows the effect of vehicle speed on disturbed width. The disturbed width of the M1A1 vehicle was calculated at speed settings of $1\,\mathrm{m/s}$, $4\,\mathrm{m/s}$, and $8\,\mathrm{m/s}$, respectively. The disturbed width is sensitive to vehicle speed when the turning radius is small. An increase of speed will cause a significant increase of disturbed width at a smaller turning radius. However, the effect of speed diminishes when the turning radius increases.

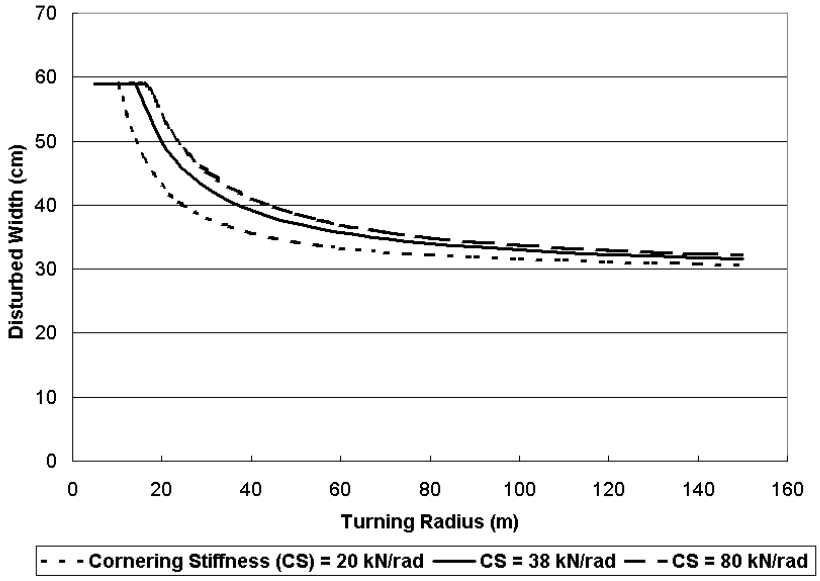

Figure 7.24: Model sensitivity to cornering stiffness of tires

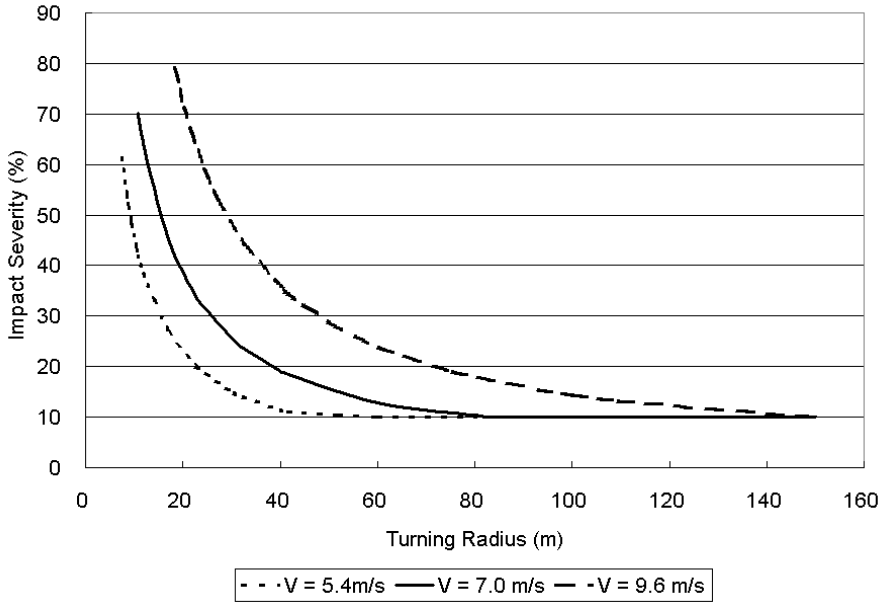

Figure 7.25: Model sensitivity to speed for wheeled vehicle

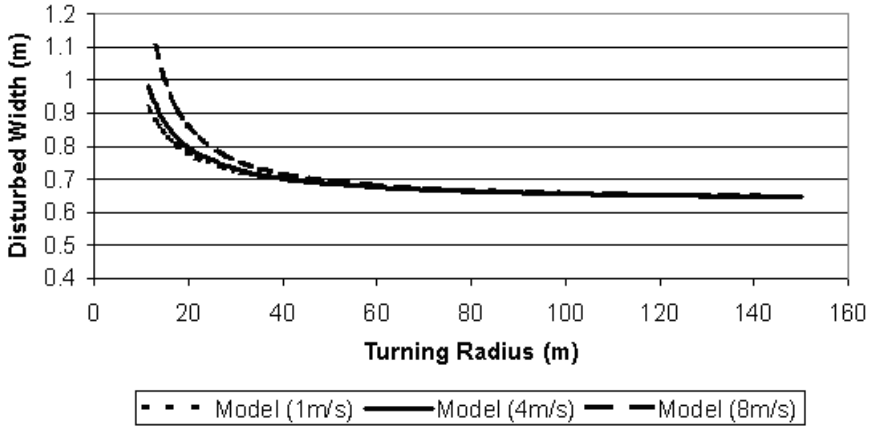

Figure 7.26: Model sensitivity to speed for tracked vehicle

7.6.4 Sensitivity of DW to track length for tracked vehicle

Figure 7.27 shows the effect of track length on disturbed width of the M1A1 tank. The sensitivity of disturbed width to track length is similar as the sensitivity to vehicle speed. The disturbed width is much more sensitive to track length at smaller turning radius. An increase of track length will cause an obvious increase of disturbed width at a smaller turning radius. This influence diminishes as the turning radius increases.

7.6.5 Sensitivity of DW to track width for tracked vehicle

Figure 7.28 shows the effect of track width on disturbed width of the M1A1. Contrary to track length, the influence of track width on disturbed width is equivalent at different turning radii. An increase of track width will have a similar increase of disturbed width at a lower turning radius as at a higher turning radius.

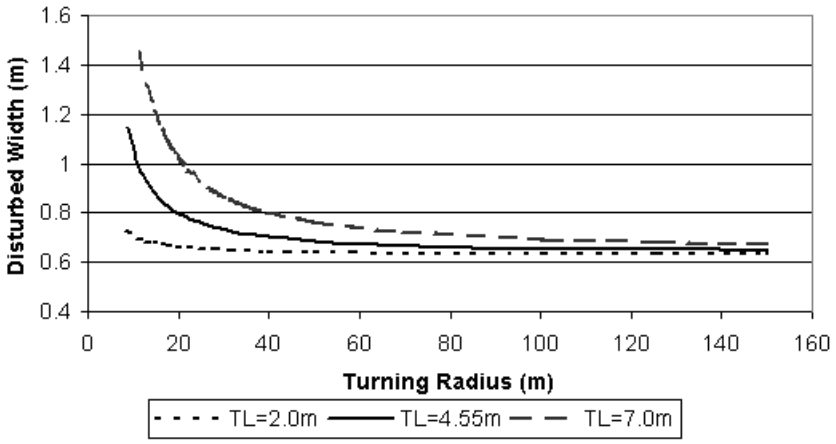

Figure 7.27: Model sensitivity to track length

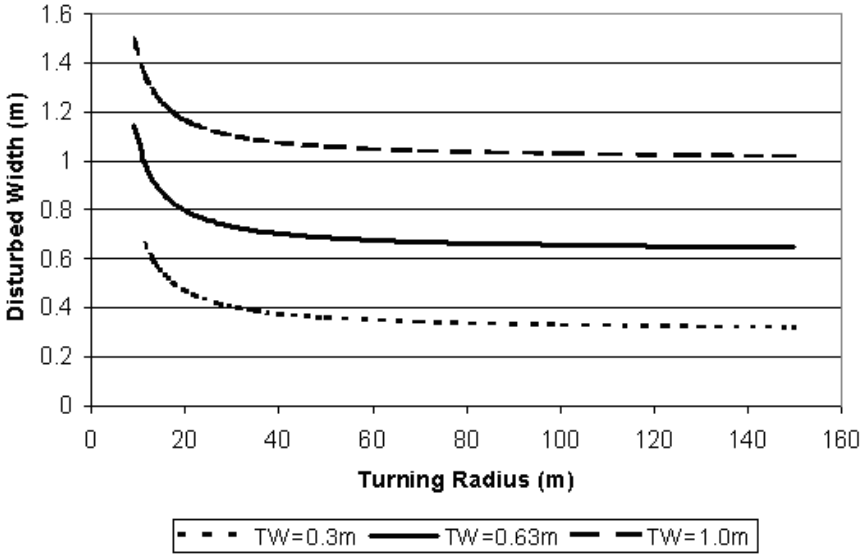

Figure 7.28: Model sensitivity to track width

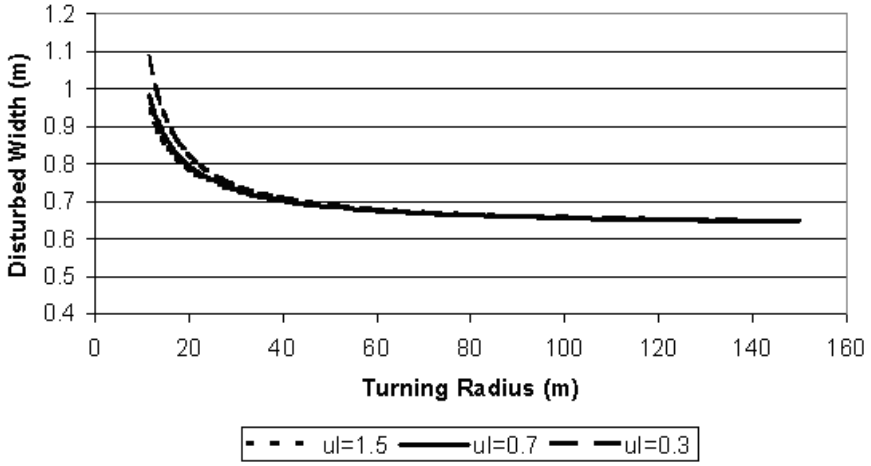

Figure 7.29: Model sensitivity to lateral resistance coefficient of soil

7.6.6 Sensitivity of DW to soil lateral resistance coefficient for tracked vehicle

Figure 7.29 shows the relationship between disturbed width and lateral resistance coefficient of soil. A smaller lateral resistance coefficient of soil will cause a bigger disturbed width at a lower turning radius. This influence diminishes as the turning radius increases.

7.6.7 Sensitivity of IS to the shear deformation modulus of soil for tracked vehicle

Figure 7.30 shows the relationship between the impact severity of the M1A1 tank and the shear deformation modulus (K) of soil. The shear deformation modulus changes the shape of the curve that defines the relationship between disturbed width and impact severity. As the modulus increases from $1\,\mathrm{cm}$ to $8\,\mathrm{cm}$, the gradient of the curve decreases.

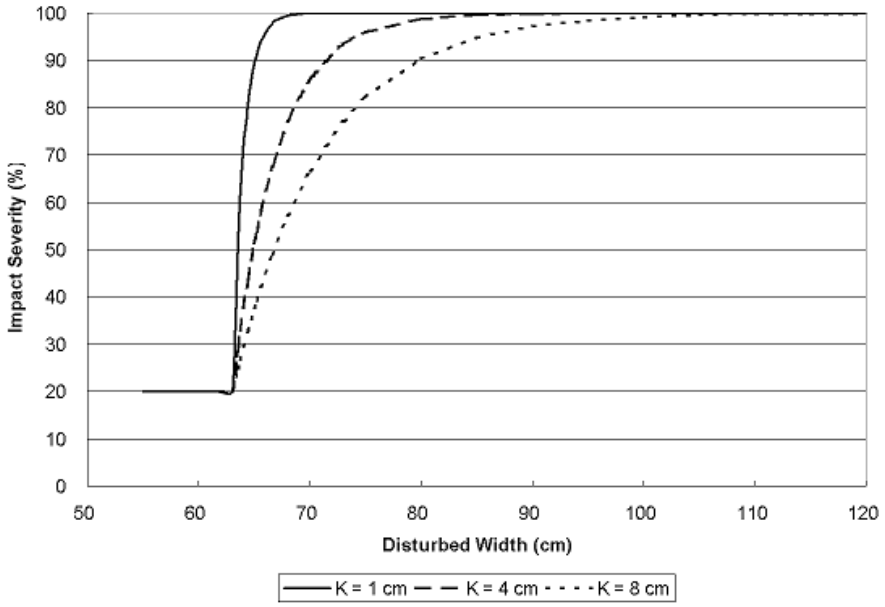

Figure 7.30: Model sensitivity to the shear deformation modulus of soil

7.7 Comparison between the theoretical model equations and best-fit equations

A comparison between the theoretical model equations and best-fit equations of the field data provides another perspective to evaluate the accuracy of the theoretical models. Using the impact severity test of the eight-wheeled vehicle discussed in section 7.2 as an example, this section compares the average percentage error between the theoretical model and the best-fit equations of the field data. Two data sets were discussed in section 7.2. The high speed data set had an average velocity of $9.6\,\mathrm{m/s}$. The low speed data set had an average velocity of $5.4\,\mathrm{m/s}$.

For the high speed data set, Equation 7.18 is a best-fit equation of the field measurement data in the form of Equation 7.5 of the theoretical impact severity model. The best-fit equation was generated through regression of the field data, thus provided a comparison of the model.

$$IS_{theory} = \frac{1093}{TR} \times 100\% \tag{7.18}$$

Figure 7.31 shows the field measurement data, the theoretical impact severity model, as well as the best-fit equation. The average percentage error between the predicted impact severity value and the measured value is $48.5\,\%$ with a standard deviation of $55.5\,\%$. The average percentage error between the best-fit equation and the measured value is $28.5\,\%$ with a standard deviation of $36.6\,\%$.

For the low speed data set, Equation 7.19 is a best-fit equation of the field measurement data in the form of Equation 7.6 of the theoretical impact severity model.

$$IS_{theory} = \frac{503.6}{TR} \times 100\% \tag{7.19}$$

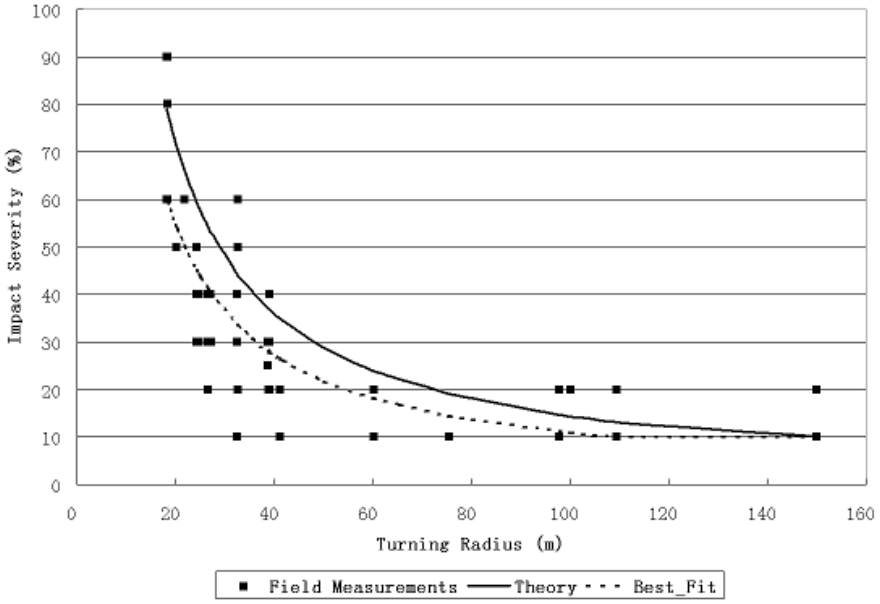

Figure 7.31: Comparison between the theoretical model and best-fit equation (high speed)

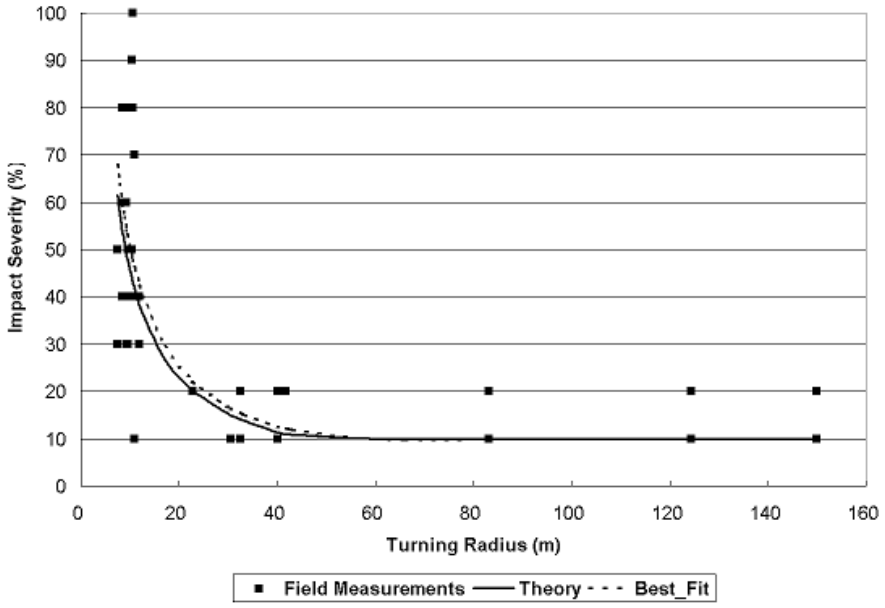

Figure 7.32: Comparison between the theoretical model and best-fit equation (low speed)

Figure 7.32 shows the field measurement data, the theoretical impact severity model, as well as the best-fit equation. The average percentage error between the predicted impact severity value and the measured value is $34.2\,\%$ with a standard deviation of $55.8\,\%$. The average percentage error between the best-fit equation and the measured value is $37.8\,\%$ with a standard deviation of $54.4\,\%$.

The example shows that the average percentage errors of the theoretical impact severity model of the LAV are comparable with that of the best fit equations. The comparison of other theoretical models with their corresponding best-fit equations of the field data has similar results. These theoretical models can represent the field data with similar accuracy as their best-fit equations.

Chapter 8

Comparison of terrain impact between wheeled vehicles and tracked vehicles

This chapter studies the interaction effect of speed and turning radius on terrain impact severity of both tracked vehicles and wheeled vehicles. Previous chapters have discussed how vehicle dynamic conditions may influence the terrain impact severity. An interaction effect of speed and turning radius on terrain impact severity was observed from field test data. A statistical analysis method was designed in this chapter to study the influence of the interaction effect on terrain impact severity and compare the difference of the effect between wheeled vehicles and tracked vehicles.

8.1 Introduction of the field data to be compared

The impact severity data of two field tests were studied. One was for a wheeled vehicle in Fort Lewis, WA, in June 2002. The other field test was for a tracked vehicle in Fort Riley, KS, in October 2004. The wheeled vehicle was a Light Armored Vehicle (LAV); the tracked vehicle was a M1A1 tank. Descriptions of the military installations and the vehicles can be found in the previous chapters. As discussed in previous chapters, the measurement

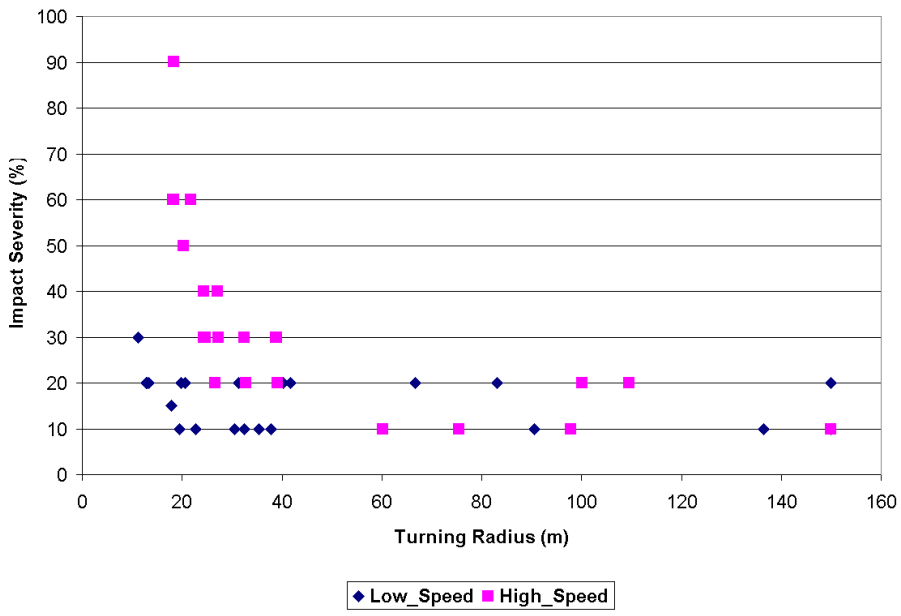

Figure 8.1: Impact severity measurement of the wheeled vehicle (LAV)

of impact severity is based on an initial impact severity guideline (Haugen, 2002). The guideline scales impact severity from 0% to 100%. The test vehicles were operated in a spiral pattern at both high speed and low speed settings, so as to get a variety of turning radii along with speed information.

Figures 8.1 and 8.2 show the raw data of field measurement. Both speed and turning radius can influence the magnitude of impact severity. As the turning radius decreases, the impact severity increases. An increase of speed of the wheeled vehicle at a lower turning radius causes a higher impact severity, but the influence of speed diminishes as the turning radius increases. The influence of vehicle speed of the tracked vehicle on impact severity is not as obvious as that of the wheeled vehicle. The wheeled vehicle shows a stronger effect of the interaction of speed and turning radius on terrain impact severity than the tracked vehicle.

The field data were divided into three groups: data with small turning radius, data with medium turning radius, and data with large turning radius. The two variables, vehicle speed

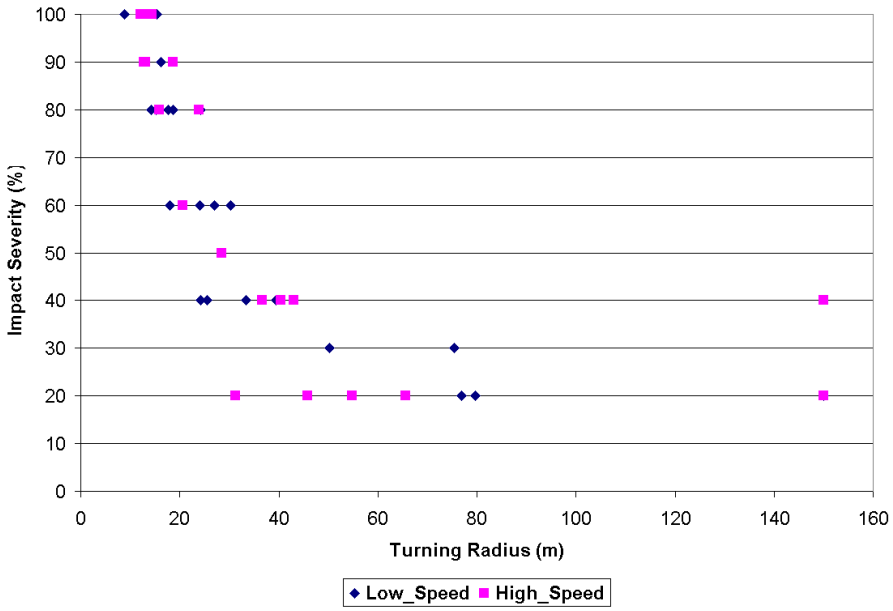

Figure 8.2: Impact severity measurement of the tracked vehicle (M1A1)

Table 8.1: Treatments of vehicle speed and turning radius combination

	Large Turning Radius	Medium Turing Radius	Small Turning Radius
LS *	IS† @ Large TR‡ & LS	IS @ Medium TR & LS	IS @ Small TR & LS
HS§	IS @ Large TR & HS	IS @ Medium TR & HS	IS @ Small TR & HS

Table 8.2: Mean and standard deviation of speeds (m/s)

	Wheeled Vehicle (LAV)	Tracked Vehicle (M1A1)
Low Speed	4.8 (0.30)	2.7 (0.36)
High Speed	9.5 (0.78)	5.1 (0.82)

and turning radius, were used to create a table. The different settings of speed define the rows in the table. The levels of turning radius define the columns. Table 8.1 shows 6 treatments resulting from the two variables. Each treatment in Table 8.1 has 8 measurements of impact severity for each vehicle.

In normal driving conditions, the LAV wheeled vehicle operates at a higher speed than the M1A1 tracked vehicle. In the field test, speeds were determined by the operation as typical high speed and low speed maneuvers. In this test, the average values of low speed and high speed of the LAV were greater than those of the M1A1. Table 8.2 shows the average speeds of the field test for both vehicles.

During the field test, the vehicles were driven from going straight to the minimum operating turning radius of the vehicles. The turning radii of the test vehicles were derived from GPS tracking data and ranged from less than $10\,\mathrm{m}$ up to $150\,\mathrm{m}$. The data were manually divided into three groups according to the magnitude of turning radius. Table 8.3 shows the average value of turning radius of both vehicles.

*Low Speed
†Impact Severity
‡Turning Radius
§High Speed

Table 8.3: Mean and standard deviation of turning radii (m)

	Wheeled Vehicle (LAV)	Tracked Vehicle (M1A1)
Small Turning Radius	18.9 (4.4)	14.8 (2.7)
Medium Turing Radius	34.5 (5.1)	31.2 (7.8)
Large Turning Radius	117.0 (34.7)	119.0 (42.1)

Figures 8.3 and 8.4 more clearly show the interaction relationship between turning radius and speed. Height of the columns in both figures, with standard deviation bars indicated, stands for the mean value of impact severity. The mean values of impact severity in both speed settings are in the sequence of small turning radius, medium turning radius, and large turning radius. Figure 8.3 shows that although there is not much difference of impact severity value for a wheeled vehicle driving in high speed or low speed at a large turning radius, a small turning radius combined with a high speed can cause much higher impact severity than with a low speed. This property does not show in Figure 8.4 for the tracked vehicle. The effect of vehicle speed of tracked vehicles is not as obvious as that of wheeled vehicles.

8.2 ANOVA of the data

The same information can be more accurately expressed from a two-factor ANOVA analysis. Table 8.4 shows the ANOVA results of the wheeled vehicle data. Interaction of speed and turning radius on impact severity accounts for $18.75\,\%$ of the total variance. The P value is less than 0.0001, which means that if there is no interaction overall, there is a less than $0.01\,\%$ chance of randomly observing so much interaction in an experiment of this size. The interaction of turning radius and speed on impact severity is considered extremely significant. Speed accounts for $20.35\,\%$ of the total variance. Turning radius accounts for $31.31\,\%$ of the total variance. Both effects are considered extremely significant.

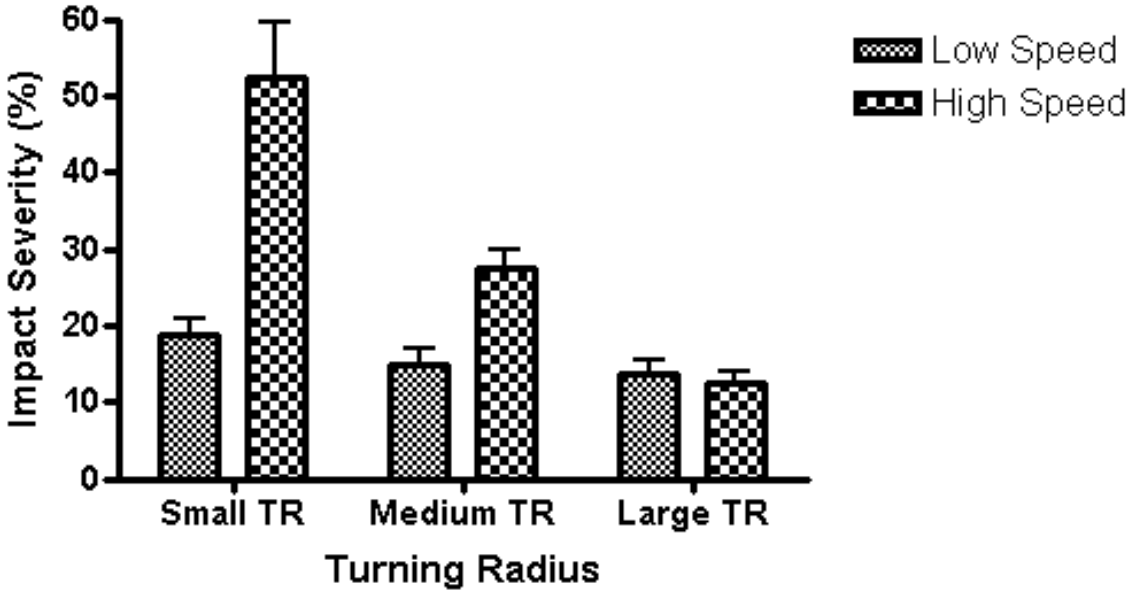

Figure 8.3: Mean impact severity of the wheeled vehicle (LAV)

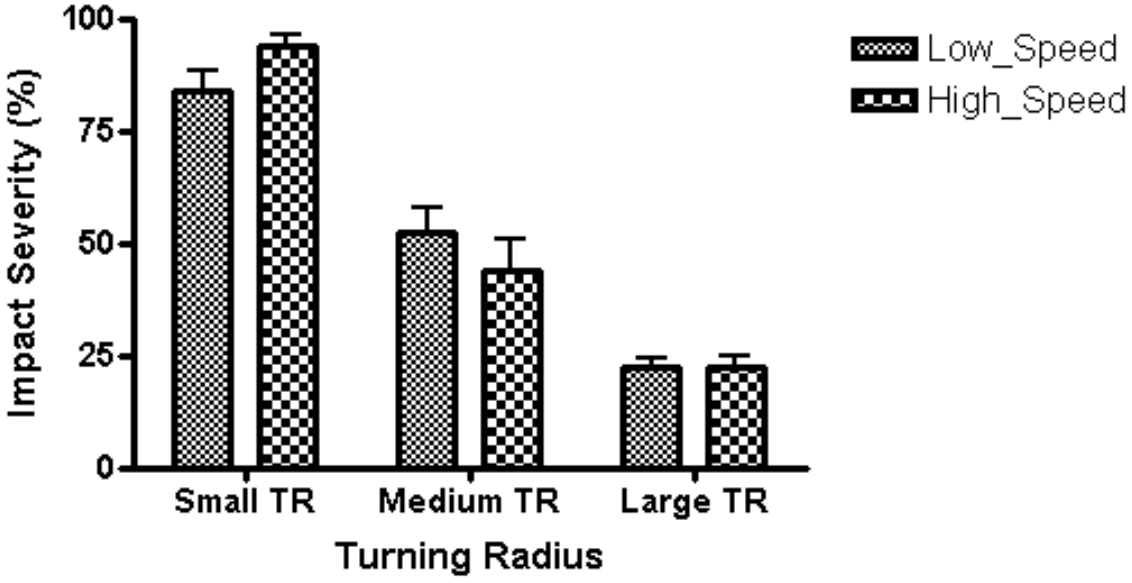

Figure 8.4: Mean impact severity of the tracked vehicle (M1A1)

Table 8.4: ANOVA results of the wheeled vehicle

Source of Variation	Percent of total variation	P value
Interaction	18.75	$P < 0.0001$
Speed	20.35	$P < 0.0001$
Turning Radius	31.31	$P < 0.0001$

Table 8.5: ANOVA results of the tracked vehicle

Source of Variation	Percent of total variation	P value
Interaction	1.64	0.1121
Speed	0.00	0.9076
Turning Radius	83.38	$P < 0.0001$

Table 8.5 shows the ANOVA results of the tracked vehicle. Interaction of turning radius and speed on impact severity accounts for only $1.64\,\%$ of the total variance. The P value is 0.1121, which means that if there is no interaction overall, there is an $11\,\%$ chance of randomly observing so much interaction in an experiment of this size. The interaction of turning radius and speed on impact severity is considered not significant. Speed accounts for less than $0.1\,\%$ of the total variance. The effect of speed is considered not significant. Turning radius accounts for $83.38\,\%$ of the total variance. The effect of turning radius is considered extremely significant.

In the speed range tested in the field, speed and turning radius of wheeled off-road vehicles had strong interaction on terrain impact severity. The interaction accounts for $18.75\,\%$ of the total variance. The worst scenario for impact severity happens when the wheeled vehicle negotiates a sharp turn at a high speed. However, the interaction of turning radius and speed for tracked vehicles was considered not significant. The interaction accounts for only $1.64\,\%$ of the total variance. A smaller turning radius of tracked vehicle always causes higher impact severity regardless of the magnitude of speed.

Chapter 9

Conclusions

9.1 Summary

The major objective of this study was to develop theoretical models for the estimation of disturbed width and impact severity for off-road vehicles. Since there were two indexes (disturbed width and impact severity) to describe terrain impact as well as two kinds of off-road vehicles (wheeled and tracked) to be studied, four individual models were developed: disturbed width model for wheeled vehicles, disturbed width model for tracked vehicles, impact severity model for wheeled vehicles, and impact severity model for tracked vehicles. After the development of these models, field tests at different test sites using different types of vehicles were conducted in order to validate these models.

Disturbed width models were developed for both tracked vehicles and wheeled vehicles. Field tests of disturbed width of wheeled vehicles, the eight-wheeled LAV and the four-wheeled HMMWV, were conducted. The average percentage errors of the disturbed width model for the eight-wheeled vehicle and the four-wheeled vehicle were $19.5\,\%$ and $8.6\,\%$, respectively. Field tests of tracked vehicles showed that the average percentage errors of

the theoretical models for the M1A1, M577, and M548, were $10\,\%$, $27.3\,\%$, and $8.5\,\%$, respectively.

The impact severity models were developed and tested for both wheeled vehicles and the tracked vehicles. The average percentage error of the wheeled vehicle (LAV) was $48.5\,\%$ for the high speed test and $34.2\,\%$ for the low speed test. For the tracked vehicles, M1A1 and M577, the average percentage errors were less than $25.0\,\%$ and $21.4\,\%$, respectively.

Comprehensive terrain impact models of both wheeled vehicles and tracked vehicles were developed and tested. Both the disturbed width model and the impact severity model can represent the field test results. The combination of the disturbed width model and the impact severity model helps to predict both the size of the disturbed area and the severity of the terrain impact. The evaluation of terrain impact caused by individual vehicles using these models can help land managers to assess broad-scale spatial impacts of off-road vehicle and provide better management of the land resources.

9.2 Advantages of the terrain impact models

The theoretical models can help the users better understand the mechanisms of terrain impact due to vehicular activities. Most of the previous methods for assessing terrain impact in the military are empirical models that were developed from statistically-based replicated plot studies. For example, in the ATTAC methodology the terrain impact is normalized in terms of Maneuver Impact Miles (MIM) (Anderson and Sullivan, 2002). One MIM is the equivalent impact of an M1A2 tank traveling 1 mile while participating in an armor battalion field training exercise (Mendoza et al., 2002). The theoretical models, on the other hand, are based on vehicle properties, design characteristics, and terrain properties. Model inputs were selected based on the dynamic analysis of the vehicle-terrain

system. The inputs included a variety of site-specific factors such as the terrain properties and vehicle dynamic properties.

The limitations of the empirical methods are that only one or a few vehicle types were included as treatments and only currently used vehicles have been evaluated (Anderson et al., 2005). The fact is that a wide variety of off-road vehicles are in use in different areas, and newly developed vehicles are fielded now and then. Individual vehicles are often in more than one configuration, each with unique static vehicle properties (Anderson et al., 2005). Comparing with the limitations of the empirical methods, the theoretical models developed in this dissertation are able to assess terrain impact of a wide range of vehicles by selecting appropriate information of each individual vehicle and soil conditions as inputs. The assessment can be performed even before vehicles are available for testing.

9.3 Comparison of the mechanisms of terrain impact between wheeled vehicles and tracked vehicles

According to the disturbed width models of both wheeled vehicles and tracked vehicles, the disturbed width of off-road vehicles is not only determined by static vehicle properties, but also influenced by terrain properties and vehicle dynamic properties, such as vehicle speed and turning radius. However, the mechanism of the influence of vehicle speed and turning radius on disturbed width of wheeled vehicles are different from that of tracked vehicles. For wheeled vehicles, the centrifugal force developed at high speed and small turning radius produces cornering forces on the tires. The cornering forces cause the tires to produce slip angles. The slip angles need to be determined for an accurate calculation of the disturbed width of wheeled vehicles. For tracked vehicles, the centrifugal force causes the center of turn shifting forward in the vehicle traveling direction. The forward shifting of the vehicle turning center increases the disturbed width.

The development of the impact severity models for both wheeled vehicles and tracked vehicles was based on the following principle: the more the ratio of the soil shear stress to the soil shear strength, the more the soil impact severity. However, the calculation of the soil lateral shear stress of wheeled vehicles was different from that of tracked vehicles. For wheeled vehicle, the soil shear stress was directly calculated from the centrifugal force and the tire-terrain contact area. For tracked vehicles, the lateral shear stress of the soil was mainly resulted from the lateral shear displacement of the soil that was caused by the lateral movement of the tracks. The lateral shear displacement of the soil and the soil shear deformation modulus were used for the calculation of the impact severity of tracked vehicles.

The mechanism of wheeled vehicles to laterally shear the soil is different from that of tracked vehicles when conducting a turn. This difference not only resulted in different calculation methods of the soil lateral shear stress, but also produced different characteristics of the interaction of vehicle speed and turning radius on the impact severity. For wheeled vehicles, the lateral shearing stress of soil in the tire-terrain contact area was mainly due to the centrifugal force of the vehicle when performing a turn at a certain speed. A higher magnitude of centrifugal force, which is determined by both vehicle speed and turning radius, will cause a higher impact severity. A strong interaction of vehicle speed and turning radius on impact severity demonstrated the characteristics of such a soil lateral shear mode of wheeled vehicles. While for tracked vehicles, the lateral shearing stress of soil in the track-terrain contact area was mainly due to the lateral movement of tracks during a turn. This soil lateral shear mode contributed to a weak interaction of speed and turning radius on impact severity. When a tracked vehicle negotiated a turn at either a high speed or a low speed during normal maneuvers, the lateral movement of the tracks was about the same displacement and would produce comparable soil lateral shear stress.

Although the terrain impact models were developed separately for wheeled vehicles and tracked vehicles, it is applicable to compare the prediction of terrain impact (DW and IS) of the wheeled vehicles with that of the tracked vehicles. Although the calculation methods are different, it is straightforward to compare the disturbed width between wheeled vehicles and tracked vehicles. The calculations of the soil lateral shear stress are also via different methods for wheeled vehicles and tracked vehicles. However, the unification of terrain impact severity to the ratio between soil lateral shear stress and soil shear strength makes the comparison of impact severity between these two vehicle types feasible.

9.4 Future directions

The current models do not consider the scenario of operating vehicles on a slope. If the slope is considerately steep, the accuracy of the models deteriorates. Introduction of the influence of slope on the terrain impact would improve the utilities of the models. A limitation of the wheeled models is that the models can only be used on 2-axle vehicles or 4-axle vehicles. If there are some current vehicles or vehicles to be deployed in the future that have configurations other than a 2-axle or a 4-axle, the wheeled models need to be extrapolated to accommodate their configurations. The wheeled vehicle models could also be improved in order to be applied on wheeled vehicles that use different tire sizes on their axles.

More field tests need to be conducted in order to fully test the models. For example, the moisture content of some of the test fields in wet season is very different from that in dry season. The soil strength parameters change with soil moisture content. Field tests conducted in both dry and wet seasons at the same test site could evaluate the influences of soil moisture content on terrain impact. Vegetation types could also influence the impact

severity, thus field tests of a vehicle on different vegetation types help to evaluate their influences. If these influences are not negligible, some constants may be needed to customize the models according to the moisture content and/or vegetation type of the field.

Bibliography

Bibliography

Abbott, E. and Powell, D. (1999). Land-vehicle navigation using GPS. *Proceeding of the IEEE*, 87(1):145–162.

Abebe, A., Tanaka, T., and Yamazaki, M. (1989). Soil compaction by multiple passes of a rigid wheel relevant for optimization of traffic. *Journal of Terramechanics*, 36(2):139–148.

Abele, G., Brown, J., and Brewer, M. (1984). Long-term effects of off-road vehicle traffic on tundra terrain. 21(3):283–294.

Althoff, P. and Thien, S. (2005). Impact of M1A1 main battle tank disturbance on soil quality, invertebrates, and vegetation characteristics. *Journal of Terramechanics*, 42(3-4):159–176.

Anderson, A., Chenkin, L., Winters, L., Hunt, R., Couvillon, C., McFerren, D., Sekscienski, S., and Sydelko, P. (1996). Evaluation of landvalue study (ELVS) / army training and testing area carrying capacity (ATTACC). In *5th Annual LRAM/ITAM Workshop Proceedings*, pages Pp.8–17, LaCrosse, WI.

Anderson, A., Palazzo, A., Ayers, P., Fehmi, J., Shoop, S., and Sullivan, P. (2005). Assessing the impacts of military vehicle traffic on natural areas: Introduction to the special issue and review of the relevant military vehicle impact literature. *Journal of terramechanics*, 42(3-4):143–158.

Anderson, A. and Sullivan, P. (2002). Estimating army training and testing area carrying capacity (ATTACC) vehicle severity and local condition factors. In *14th International Conference of the ISTVS*, Vicksburg, MS USA.

ASAE (1999). ASAE standard: Procedures for using and reporting data obtained with the soil cone penetrometer.

Ayers, P. (1994). Environmental damage from tracked vehicle operation. *Journal of Terramechanics*, 31(3):173–183.

Ayers, P., Vance, M., Haugen, L., and Anderson, A. (2000). An evaluation of DGPS-based continuously operating vehicle monitoring systems to determine site-specific event severity factors. Technical Report ERDC/CERL TR-00-43, Construction Engineering Research Laboratory.

Ayers, P. D. (1987). Moisture and density effects on soil shear strength parameters for coarse grained soils. *Transactions of the ASAE*, 30(5):1282–1287.

Ayers, P. D. and Perumpral, J. V. (1982). Moisture and density effect on cone index. *Transactions of the ASAE*, 5:1169–1972.

Ayers, P. D., Wu, C., and Anderson, A. B. (2004). Evaluation of autonomous and differential GPS for multi-pass vehicle identification. In *ASAE paper number:041061*, St. Joseph, MI. ASAE.

Bekker, M. (1969). *Introduction to terrain-vehicle systems*. University of Michigan Press, Ann Arbor, MI.

Braunack, M. (1985). The effect of tracked vehicles on soil strength and micro-relief of a calcareous earth (gc 1.12) north of woomera, south australia. *Aust. Rangel J.*, 7(1):17–21.

Braunack, M. (1986). The residual effects of tracked vehicles on soil surface properties. *Journal of Terramechanics*, 23(1):37–50.

Braunack, M. and Williams, B. (1993). The effect of initial soil water content and vegetative cover on surface soil disturbance by tracked vehicles. *Journal of Terramechanics*, 30(4):299–311.

Cohron, G. (1962). The soil sheargraph. Technical Report ASAE Technical Paper No. 62-133, ASAE, St. Joseph, Mich.

Council on Environmental Quality (1989). Defense lands and installations. Environmental quality: Annual report, 1987-88. Technical report, Washington, DC.

Diersing, V., Shaw, R., Warren, S., and Novak, E. (1988). A user's guide for estimating allowable use of tracked vehicles on nonwooded military training lands. *Journal of Soil and Water Conservation*, pages 191–195.

Donagh, P. M., Garibaldi, J., Rivero, L., Fernandez, R., and Kobayashi, S. (2002). Neotropical forest harvesting impact in Misiones, Argentina: Soil compaction and traffic intensity. Technical Report No. 025009, ASAE, St. Joseph, Mich.

Dougherty, M. (2000). A review of neural networks applied to transport. *Transportation Research*, 3(4):247–60.

Dwyer, M. . (1984). Computer models to predict the performance of agricultural tractors on heavy draught operations. In *Proceedings of the 8th International conference of ISTVS*, pages III: 933–952, Cambridge, England.

Freitag, D. . (1965). A dimensional analysis of the performance of pneumatic tires on soft soils. Technical Report No. 3-688, US Army Waterways Experiment Station.

Gatziolis, D., Fried, J., and Ramm, C. (2000). Monitoring the impacts of tracked vehicle training area use at Ft. Hood, TX: a GIS approach. In *The Second International Conference on Geospatial Information in Agriculture and Forestry*, Lake Buena Vista, Florida.

Godwin, R., Warner, N., and Smith, D. (1991). The development of a dynamic drop-cone device for the assessment of soil strength and the effects of machinery traffic. *Journal of agricultural engineering research*, 48:123–131.

Goran, W., Radke, L., and Severinghaus, W. (1983). An overview of the ecological effects of tracked vehicles on major U.S. Army installations. Technical Report N-142, Construction Engineering Research Laboratory.

Grantham, W., Redente, E., Bagley, C., and Paschke, M. (2001). Tracked vehicle impacts to vegetation structure and soil erodibility. *Journal of Range Management*, 54(6):711–716.

Haugen, L. (2002). Design and testing of a vehicle tracking system for monitoring environmental impact at U.S. army training installations. Master's thesis, Colorado State University, Fort Collins, Colorado.

Haugen, L., Ayers, P., and Anderson, A. (2003). Vehicle movement patterns and impact during military training exercises. *Journal of Terramechanics*, 40(2):83–95.

Haugen, L., Ayers, P., and Anderson, A. (2004). Measurement and comparison of military vehicle vegetative impacts. *Journal of Terramechanics*. (Accepted).

Horn, R., Blackwell, P., and White, R. (2004). The effect of speed of wheeling on soil stresses, rut depth and soil physical properties in an ameliorated transitional red-brown earth. *Soil & Tillage Research*.

Janosi, Z. and Hanamoto, B. (1961). An analysis of pneumatic tire performance on deformable soil. In *Proceedings of the 1st International ISTVS Conference*, pages 707–726, Torino-Saint Vincent, Italy.

Janzen, D. C. (1990). An industry response to compaction concerns in agriculture. Technical Report No. 90-1074, ASAE, St. Joseph, Mich.

Kogure, K., Ohira, Y., and Yamaguchi, H. (1982). A simplified method for the estimation of soil thrust exerted by a tracked vehicle. *Journal of Terramechanics*, 19(3):165–181.

Koolen, A. and Kuipers, H. (1983). *Agricultural Soil Mechanics*. Springer-Verlag, Berlin, Germany.

Le, A. (1999). *Modeling and control of tracked vehicles*. PhD thesis, the University of Sydney, Sydney.

Leatherman, S. and Godfrey, P. (1979). The impact of off-road vehicles on coastal ecosystems in Cape Cod national seashore: an overview. Technical Report UM/NPSCRU Report No. 34, National park Service Cooperative Research Unit.

Lombardi, A. (2004). Land condition trend analysis (LCTA) coordinator for Fort Lewis, WA. Personal communication.

MacLaurin, E. (1997). The use of mobility numbers to predict the tractive performance of wheeled and tracked vehicles in soft cohesive soils. In *Proceedings of the 7th European ISTVS Conference*, pages 391–398, Ferrara, Italy.

Markgraf, M., Montenbruck, O., and Leung, S. (2002). A flexible GPS tracking system for suborbital and space vehicles. In *9th St. Petersburg International Conference on Integrated Navigation Systems*, St. Petersburg, Russia.

Marsili, A., Servadio, P., Pagliai, M., and Vignozzi, N. (1998). Changes of some physical properties of a clay soil following passage of rubber- and metal-tracked tractors. *Soil & Tillage Research*, 49(3):185–199.

Matthes, R. K. and Watson, W. F. (1989). Measurements of pressure at the soil-tire interface of a rubber-tired skidder. Technical Report ASAE Paper No. 89-7066, ASAE, St. Joseph, Mich.

McKyes, E. (1989). *Agricultural engineering soil mechanics*. ELSEVIER, Amsterdam-Oxford-New York-Tokyo.

Mendoza, G., Anderson, A., and Gertner, G. (2002). Integrating multi-criteria analysis and GIS for land condition assessment: Part I - evaluation and restoration of military training areas. *Journal of Geographic Information and Decision Analysis*, 6(1):1–16.

Moen, R., Pastor, J., Cohen, Y., and Schwartz, C. C. (1996). Effects of moose movement and habitat use on GPS collar performance. *J. Wildl. Manage.*, 60:659–668.

Oljaca, M. (1994). Damage to soil mechanical properties caused by iron and rubber tracks. *Journal of Terramechanics*, 31(5):279–284.

Payne, G., Foster, J., and Leininger, W. (1983). Vehicle impacts on northern great plains range vegetation. *Journal of Range Management*, 36(3):327–331.

Petelkau, H. and Dannowski, M. (1990). Effect of repeated vehicle traffic in traffic lanes on soil physical properties, nutrient uptake and yield of oats. *Soil & Tillage Research*, 15:217–225.

Prose, D. (1985). Persisting effects of armored military maneuvers on some soils of the Mojave desert. *Environ. Geol. Water Sci.*, 7(3):163–170.

Public Land Law Review Commission (1970). One third of the nation's land. A report to the president and to the congress. Technical report, U.S. Government Printing Office, Washington, DC.

Pytka, J. (2005). Effects of repeated rolling of agricultural tractors on soil stress and deformation state in sand and loess. *Soil & Tillage Research*, 82(1):77–88.

Raper, R., Bailey, A., Burt, E., Way, T., and Liberati, P. (1995). Inflation pressure and dynamic load effects on soil deformation and soil-tire interface stresses. *Transactions of the ASAE*, 38(3):685–689.

Saarilahti, M. (2002). Soil interaction model. Technical Report Quality of life and management of living resources contract No. QLK5-1999-00991, Department of Forest Resource Management, University of Helsinki.

Schwanghart, H. (1991). Measurement of contact area, contact pressure and compaction under tires in soft soil. *Journal of Terramechanics*, 28(4):309–318.

Shaw, R. and Diersing, V. (1989). Evaluation of the effects of military training on vegetation in southeastern Colorado. *Headwaters hydrology*, pages 223–231.

Shaw, R. and Diersing, V. (1990). Tracked vehicle impacts on vegetation at the Pinon Canyon Maneuver Site, Colorado. *J. Environ. Qual.*, 19(234-243).

Simmons, K. (2004). Vegetative recovery of military vehicle impacts at Fort Lewis, WA. Master's thesis, the University of Tennessee, Knoxville, TN.

Slaughter, C., Racine, C., Walker, D., Johnson, L., and Abele, G. (1990). Use of off-road vehicles and mitigation of effects in Alaska permafrost environments: A review. *Environmental management*, 14(1):63–72.

Smith, D. and Dickson, J. (1990). Contributions of vehicle weight and ground pressure to soil compaction. *J. agric. Engng Res.*, 46:13–29.

Soil Survey Division Staff (1993). Soil survey manual. *U.S. Department of Agriculture Handbook 18*.

Stombaugh, T., Shearer, S. A., Fulton, J. P., and Ehsani, R. (2002). Elements of a dynamic GPS test standard. Technical Report ASAE Paper No. 021150, ASAE, St. Joseph, MI.

Sullivan, P. M. and Anderson, A. B. (2000). A methodology for estimating army training and testing area carrying capacity (ATTACC) vehicle severity factors and local condition factors. Technical Report ERDC TR-00-2, Engineer Research and Development Center, US Army Corps of Engineers.

Taylor, R. K. and Schrock, M. D. (2003). Dynamic testing of GPS receivers. Technical Report ASAE Meeting Paper No. 03-1013, ASAE, St. Joseph, Mich.

Thurow, T. (1990). Soil compaction evaluation at Fort Hood, Texas. Technical Report Contract Number DACA88-89-M-1249, Department of Range Science, Texas A&M University.

Thurow, T., Warren, S., and Carlson, D. (1993). Tracked vehicle traffic effects on the hydrologic characteristics of central Texas rangeland. *Transactions of the ASAE*, 36(6):1654–1650.

Trimble (2004). *AgRemote software guide for AgGPS receivers*. Trimble Navigation Limited.

Turner, L., Anderson, M., Larson, B., and Udal, M. (2001). Global positioning systems (GPS) and grazing behavior in cattle. In *Livestock Environment VI: Proceeding of the 6th international Symposium*, pages 640–650.

Tweddale, S., Charles, A., Echschlaeger, L., and Seybold, W. (2000). An improved method for spatial extrapolation of vegetative cover estimates (USLE/RUSLE C Factor) using LCTA and remotely sensed imagery. Technical Report USAEC Report SFIM-AEC-EQ-TR-200011 and ERDC/CERL TR-00-7, USAEC.

Veal, M., Tayler, S., McDonald, T., McLemore, D., and Dunn, M. (2001). Accuracy of tracking forest machines with GPS. *Transactions of the ASAE*, 44(6):1903–1911.

Webb, R. and Wilshire, H. (1983). *Environmental effects of off-road vehicles*. Springer-Verlag, New York, New York 10010, USA.

Wilshire, H. (1976). Off-road vehicle effects on California's Majave desert. *California Geology*, 6:123–132.

Wilson, S. (1988). The effect of military tank traffic on prairie: a management model. *Environmental management*, 12(3):397–403.

Wong, J. (1980). Data processing methodology in the characterization of the mechanical properties of terrain. *Journal of Terramechanics*, 17(1):13–41.

Wong, J. (2001). *Theory of ground vehicles*. John Wiley and Sons, New York, N.Y., 3rd ed. edition.

Wong, J., Radforth, J., and Preston-Thomas, J. (1982). Some further studies on the mechanical properties of muskeg in relation to vehicle mobility. *Journal of Terramechanics*, 19(2):107–127.

Zito, R., D'Este, G., and Taylor, M. (1995). Global positioning systems in the time domain: how useful a tool for intelligent vehicle-highway systems? *Transportation Research Part C*, 3(4):193–209.

Appendix

Appendix A

GIS figures of the field tests

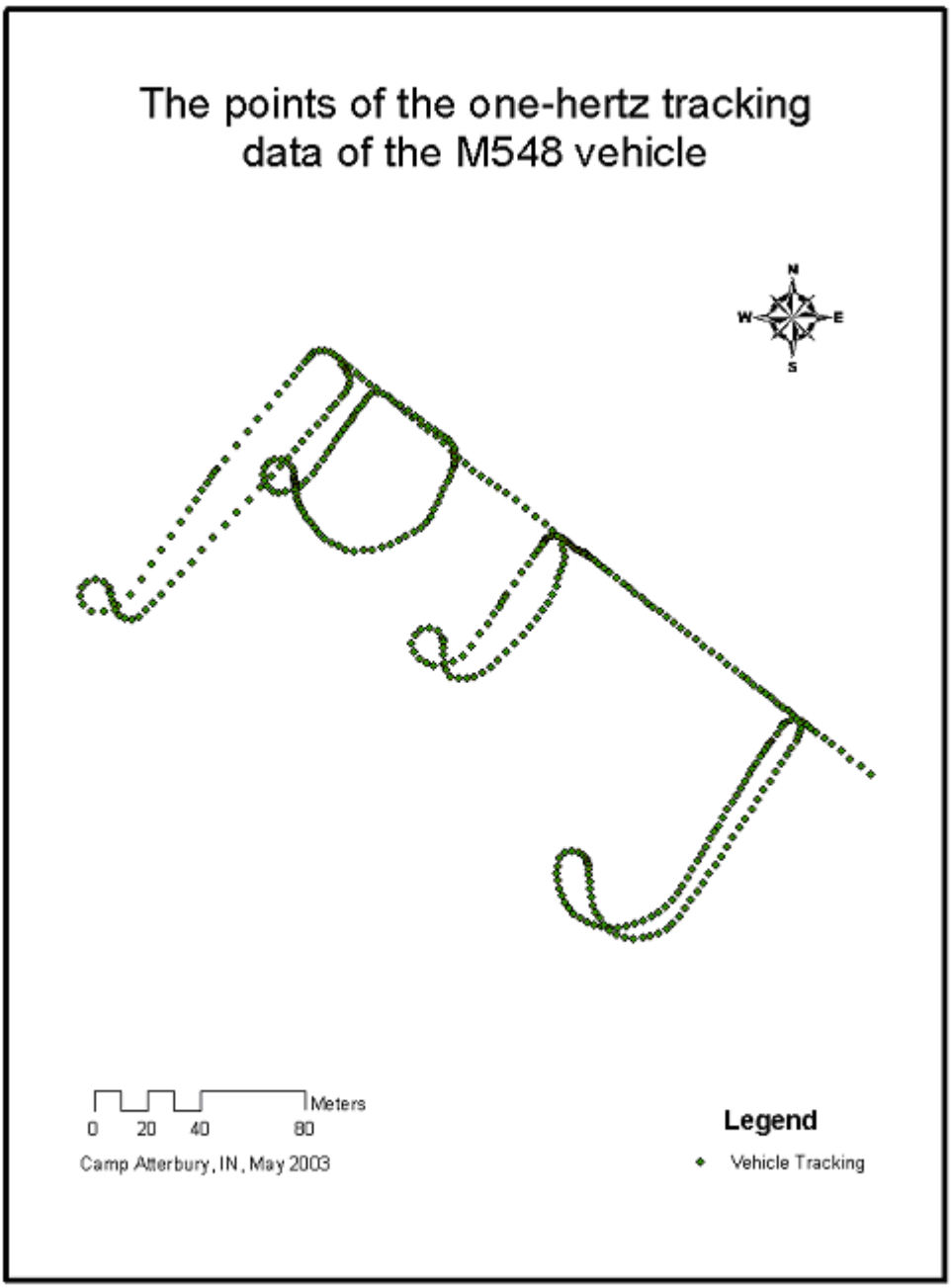

Figure A.1: The vehicle tracking data of the M548 at Camp Atterbury, IN

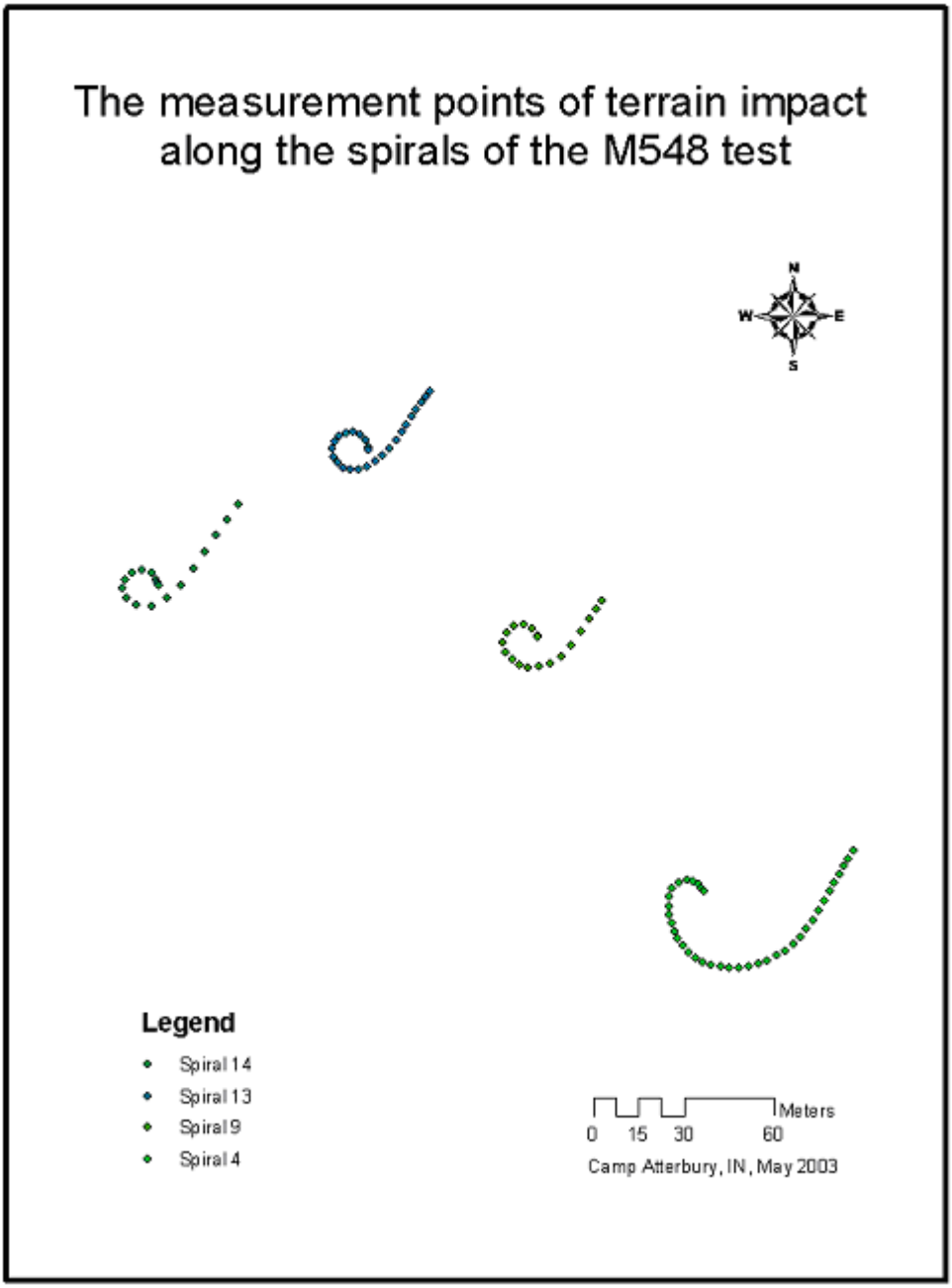

Figure A.2: The points of measurement of terrain impact of the M548 at Camp Atterbury, IN

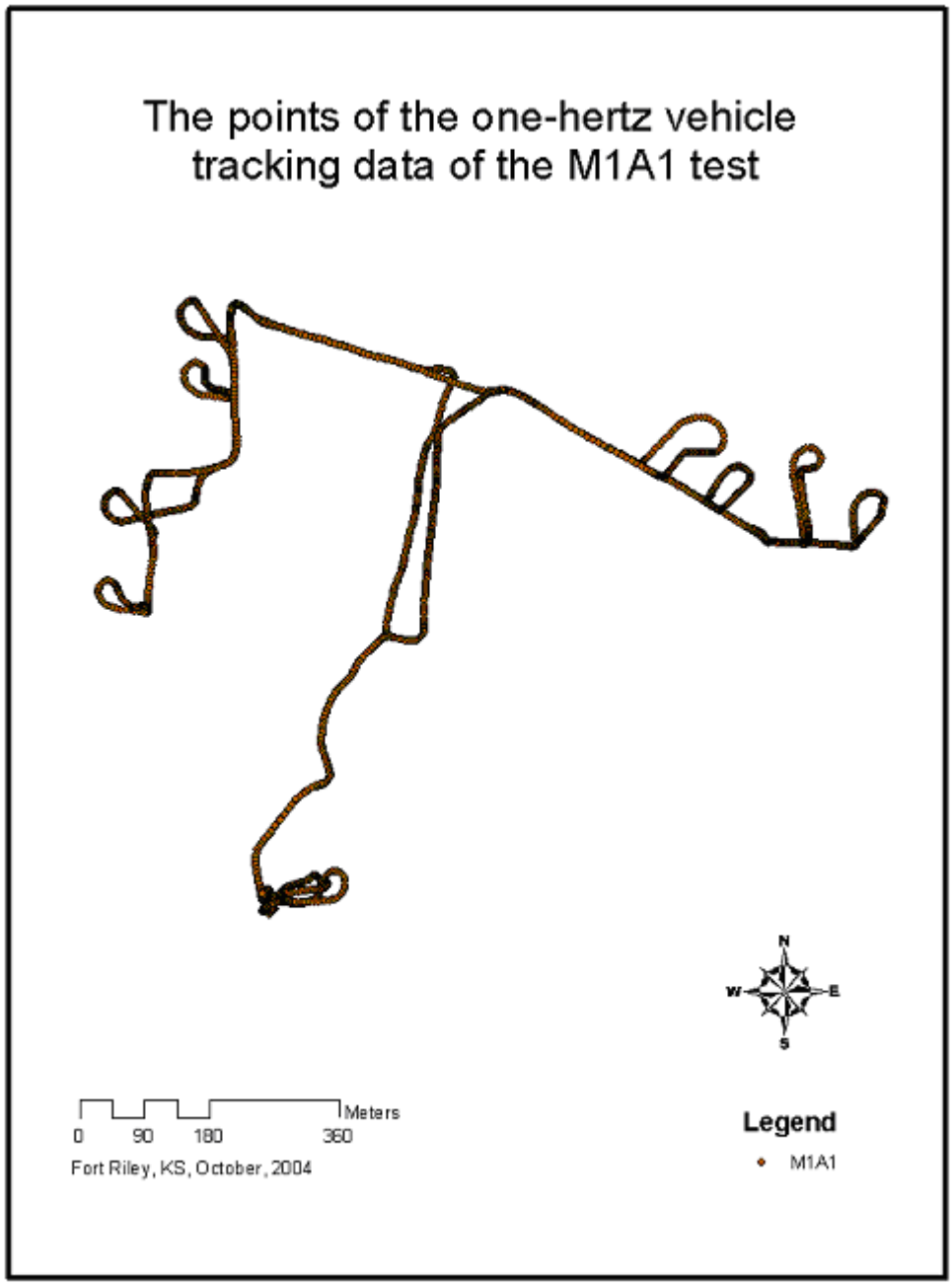

Figure A.3: The vehicle tracking data of M1A1 at Fort Riley, KS

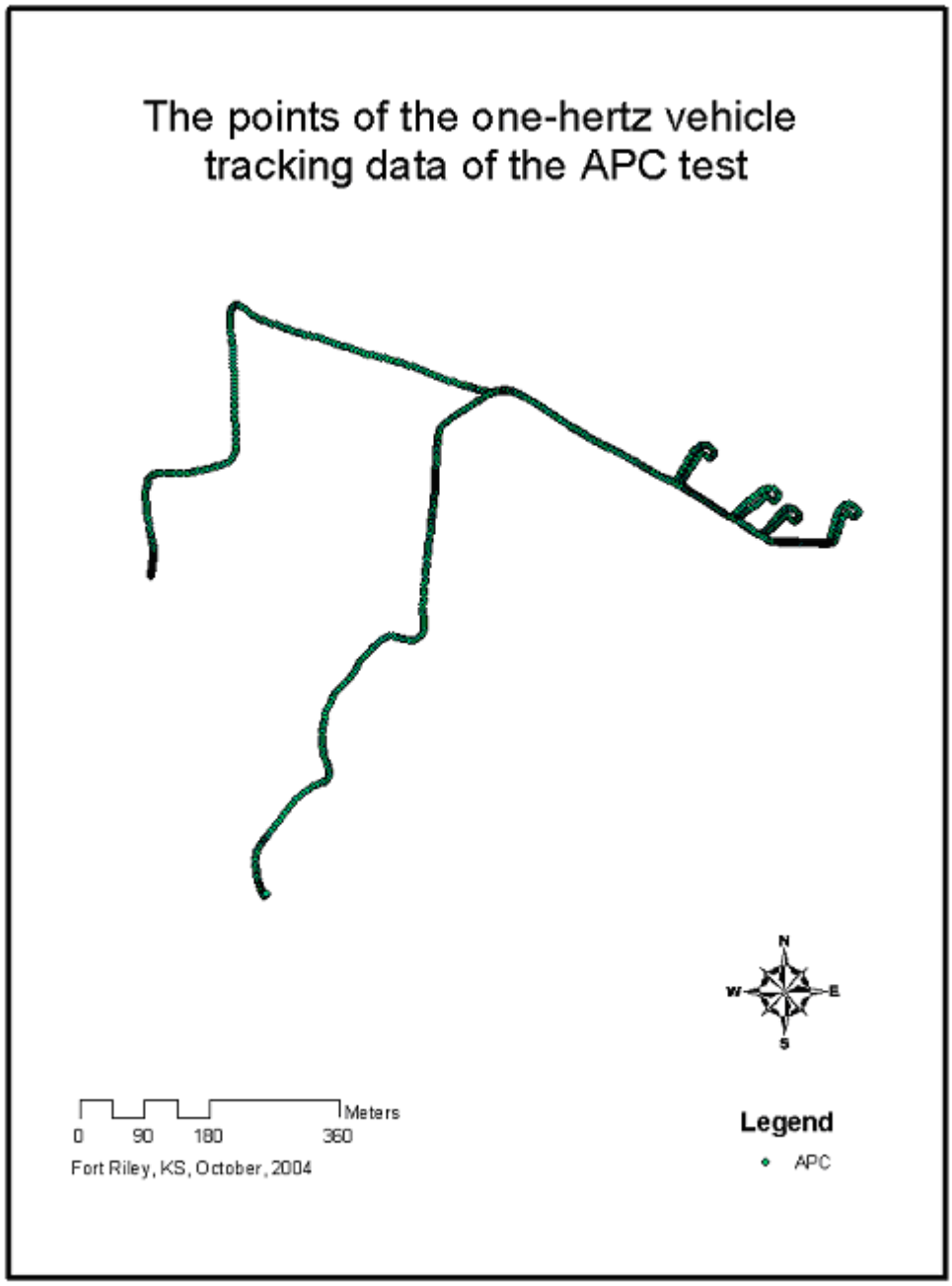

Figure A.4: The vehicle tracking data of APC at Fort Riley, KS

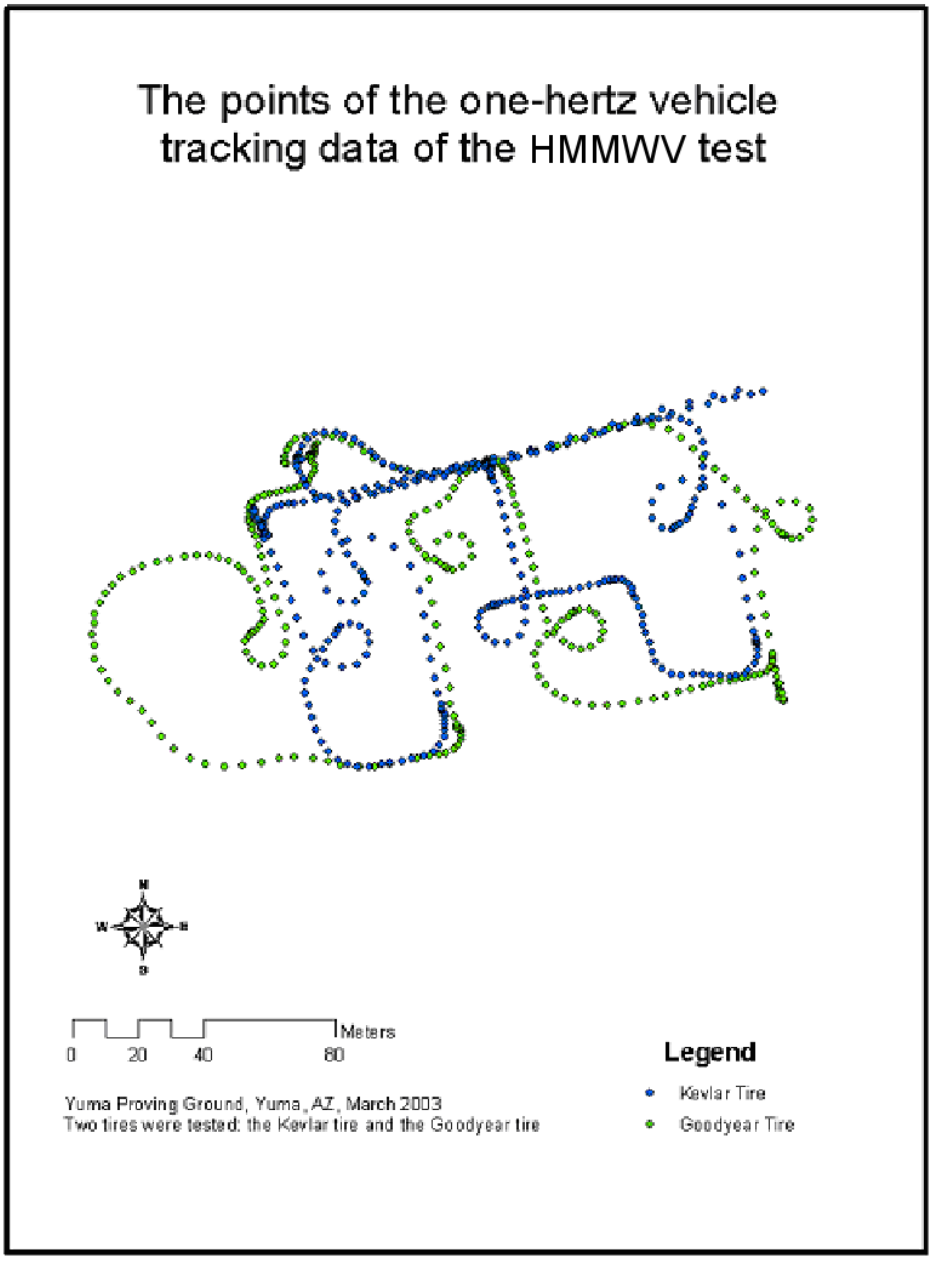

Figure A.5: The vehicle tracking data of the HMMWV test at YPG, Yuma, AZ

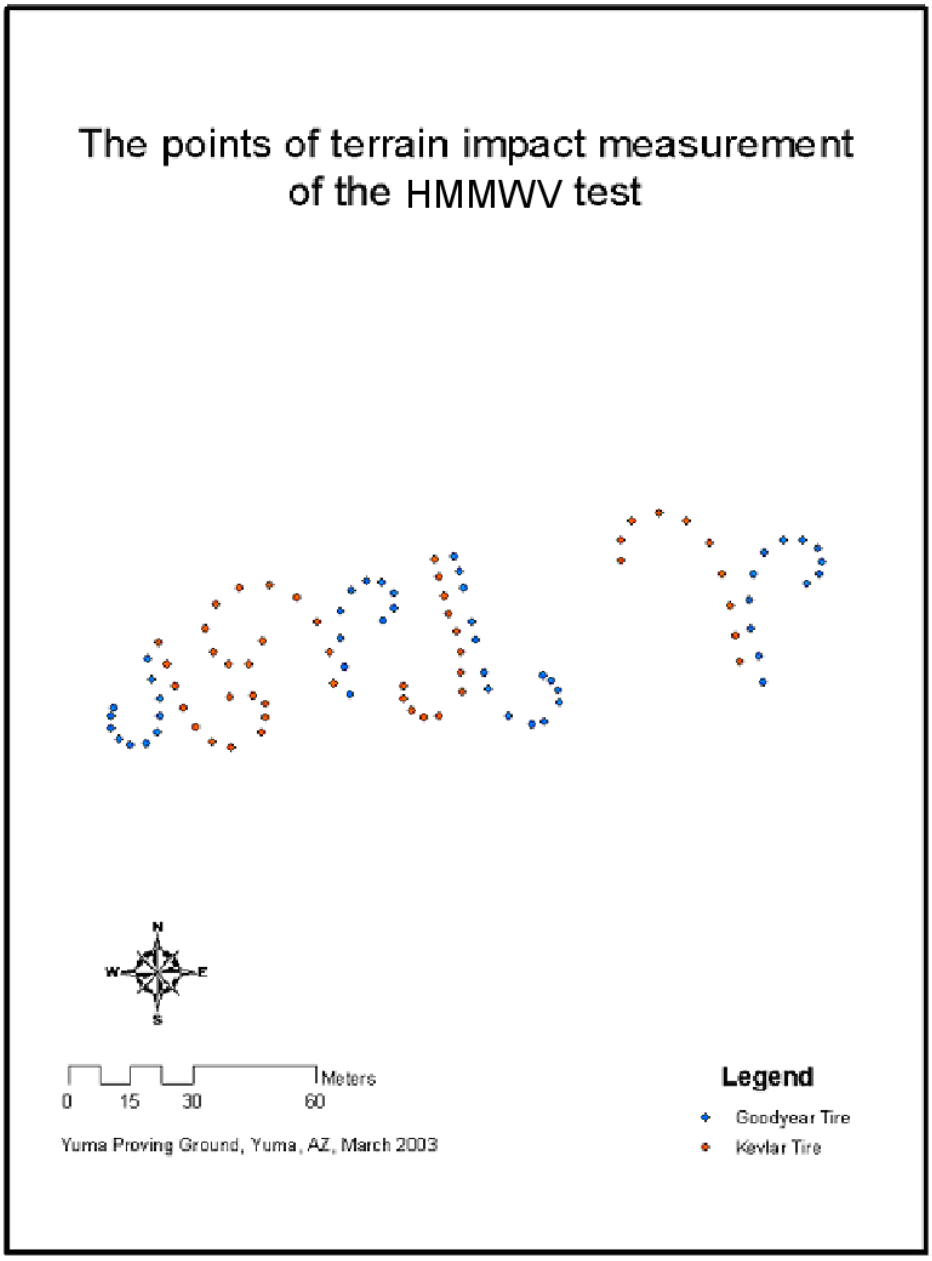

Figure A.6: The points of the terrain impact measurement of the HMMWV test at YPG, Yuma, AZ

Appendix B

General site information of the field tests

FORT LEWIS, WA JUNE 2002

SOIL TYPE and PARTICLE SIZE

Sandy Loam

67% Sand

29% Silt

4% Clay

MOISTURE CONTENT

Average 37% by weight basis (n=92)

CONE PENETROMETER

Information not available.

DROP CONE

Average 5.2 cm (n=169)

SPECIES

”The project site contained sod-forming grassy vegetation. Most of these grasses were non-native perennials. The most common type of grass at the site was Colonial bentgrass (Agrostis tenuis).” (Haugen et al., 2004)

TORSIONAL SHEAR (control)

Cohesion - 0.33 psi

Friction Angle - 43.5 degrees

9 psi shear strength @ 10 psi normal stress

ORGANIC

28% organic matter

4% root mass

YAKIMA TRAINING CENTER, WA JUNE 2002 M1 SITE

GENERAL SITE INFO

SOIL TYPE and PARTICLE SIZE

Sandy loam

55-56% sand

34-35% silt

10% clay

MOISTURE CONTENT

Information not available.

CONE PENETROMETER

Information not available.

DROP CONE

Information not available.

SPECIES

”Dominant native plants are bluebunch wheatgrass and big sagebrush; cheatgrass is an important invader” (Goran et al., 1983).

TORSIONAL SHEAR

Average Cohesion - 1.63 psi (stdv - .52 psi)

Average Friction Angle - 31.8 degrees (stdv - 1.2 degrees)

Average 7.2 psi shear strength @ 10 psi normal stress (n=2)

ORGANIC

Average 1.4% organic matter (n=2)

YUMA PROVING GROUND, AZ MARCH 2003 SAND SITE

GENERAL SITE INFO

SOIL TYPE and PARTICLE SIZE

Sand

96% sand

2% silt

2% clay

MOISTURE CONTENT

Average 32% (n=8)

CONE PENETROMETER

Average 260 kpa at surface (n=32)

Average 484 kpa at 5 cm depth (n=32)

Average 725 kpa at 10 cm depth (n=32)

Average 2882 kpa at 15 cm depth (n=32)

Average 5144 kpa at 20 cm depth (n=23)

Average 6067 kpa at 25 cm depth (n=10)

DROP CONE

Average 10.3 cm (n=114)

SPECIES

Information not available.

TORSIONAL SHEAR

Average Cohesion - 1.60 psi (stdv - .48 psi)

Average Friction Angle - 18.0 degrees (stdv - 4.7 degrees)

Average 5 psi shear strength @ 10 psi normal stress (n=8)

ORGANIC

Information not available.

CAMP ATTERBURY, IN MAY 2003

GENERAL SITE INFO

SOIL TYPE and PARTICLE SIZE

Sandy Loam

55% Sand

30% Silt

15% Clay

MOISTURE CONTENT

Average TDR 28% by volume (n=117)

CONE PENETROMETER The Investigator TM Soil Compaction Meter

Average 326 kpa at surface (n=21)

Average 1281 kpa at 5 cm depth (n=21)

Average 1939 kpa at 10 cm depth (n=21)

Average 2742 kpa at 15 cm depth (n=21)

Average 3165 kpa at 20 cm depth (n=21)

Average 2869 kpa at 25 cm depth (n=20)

Average 2978 kpa at 30 cm depth (n=20)

Average 2846 kpa at 35 cm depth (n=20)

Average 2812 kpa at 40 cm depth (n=19)

Average 2919 kpa at 45 cm depth (n=18)

DROP CONE

Average 7.1 cm (n=254)

SPECIES

Dominant native plants are bluebunch wheatgrass and big sagebrush; cheatgrass is an important invader (Goran et al., 1983).

TORSIONAL SHEAR

Average Cohesion - 2.84 psi (stdv - 1.36 psi)

Average Friction Angle - 40.4 degrees (stdv - 5.6 degrees)

Average 11.7 psi shear strength @ 10 psi normal stress (n=20)

ORGANIC

4.6% organic matter

2.5% root mass

Vita

Qinghe Li was born in Anyang, China. He received both a Bachelor of Science degree, in 1997 and a Master of Science degree in 2000 from the Department of Vehicle Engineering of China Agricultural University, Beijing, China. In the spring of 2000, he started to work for the Chinese Academy of Agricultural Mechanization Sciences, Beijing, China, as a research engineer until the summer of 2002. In the fall of 2002, he was enrolled in the Department of Biosystems Engineering and Soil Science of The University of Tennessee as a doctoral student. During the summer of 2005, he worked as a research intern at Pacific Northwest National Lab, Richland, WA. Qinghe Li received a Doctor of Philosophy degree in the August of 2006.